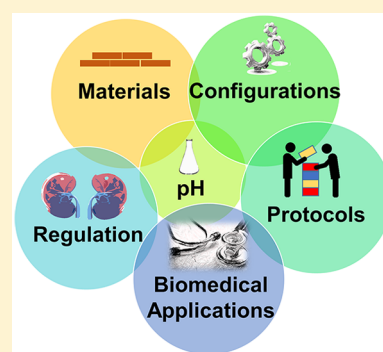


## Recent Progress in Electrochemical pH-Sensing Materials and Configurations for Biomedical Applications

M. T. Ghoneim,<sup>†</sup> A. Nguyen,<sup>‡</sup> N. Dereje,<sup>§</sup> J. Huang,<sup>#</sup> G. C. Moore,<sup>⊥</sup> P. J. Murzynowski,<sup>||</sup> and C. Dagdeviren<sup>\*,†</sup><sup>†</sup>MIT Media Lab, <sup>§</sup>Department of Mechanical Engineering, and <sup>#</sup>Department of Aeronautics and Astronautics, Massachusetts Institute of Technology (MIT), Cambridge, Massachusetts 02139, United States<sup>‡</sup>Department of Biological Engineering, <sup>⊥</sup>Department of Materials Science and Engineering, and <sup>||</sup>Department of Electrical Engineering and Computer Science, Massachusetts Institute of Technology (MIT), Cambridge, Massachusetts 02142, United States

**ABSTRACT:** pH-sensing materials and configurations are rapidly evolving toward exciting new applications, especially those in biomedical applications. In this review, we highlight rapid progress in electrochemical pH sensors over the past decade (2008–2018) with an emphasis on key considerations, such as materials selection, system configurations, and testing protocols. In addition to recent progress in optical pH sensors, our main focus in this review is on electromechanical pH sensors due to their significant advances, especially in biomedical applications. We summarize developments of electrochemical pH sensors that by virtue of their optimized material chemistries (from metal oxides to polymers) and geometrical features (from thin films to quantum dots) enable their adoption in biomedical applications. We further present an overview of necessary sensing standards and protocols. Standards ensure the establishment of consistent protocols, facilitating collective understanding of results and building on the current state. Furthermore, they enable objective benchmarking of various pH-sensing reports, materials, and systems, which is critical for the overall progression and development of the field. Additionally, we list critical issues in recent literary reporting and suggest various methods for objective benchmarking. pH regulation in the human body and state-of-the-art pH sensors (from *ex vivo* to *in vivo*) are compared for suitability in biomedical applications. We conclude our review by (i) identifying challenges that need to be overcome in electrochemical pH sensing and (ii) providing an outlook on future research along with insights, in which the integration of various pH sensors with advanced electronics can provide a new platform for the development of novel technologies for disease diagnostics and prevention.



## CONTENTS

1. Introduction	5249	5.1. Inherent Properties of Components	5260
2. The Power of Hydrogen (pH)	5250	5.2. Input Resistance of Characterization Systems	5263
2.1. Definition, Importance, and Analytical Formulation	5250	5.3. Surface Cleaning	5263
2.2. Temperature Effect	5250	5.4. Surface Resetting (Intermittent Cleaning vs In Situ Discussion)	5263
3. Materials for Electrochemical pH Sensors	5251	5.5. Time Plots and Analysis	5265
3.1. Overview	5251	5.6. Critical Point ( $P_c$ ) for Response and Drift Determination	5267
3.2. Thin Films and Nanostructures	5251	6. pH Regulation in the Human Body	5269
3.2.1. Metal Oxides Thin Films	5251	6.1. Cells	5269
3.2.2. Polymers	5252	6.2. Kidneys and Lungs	5269
3.2.3. Nanorods	5255	6.3. Blood	5269
3.2.4. Nanotubes	5255	7. pH Sensing in Biomedical Applications	5270
3.3. Summary and Conclusions	5256	7.1. Ex Vivo	5270
4. pH-Sensing Configurations	5256	7.1.1. Urine Tests	5270
4.1. Ion Sensitive Field Effect Transistor (ISFET)	5256	7.1.2. Saliva Tests	5270
4.2. Extended Gate Field Effect Transistor (EGFET)	5256	7.1.3. Tooth Decay	5270
4.3. Interdigitated Electrodes (IDEs)	5258	7.2. In Vivo	5272
4.3.1. Hybrid IDEs	5258	7.2.1. Glioblastoma	5272
4.3.2. Capacitance IDEs	5258	7.2.2. Intracellular and Extracellular pH	5273
4.4. Resistance Variation	5259		
4.5. Summary and Conclusions	5260		
5. Sensing Standards and Protocols	5260		

Received: October 30, 2018

Published: March 22, 2019



7.2.3. Oral Hygiene	5273
7.2.4. Ischemia	5275
7.2.5. Sweat Analysis	5276
8. Status Quo	5277
8.1. Wearable pH-Sensing Systems	5277
8.2. Implantable pH Sensing Systems	5279
9. Challenges	5282
9.1. Stability of pH-Sensing Devices	5282
9.2. Repeatability of pH-Sensing Devices	5283
9.2.1. Mixed Versus Specific Reactions	5284
9.3. Reproducibility of pH-Sensing Devices	5285
9.4. Modeling of pH-Sensing Devices	5286
10. Future Outlook on pH Sensing in Biomedical Applications	5288
Author Information	5289
Corresponding Author	5289
ORCID	5289
Notes	5289
Biographies	5289
Acknowledgments	5290
References	5290

## 1. INTRODUCTION

In 1889, Herman Walther Nernst postulated that the ion concentration could be measured using electrode potential. This foundation, paired with Arrhenius's definition of an acid as a proton donor, paved the way for a term specifically designated to describe hydrogen ion ( $H^+$ )/hydronium ion ( $H_3O^+$ )/proton concentration. pH was first defined in 1909 by Soren Peder Lauritz Sorenson in conjunction with his novel acid colorimetric assay, which used a hydrogen electrode paired with a calomel reference electrode (RE).<sup>1</sup> The RE maintains a constant potential, while the hydrogen electrode builds up a potential proportional to  $H^+$  concentration in a solution. The potential difference measured across the two-electrode system changes with the pH of the solution. While Sorenson's assay failed to break into the field dominated by more inexpensive and less accurate pH paper sensors, his pH term has become an essential component of modern lexicons.<sup>1</sup> Originally defined as the negative logarithm base 10 of the  $H^+$  concentration, pH has since been modified to be the negative logarithm base 10 of  $H^+$  activity.<sup>2</sup> This amendment stems from interaction of ions within a solution, which can cause some ions to deviate from ideal behavior and effectively appear inactive. To account for this phenomenon, ion activity (also referred to as effective ion concentration) is used in the definition instead of concentration. Despite Sorenson's definition and attempts to popularize electrodes in pH measurement, the glass electrode and acidimeter were the true developments that issued a new era of pH measurements. The glass electrode, invented by Duncan McInnes and Malcolm Dole in the 1920s, was capable of specific ion detection by means of a doped glass membrane.<sup>3</sup> In addition, the acidimeter, developed by Arnold O. Beckham, enabled acid strength detection.<sup>3</sup> These advances enabled accurate pH measurements and opened new routes for engineering even better sensors. Along with the well-defined term for  $H^+$  activity and progress in its measurement, the role of pH in biological systems has become more evident.

The regulation of pH is essential to maintaining healthy equilibrium in biological environments to support life. Disturbances and variations in pH can be either the cause or effect of disease and dysfunction within a biological system.

Therefore, the sensing of this essential parameter is of prime interest in current biomedical research. However, biological systems are extremely complex and constitute a myriad of chemicals and interactions. It is the act of balancing these interactions between chemicals that sustains life. This balance is achieved through equilibrium states that mandate the rates of reactions and proper activity of various fluids, and consequently the proper pH value when  $H^+$  is concerned. To this end, pH inevitably plays a role in balancing and altering these equilibria. At a macromolecular scale, nucleic acids and proteins contain proton dissociable groups, which interact with the pH of the direct environment. Specifically, enzymes—essential to catalysis—function within a specific pH range and can begin to denature at the extremes of this range. At the cellular level, the cell environment is buffered to maintain a consistent equilibrium within the cell; for example, the cytoplasm regulates under a phosphate buffer system.<sup>4</sup> Entire systems are also affected by pH, such as the circulatory system with blood regulated by a bicarbonate buffer system.<sup>5</sup> The excellent buffering ability of biological systems not only helps maintain proper equilibrium and pH ranges, but can also reliably indicate anomalies and diseases when deviations occur. Tumor cell detection is one such example. Tumors induce reduced vasculature and thus oxygen, which increases the rate of anaerobic energy production and promotes a significantly more acidic environment than neighboring tissue.<sup>6</sup> This results from the  $H^+$  donating capacity of the byproducts of anaerobic energy production, such as lactic acid, which in turn increases local  $H^+$  activity. Lactic acid is an Arrhenius acid (i.e., dissociates in water/aqueous solutions to give  $H^+$ ), which consequently increases the acidity (i.e., activity of  $H^+$ ) and lowers the pH of body fluids. Therefore, tumor tissue can be differentiated, and its progression and growth can be monitored by monitoring the pH. Methods of monitoring pH within biological systems, however, can vary depending on the situational needs and restrictions. Given the importance and strict regulation of pH in biological systems, pH sensors research has attracted the interest of many researchers. Figure 1a depicts the trend in the number of Scopus database listed publications over the past decade with “pH sensor” in the title and biomedical applications mentioned in the manuscript text.

This review provides an overview of pH sensors based on their material systems, sensing configuration, operating principles, and their suitability for biomedical applications. The regulation of pH in the human body and representative biomedical pH sensors are also discussed. Finally, state-of-the-art pH sensors are compared for suitability in biomedical applications, and insights, challenges, and future outlook are provided. The review is organized as depicted in Figure 1b. Sections 1 and 2 introduce the topic and basic definitions; Sections 3 and 4 focus on materials for pH sensors and discuss pH-sensing configurations and techniques; Section 5 discusses standards and protocols for pH-sensing systems; Sections 6 and 7 present a debrief on pH regulation in the human body, followed by highlights of specific examples on pH sensing in biomedical applications; Sections 8 and 9 discuss the status quo of wearable and implantable pH sensors, and the common challenges facing pH-sensing systems; finally, Section 10 provides a future outlook on pH-sensing systems in biomedical applications.

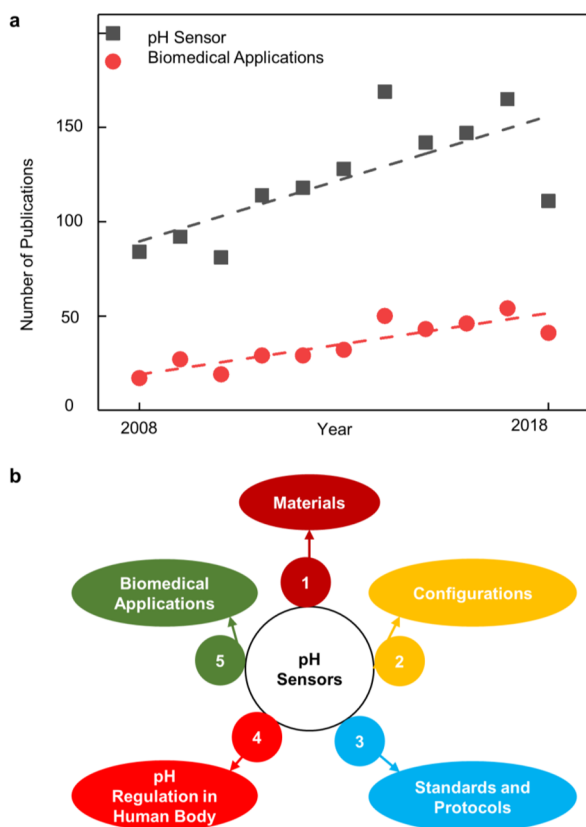


**Figure 1.** Trends in pH-sensing research and the organization. (a) Trend in the number of publications including “pH sensor” in the title (black squares) and “biomedical applications” in the abstract or text of the manuscript (red circles) between 2008 and 2018, collected from Scopus database. (b) The review content follows the depicted flowchart clockwise from (1) to (5).

## 2. THE POWER OF HYDROGEN (pH)

### 2.1. Definition, Importance, and Analytical Formulation

When pH was first defined by Sorenson in 1909, he based his calculations on electromotive force measurements which could be used in conjunction with the Gibbs energy equation (eq 1):

$$\Delta G = \Delta G^{\circ} + RT \ln Q \quad (1)$$

$\Delta G$  is the Gibbs energy change,  $\Delta G^{\circ}$  is Gibbs energy change under standard state, and  $R$ ,  $T$ , and  $Q$  are the gas constant, absolute temperature, and the reaction quotient, respectively.<sup>7</sup> Using the electromotive force, Sorenson defined pH as the negative logarithm base 10 of  $H^{+}$  concentration. With the advent of Lewis’s concept of ion activity, the Gibbs energy equation involved in Sorenson’s calculations was modified to substitute  $H^{+}$  activities for the previous  $H^{+}$  concentration values. In 1932, two main general definitions pervaded the scientific community: pH is equal to the negative logarithm base 10 of (i) concentration of  $H^{+}$  and (ii) activity of  $H^{+}$ . In 1948 both definitions fell to criticism.<sup>8</sup> Despite these issues, pH measurements were practiced under eq 2 (where pH is a function of the  $H^{+}$  activity):

$$pH(X) - pH(S) = (E_X - E_S) / \left( \frac{RT}{F \ln 10} \right) \quad (2)$$

where an unknown solution (X) with pH equal to  $pH(X)$  and an electromotive force (EMF) of  $E_X$  is measured against a reference solution (S) of known pH value of  $pH(S)$  and an EMF of  $E_S$ .  $F$  is

the Faraday constant. Hence, the difference between the solution under the test’s pH and the reference solution’s pH (i.e.,  $pH(X) - pH(S)$ ) can be linked to the measured EMF difference (i.e.,  $E_X - E_S$ ). pH as a function of  $H^{+}$  activity is now the most commonly accepted definition because of electrode dependence on ion activity. The Nernst equation links the  $H^{+}$  activity to pH.<sup>9</sup> Another reason  $H^{+}$  activity presents a better mode of measurement is the dependency of pH on temperature. This dependency is best explained by the activity of  $H^{+}$  varying in a directly proportional manner with temperature. Though the history of the definition of pH has seen many changes and modifications, today’s measurements are based on the latest definition. Developing new pH-sensing techniques and applications based on previous developments must be unhindered by any confusion surrounding the measurements.

### 2.2. Temperature Effect

The temperature dependency of pH measurements affects the consistency of results. Variations in temperature are known to cause changes in solution viscosity and ion mobility. Overall temperature can have two main effects on pH sensing: (i) reducing electrode accuracy and measurement speed and (ii) changing the results due to the coefficient of temperature variation of the material itself.<sup>10</sup> A number of sources can cause electrode variations, including effects on the electrode sensitivity, isothermal point calibration, thermal and chemical equilibrium, and membrane resistance.  $H^{+}$  activity, as defined by the Nernst equation, varies with a temperature-dependent Nernstian slope constant. This effect is typically compensated for by the initial sample temperature. The intersection point of the calibration lines of differing temperatures, also known as the isothermal point, is ideally represented by the zero potential point. However, as real electrodes possess different coefficients of temperature variation and all contribute to the total potential, the isothermal point often deviates from the ideal situation. Imbalances in thermal equilibrium can also result in pH measurement drifts over time and can be corrected for by using temperature insensitive electrode materials or a carefully maintained thermal environment.<sup>11</sup> Chemical equilibria at the electrode/electrolyte interface are also affected by thermal variation, given that temperature can affect the solubility of the metal salt, leading to slow response and drift.

The glass membrane resistance of pH-sensing electrodes increases with decreasing temperature, causing sluggish response, and at extremes, complete dysfunction. Taking into account these temperature effects will thus lead to greater accuracy of pH measurements and more repeatable results, and extend their applications in biomedical fields.

Particularly for biomedical applications of pH sensors, temperature can greatly affect results. As demonstrated by the experiments performed by Rosenthal et al., blood pH varies linearly with temperature.<sup>12</sup> The reported dependence coefficients were  $-0.0147 \text{ pH}/^{\circ}\text{C}$  and  $-0.0118 \text{ pH}/^{\circ}\text{C}$  for human blood and plasma, respectively. In addition to solution pH variation with temperature, pH sensors also demonstrate temperature dependence for biomedical application. Huang et al.’s review of pH-sensing iridium oxide film demonstrates how temperature can affect measurements and how this effect can be predicted in practical applications.<sup>13</sup> The investigation showed the intrinsic and predictable dependence of the Nernstian potential on temperature based on the Nernst equation by recording pH and temperature for four buffer solutions and temperatures. Figure 2 presents the actual measurements, with

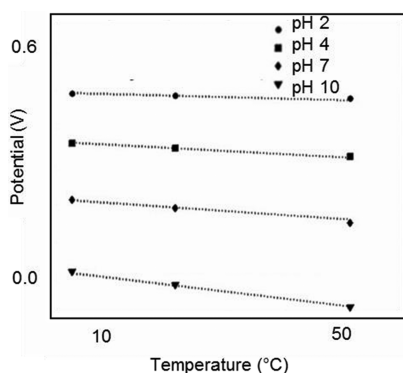


**Figure 2.** Theoretical temperature dependence of a representative IrOx pH sensor showing  $-0.3$ ,  $-0.8$ ,  $-1.3$ , and  $-2$  mV/°C at pH = 2, 4, 7, and 10, respectively.<sup>13</sup> Reproduced with permission from ref 13. Copyright 2011 Elsevier.

varying dependence of pH on temperature ranging from  $-0.3$  to  $-2.0$  mV/°C for pH 2–10, respectively; the clear relationship between the two highlights the temperature effect on pH sensors and films.<sup>13</sup> To extend this example and apply it to pH sensing within an organism, potentially acidic tumor cell detection would necessarily account for the temperature dependence of the sensor to prevent confusing healthy cells with diseased ones. Indeed, these temperature effects in pH sensing necessitate temperature correction for accurate pH measurements. Due to the strong dependence of pH on temperature, recent studies aimed at measuring both temperature and pH at the same time.<sup>14,15</sup> For instance, Zhang et al. reported on nanosensors for simultaneous monitoring of lysosomal pH and temperature, indicating the need for the temperature measurement to calibrate the pH measurement.<sup>14</sup>

### 3. MATERIALS FOR ELECTROCHEMICAL pH SENSORS

#### 3.1. Overview

Measurements within biological systems often demand special considerations, such as preserving the life of the organism or a necessary microscopic scalability, and their effect on the methodology of sensing. These considerations determine the suitability of various pH-sensing materials and their target application. Using indicator dye that is sensitive to pH and covalently attached to reagent paper presents an inexpensive and quick way of testing biological fluid.<sup>16</sup> Electrochemical method-based pH sensors span from the glass electrode of the early 1900s to the modern extended gate field effect transistor (EGFET) and ion sensitive field effect transistor (ISFET) configurations. The glass electrode pH sensor compares the potential of known to unknown  $H^+$  using a RE and a sensing half-cell. Though an accurate and reliable method, the glass electrode suffers in its need for repeated calibration and fragile construction, making it difficult to miniaturize and use effectively in vivo.<sup>16</sup> EGFET pH sensors use the physical protonation and deprotonation reactions that cause a difference in the surface potentials at the interface between the electrolyte solution and the extended gate of a transistor. The resulting electric field modifies the conductance of the field effect transistor (FET), and the current flowing in the channel between the source and the drain terminals is used to measure pH.<sup>17</sup> The ISFET is another technique where the whole transistor is immersed in the solution and its gate dielectric is exposed, i.e., replacing the transistor gate with the electrolyte. As

$H^+$  ions accumulate on the ISFET's gate dielectric, the resulting electric field modulates the current in the channel. Although these measurements can drift over time and render ISFET devices progressively less sensitive, novel fabrication techniques allow a smaller size and glass-less structure.<sup>18</sup> Interdigitated electrodes take advantage of new micro- and nanofabrication techniques to maximize the surface area to volume ratio, therefore maximizing the sensitivity of the biosensor.<sup>19</sup> Additionally, the small size reduces material costs and power consumption. The configurations of pH-sensing systems are discussed in detail in Section 4. Nonetheless, it is the extensive materials library available with pH-sensing capabilities that made these configurations possible.

#### 3.2. Thin Films and Nanostructures

**3.2.1. Metal Oxides Thin Films.** pH sensors have also been developed with numerous thin film metal oxides, including ZnO, PtO<sub>2</sub>, PbO<sub>2</sub>, IrO<sub>2</sub>, Sb<sub>2</sub>O<sub>3</sub>, RuO<sub>2</sub>, TiO<sub>2</sub>, Ta<sub>2</sub>O<sub>5</sub>, WO<sub>3</sub>, RhO<sub>2</sub>, OsO<sub>2</sub>, PdO, CuO, and SnO<sub>2</sub>.<sup>20–27</sup> These materials interface with the electrolyte results in the accumulation of  $H^+$  and hydroxide ions ( $OH^-$ )<sup>20</sup> and find applications in the electrochemical measurement of pH because of the charged nature of these ions. In such configurations, a support material is typically coated with the metal oxide to create a durable electrode.<sup>20</sup> For example, a sensor developed with Ta<sub>2</sub>O<sub>5</sub> has demonstrated Nernstian pH sensitivity ( $\sim -56.19$  mV/pH) in the pH range from 1 to 10, without suffering errors caused by acid corrosion.<sup>28</sup> Moreover, atomic force microscopy (AFM) has shown that Ta<sub>2</sub>O<sub>5</sub> has a smooth and uniform surface, without cracks or crystal grains after annealing, which is essential to a capacitance-based sensor, with an impedance characteristic that varies little in different pH solutions.<sup>28</sup> However, out of all the possible pH-sensing metal oxides mentioned, IrO<sub>2</sub>, ZnO, and doped ZnO thin films have manifested the most desirable qualities, such as high sensitivity and biocompatibility, and, consequently, most reported metal-based pH sensors utilize these materials.

IrO<sub>2</sub> pH sensors can be created with high sensitivity and even super-Nernstian response, a sensitivity higher than  $-59$  mV/pH at room temperature.<sup>22</sup> In addition, IrO<sub>2</sub> sensors achieve stability over a large range of pH values, temperatures, pressures, and media, as well as minimal potential drift, excellent chemical selectivity, durability, no requirement for pretreatment, and are biocompatible.<sup>13,20,23,29</sup> Furthermore, electroplated iridium is cost-effective, precise, and produces reproducible results.<sup>30–34</sup>

Another oxide, ZnO, is a transparent semiconductor with a direct band gap ( $E_g = 3.37$  eV) and a large exciton binding energy (60 meV).<sup>21</sup> Additional attractive qualities for pH sensing include its biosafety and biocompatibility, importance as a nanomaterial for integration with microsystems and biotechnology, polar and nonpolar surfaces, and the ability to signal each time a  $H^+$  binds to its surface because of its conductivity.<sup>35,36</sup> Surface charge will develop when an electrolyte interacts with ZnO through physical adsorption of ions or charged species on the surface.<sup>36,37</sup> ZnO also has a distinct amphoteric nature due to a high density of binding sites for  $H^+$  and  $OH^-$ .<sup>37,38</sup> In the presence of high concentration of  $H^+$ , the diffusion of  $H^+$  leads to a higher surface potential, while a high concentration of  $OH^-$  causes ZnO to give up a proton to  $OH^-$  and create a lower surface potential.<sup>37</sup> Moreover, the diverse and abundant ZnO nanostructures, such as nanowires (NWs),<sup>39–41</sup> nanoflakes (NFs),<sup>42</sup> nanobelts,<sup>43,44</sup> nanobows,<sup>45</sup> and nanohelices,<sup>46</sup> open novel designs and applications for ZnO, which

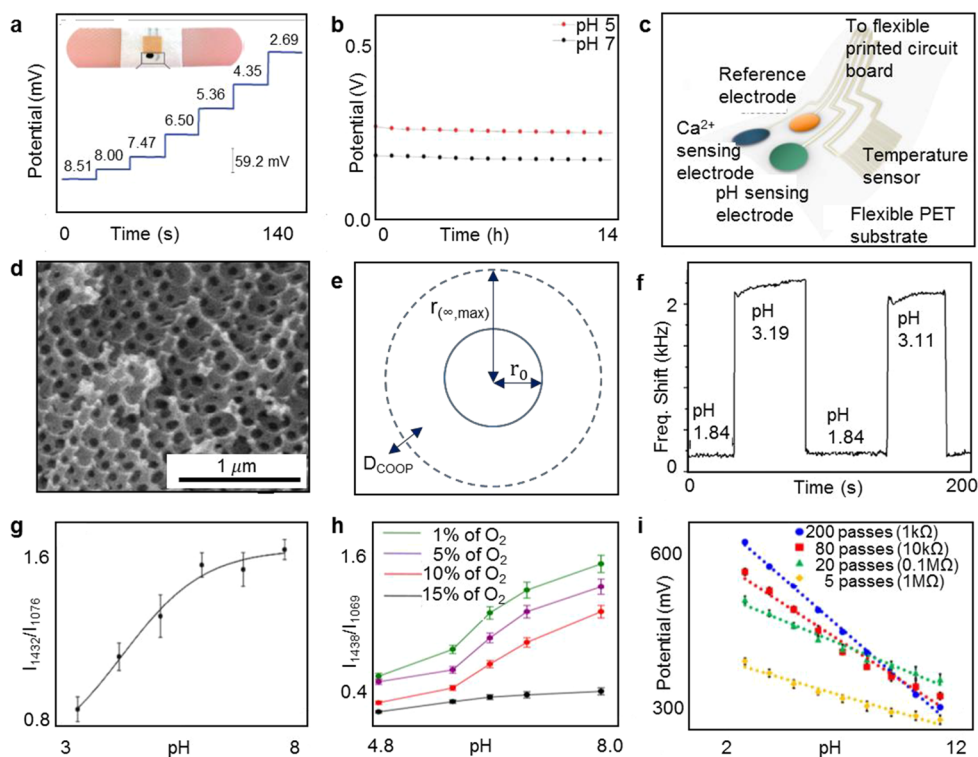


**Figure 3.** pH-sensing materials. (a) Potentiometric time-trace of a pH bandage sensor from pH 8.51 to 2.69, with sensitivity of  $-58.5$  mV/pH and response time less than 20 s. Inset shows a digital image of the printed potentiometric sensor on an adhesive bandage. Electropolymerization of polyaniline (PANI) onto the printed carbon was achieved to act as the working electrode, and the deposited polyvinyl butyral (PVB)-based membrane acts as the reference electrode (RE).<sup>59</sup> (b) Long-term stability of PANI sensors measured at pH 5 and 7 buffer solutions showing drift values of 0.64 mV/h and 0.49 mV/h, respectively.<sup>60</sup> (c) Schematic of a flexible sensor array containing  $\text{Ca}^{2+}$ , pH, and temperature sensors patterned on a flexible polyethylene terephthalate (PET) substrate. The inset shows a photograph of a flexible sensor array.<sup>68</sup> (d) SEM image of dried inverse hydrogel opal.<sup>73</sup> (e) Spherical hydrogel schematic, showing shrinking and swelling,  $r_0$  is the initial radius,  $r_\infty$  is the maximum radius at swelling equilibrium, and  $D_{\text{coop}}$  is the cooperative diffusion coefficient accounting for solvent diffusion and consequent polymer chains motion. (f) Response of poly(vinyl alcohol)-poly(acrylic acid) (PVA-PAA) hydrogel quartz crystal microbalance sensor at 3–10 pH values, with sensitivity of 13.2 kHz/pH and swelling and shrinking times of 500 and 800 ms, respectively.<sup>75</sup> (g) Normalized intensity of 1432 cm at 3–8 pH values. For each specific pH value, the surface enhanced Raman spectroscopy (SERS) measurements were performed 10 times, and the average results were adopted, with error bars representing the standard derivation.<sup>76</sup> (h) Plots of the intensity ratio  $I_{1438}/I_{1069}$  as a function of pH, in the 3–8 range, under 1%  $\text{O}_2$ , 5%  $\text{O}_2$ , 10%  $\text{O}_2$ , and 15%  $\text{O}_2$  conditions.<sup>77</sup> (i) Calibration curves of single-walled carbon nanotubes (SWCNTs) pH-sensing electrodes on glass in pH 3–11, showing sensitivity of  $-48.1$  mV/pH,  $-36.2$  mV/pH,  $-22.6$  mV/pH, and  $-16.4$  mV/pH for 200, 80, 20, and 5 passes, respectively.<sup>78</sup> Reproduced with permission from refs 59, 60, 68, 73, 75, 76, 77, and 78. Copyright 2014 John Wiley and Sons, Inc. Copyright 2017 Elsevier. Copyright 2016 American Chemical Society. Copyright 2010 Elsevier. Copyright 2004 Elsevier. Copyright 2011 American Chemical Society. Copyright 2016 American Chemical Society. Copyright 2016 Elsevier.

can easily be altered by slightly modifying the conditions for preparation.<sup>38,47–52</sup>

ZnO is often n-type in its natural state,<sup>53</sup> but doping can be utilized to adjust ZnO conductivity for different purposes.<sup>54</sup> Iron, for example, has shown multiple potential benefits as a dopant material through its use in controlling the electrical conductivity, energy band structure, and carrier concentration of ZnO. Furthermore, iron doping of ZnO results in the reduction of ZnO nanostructure dissolution rates.<sup>55,56</sup> Aluminum is another common dopant for ZnO and results in increased pH sensitivity.<sup>57,58</sup> One of the main problems with doping is that the dopant may disrupt material morphology, but arrays of well-aligned In doped ZnO nanorods (In:ZnO) have been reported.<sup>53</sup>

**3.2.2. Polymers.** Besides inorganic pH-sensing oxides, the ion-exchanging ability seen in conductive polymers serves well for potentiometric sensors and has earned them considerable attention when developing pH sensors.<sup>16</sup> Yet, the type of polymer chosen depends on the application along with sensitivity and selectivity requirements.<sup>16</sup>

A popular polymer used is polyaniline (PANI) because of its high conductivity, ease of synthesis, and stability.<sup>16</sup> Andrade et al. developed a potentiometric sensor embedded into an adhesive bandage using PANI as the working electrode and polyvinyl butyral polymer (PVB) as the reference electrode (Figure 3a, inset).<sup>59</sup> The working electrode is where the reaction of interest takes place, resulting in a reduction potential that is pH dependent, and the reference electrode is an electrode of known stability and known potential in the pH range of interest. A potentiometric sensor uses the relation between test solution's pH and the difference in reduction potentials between the working and reference electrodes. The results showed a Nernstian response of  $-58$  mV/pH between pH 4.35 and 8 with a response time of less than 20 s (Figure 3a). After 1000 bending cycles, the bandage still performed well at  $-58.5$  mV/pH. Another flexible and thin pH sensor based on a PANI array was developed by Yoon et al., and its performance closely matched a commercial pH meter.<sup>60</sup> Within a pH range of 2.38–11.61, it demonstrated a linear Nernstian response of  $-60.3$  mV/pH with a response time of less than one second. At a pH of

S, it showed a potential drift of 0.64 mV/h and 0.49 mV/h at pH 7 from 5 to 12 h (Figure 3b).<sup>60</sup> Flexible pH sensors are, especially, appealing for their integration ability with logic, memory, and other sensing devices from the growing field of flexible electronics<sup>61–67</sup> for fully flexible wearable systems (Section 8.1). PANI has also been used in the development of a wearable electrochemical device with the purpose of continuous monitoring of Ca<sup>2+</sup> and pH in body fluids, as illustrated in Figure 3c.<sup>68</sup> This device had an average slope of –62.5 mV/pH when tested at pH 4–7 and a potential drift of 0.7 mV/h over 1 h, resulting in a 1.1% error in pH value.<sup>68</sup> The biocompatibility of PANI was studied, and the results showed that PANI does not induce skin irritation or provoke any sensitization.<sup>69</sup>

Further studies have been performed on the combination of multiple polymers. For instance, PANI has proved useful in enhancing the performance of other materials, such as graphene (Gr).<sup>70</sup> An amperometric sensor using the fabricated Gr-PANI composite demonstrated a shorter response time with an improved sensitivity at –50.14  $\mu\text{A}/(\text{pH}\cdot\text{cm}^2)$  between pH 1–5 and 139.2  $\mu\text{A}/(\text{pH}\cdot\text{cm}^2)$  between pH 7–11.70 A pH-sensing membrane was developed by incorporating the ionic *n*-cetylpyridinium hexafluorophosphate (CPFP) and poly(vinyl chloride) with quinhydrone (QH).<sup>71</sup> In the pH range of 2–9.5, the sensor showed a sensitivity of –57.5 mV/pH and a response time of less than 10 s.<sup>71</sup> After a month, the sensor lost only 5% of its sensitivity.<sup>71</sup> Another potentiometric pH sensor was developed by coating a platinum electrode with 0.5  $\mu\text{m}$  thick mix of 120 mg of LiClO<sub>4</sub> and 10  $\mu\text{L}$  of pyrrole dissolved in 5 mL of acetonitrile.<sup>16</sup> In the pH range 2–11, the electrode exhibited a response time of less than one second and a drift of 0.25 mV/day.

Conductive polymers offer a good option for pH-sensing materials, due to their ion-exchanging properties. Many polymers have been studied; the most popular being PANI. Table 1 summarizes key developments in polymeric pH sensors. Evidently, the table shows excellent sensitivity (–57.5 to –62.5 mV/pH) and stability (0.25–0.7 mV/h drift) for polymeric materials as pH sensors, with PANI in open circuit potential (OCP) as the most common system.

**3.2.2.1. Hydrogels.** There are many types of polymers, and stimuli-responsive hydrogels are a special class of them. In response to stimuli, they can characteristically alter their volume, absorbing, and releasing amounts of aqueous solution.<sup>79</sup> As polymers with cross-linked molecule chains, they are very useful for detecting changes in temperatures, light, and even pH. Figure 3d shows a scanning electron microscopy (SEM) image of a dried inverse hydrogel opal.

A key characteristic of hydrogels is their swelling and shrinking properties. On the basis of the Tanaka-Fillmore theory, when uninfluenced by the surrounding, the behavior of swelling for a spherical hydrogel (as represented in Figure 3e) can be found through eq 3,

$$r(t) = r_0 + (r_{\infty(\text{max})} - r_0)(1 - e^{-t/\tau}) \quad (3)$$

and shrinking may be found through the eq 4,

$$r(t) = r_0 + (r_{\infty(\text{max})} - r_0)e^{-t/\tau} \quad (4)$$

where the swelling characteristic time constant,  $\tau$ , is found through eq 5,

Table 1. Summary of the Key Developments in Polymeric pH Sensors

ref	setup	sensing material	reference material	biocompatibility	sensitivity	response time	stability	pH range
Korostynska et al. <sup>16</sup>	open circuit potential (OCP)	120 mg of lithium perchlorate (LiClO <sub>4</sub> ) and 10 $\mu\text{L}$ of pyrrole (PPy) dissolved in 5 mL of acetonitrile	Ag	yes	followed a Nernstian response (~ –60 mV/pH)	<1 s	drift of 0.25 mV/day	2–11
Yoon et al. <sup>72</sup>	OCP	polyaniline (PANI) nanopillar array	Ag/AgCl	yes	linear Nernstian response of –60.3 mV/pH	<1 s	drift of 0.64 mV/h at pH 5, 0.49 mV/h at pH 7 (from 5 to 12 h)	2.38–11.61
Guinovart et al. <sup>59</sup>	OCP	electropolymerized PANI	poly(vinyl butyral (PVB) polymer		Nernstian response of –58 mV/pH and post 100 bending cycles: –58.5 mV/ph	<20 s	yields a stable signal in less than 20 s	4.35–8
Sha et al. <sup>70</sup>	amperometric	graphene-PANI (Gr-PANI)	Ag/AgCl		–50.14 $\mu\text{A}/(\text{pH}\cdot\text{cm}^2)$ in pH 1–5, and 139.2 $\mu\text{A}/(\text{pH}\cdot\text{cm}^2)$ in pH 7–11			1–11
Ping et al. <sup>71</sup>	OCP	poly(vinyl chloride) (PVC) and <i>n</i> -cetylpyridinium hexafluorophosphate (CPFP) incorporated with quinhydrone (QH)	Ag/AgCl		–57.5 mV/pH	<10 s	relative standard deviation of responses less than 4% after 5 h, and lost 5% of its sensitivity after a month	2–9.5
Nyein et al. <sup>68</sup>	OCP	PANI	PVB coated Ag/AgCl	yes	average slope of –62.5 mV/pH		drift of 0.7 mV/h, 1.1% error in pH value in 1 h	4–7

$$\tau = \frac{r^2}{D_{\text{coop}}} \quad (5)$$

and  $r$  is the final radius,  $r_{\text{coo,max}}$  is the maximal radius in the swelling equilibrium,  $r_0$  is the initial radius,  $t$  is the time, and  $D_{\text{coop}}$  is the cooperative diffusion characteristic.<sup>74</sup> However, a more complex model must be used when considering the surrounding environment.

Swelling kinetics and properties greatly influence the response time of a hydrogel pH sensor. For instance, Richter et al. showed that swelling for a quartz crystal microbalance sensor, coated with poly(vinyl alcohol)-poly(acrylic acid) (PVA-PAA) hydrogel, had a short response time of 500 ms due to its high ionic strength, a shrinking time of 800 ms, and sensitivity of 13.2 kHz/pH, in the 3–10 pH range.<sup>75</sup> Figure 3f shows the response time from the experiment.

In order to apply the hydrogel properties in pH sensors, sensor transducers (either optical, oscillating, or conductometric) are used to provide electrical signals from the hydrogel's swelling properties.<sup>74</sup> Although significant progress has been made in optical pH sensors over the past few decades,<sup>80–89</sup> this review is dedicated to electrochemical pH sensors—due to the extensiveness and importance of the topic. One example of a conductometric transducer is found in Sheppard et al.'s hydrogel-coated interdigitated electrode array, where resistance was shown to decrease with an increase in conductivity as the hydrogel swelled.<sup>90</sup> Hydrogels are advantageously shown to be extremely sensitive (up to 10<sup>-5</sup> pH units), inexpensive, efficient, and have diverse functions that are useful for a variety of applications.<sup>91</sup> However, the disadvantage of hydrogels is that they have a small working range<sup>74</sup> and require complex setups. Richter et al. found that initial readings from hydrogels may be inaccurate.<sup>92</sup> Despite the disadvantages, hydrogels are still a promising material for pH sensing, as they have unique properties that allow the sensors to be ultrasensitive and utilized in many circumstances. Table 2 provides a summary of hydrogel pH sensors with important reported parameters such as sensitivity, response time, and stability. The table shows the excellent ability of hydrogels' swelling and shrinking in the 500–800 ms range, respectively. However, swelling of 120 s and shrinking of 130 s have also been reported, for a different type of hydrogels, highlighting the strong dependence of the response on the hydrogel's composition. In addition, the versatility of hydrogels enables its usage with many configurations, including potentiometric, interdigitated electrodes (Section 4.3), and resistance variation (Section 4.4). Consequently, the sensitivity of hydrogel sensors can be quantified as a frequency/wavelength shift (kHz/pH or nm/pH), voltage difference (mV/pH), and change in resistance ( $\Omega$ /pH), adding to the versatility of the material.

For reference, the uncommon setups, such as quartz crystal microbalance, magnetoelastic, Raman spectroscopy, and White emission, mentioned in Table 2, are briefly explained in this paragraph. The other common setups, such as interdigitated electrodes, and resistance-based sensors are explained in Section 4. The process for quartz crystal microbalance uses microgravimetric transducer principles to measure changes in frequency as pH changes.<sup>75</sup> Another sensing technique is through magnetoelastic sensing, which measures pH sensitivity through changes in resonance frequency. In this technique, a pickup coil detects a magnetic flux caused by mechanical deformations of the sensor, which occur as a result of magnetic field impulses.<sup>79</sup> For surface enhanced Raman spectroscopy

Table 2. Summary of the Key Variables of Hydrogel pH Sensors

ref	setup	sensing material	sensitivity	response time	stability	pH range
Zhao et al. <sup>93</sup>	fiber optics	acrylamide, N,N'-methylene diacrylamide, N,N,N,N'-tetramethylethylenediamine and methacrylic acid hydrogel	13 nm/pH	rise time: 24 s and fall time: 20 s	3 sensors after 10 days display sensitivities of 4.282, 4.279, and 4.280 nm/pH in the lower pH region	1–12
You et al. <sup>94</sup>	surface enhanced Raman spectroscopy (SERS)	alginate solution, poly(diallyldimethylammonium chloride), poly(sodium 4-styrenesulfonate), and D-(+)-glucono-1,5-lactone	0.07/pH			4.43–8.07
Mishra et al. <sup>95</sup>	fiber optics	acrylamide, bis(acrylamide) solutions, and methacrylic acid hydrogel	~0.66 nm/pH	<2 s		2–12
Shaibani et al. <sup>96</sup>	potentiometric	poly(vinyl alcohol)/poly(acrylic acid) (PVA/PAA) hydrogel nanofibers	74 mV/pH		deviation of $\pm 0.07$ units pH over 50 min	
Benson et al. <sup>91</sup>	white emission	bovine serum albumin, coumarin 460, fluorescein, and 5(6)-carboxy-x-rhodamine hydrogel	slope of 0.16/pH unit			1–11

Table 3. Summary of the Representative Works on Nanorod Based pH Sensors

ref	sensing material	reference material	setup	biocompatibility	sensitivity	pH range
Al-Hilli et al. <sup>101</sup>	ZnO nanorod	Ag/AgCl	open circuit potential (OCP)	yes	−59 mV/pH at room temp	1–14
Chen et al. <sup>98</sup>	iridium nitride nanorod	Ag/AgCl	extended gate field effect transistor (EGFET)		current: 26 $\mu$ A/pH voltage: −22.66 mV/pH	4–10
Ma et al. <sup>77</sup>	4-nitrothiophenol on gold nanorods		surface enhance Raman spectroscopy (SERS)	yes		3–8
Lee et al. <sup>99</sup>	ZnO-based nanorod/gate-recessed AlGaIn/GaN	Ag/AgCl	ion sensitive field effect transistor (ISFET)	yes	−57.66 mV/pH	4–12
Zong et al. <sup>76</sup>	gold nanorods	<i>p</i> -amino-thiophenol	Raman scattering	yes		3–8

(SERS), the surface plasmon resonance (SPR), where incident light causes conduction electrons at the interface to oscillate resonantly, near particular metal surfaces creates an enhanced electromagnetic field. This in turn increases the Raman scattering intensity significantly.<sup>94</sup> Noteworthy, assessing Raman shifts via a single point can be misleading, due to nonuniformities and irregularities. Instead, a Raman map of a reasonable area would be more objective for Raman peaks and shifts observations.<sup>97</sup> The pH-sensitive Raman molecule (MBA) is affected when a decreasing peak intensity ratio is created from a decreasing pH.<sup>94</sup> The last method is white emission. With changes in pH, white-emitting hydrogels can change from white to a nonwhite color and allow for the detection of pH changes from the intensity ratios of principal color components.<sup>91</sup> Because hydrogels can be used in a variety of setups, they have gained considerable attention like metal oxides and other nanostructures.

**3.2.3. Nanorods.** Compared to metal oxides and polymers, nanorods have gained more attention for pH sensing due to their higher surface-to-volume ratio, a characteristic imperative for improving the sensitivity of pH sensing.<sup>98</sup> The nanorods can have a significant effect on sensing performance when applied to different testing setups. Different sensing materials have been studied; the most popular being ZnO due to its chemical stability, nontoxicity, electrochemical activity, fast response, and low costs.<sup>99,100</sup> Other nanorod materials investigated were gold, iridium nitrate, and tungsten oxide.

Al-Hilli et al. explored the electrochemical potential response of ZnO nanorods between a pH of 1 and 14. The results showed a sensitivity of −59 mV/pH at room temperature, performing better than a ZnO EGFET.<sup>101</sup> A similar study explored the sensing characteristics of the ZnO-based nanorod using gate-recessed AlGaIn/GaN ISFETs.<sup>99</sup> The developed biosensor exhibited a sensitivity of −57.66 mV/pH in a pH range of 4–12.99 The performance was attributed to the larger sensing area from combining ZnO nanorods and AlGaIn/GaN.<sup>99</sup>

Another popular nanorod material studied is gold (Au) nanorods. One study demonstrated hydrochloric acid (HCl) treated gold nanorods (GNRs) as an intracellular pH (pHi) sensor based on the SERS method.<sup>76</sup> The results, in the 3–8 pH range, are shown in Figure 3g.<sup>76</sup> The study found that by reducing the cytotoxicity of GNRs with HCl treatment bioapplications become possible.<sup>76</sup> Experimentation has also been done on GNRs coated with 4-nitrothiophenol as a SERS nanoprobe.

The purpose of this experiment was to report a new nanoprobe for pH sensing under different levels of hypoxia by SERS.<sup>77</sup> Hypoxia is a condition of low oxygen levels that can detrimentally affect cells and tissues.<sup>102</sup> The nanoprobe proved to be effective in measuring between 4.5 and 7.5 pH values at

different O<sub>2</sub> concentrations (Figure 3h).<sup>77</sup> The performance of an EGFET pH sensor fabricated with 1-D iridium nitrate nanorods was also investigated. However, over a pH range of 4–10, the sensor exhibited a sensitivity level of only −22.66 mV/pH, a value much lower than the theoretical limit.<sup>98</sup> Table 3 summarizes key works on nanorod-based pH sensors. The table shows that even functionalized nanorods have relatively limited pH range, compared to polymeric thin films (Section 3.2.2) in general and hydrogels (Section 3.2.2.1) specifically, except for ZnO nanorods that showed a sensitivity of −59 mV/pH in the 1–14 pH range.

**3.2.4. Nanotubes.** Besides nanorods, researchers have taken a step further to increase pH-sensing capabilities by using nanotubes.<sup>78,103–107</sup> Nanotubes have a hollow center allowing solutions to come into contact with almost twice the amount of surface area it would on a nanorod. As a result, they are much more sensitive to their surrounding environment.<sup>103</sup> Nanotubes also display high mechanical stability, mass production capability, ease of chemical functionalization, and adjustable electrical properties, making them a better candidate for pH-sensing material.<sup>78</sup> Carbon nanotubes, specifically, have been extensively studied for pH sensing.

Li et al. proposed a microfluidic pH-sensing chip that was developed based on single-walled carbon nanotube thin films (CNTFs).<sup>104</sup> The developed chip performed at a sensitivity of −59.71 mV/pH with a standard deviation of 1.5 mV/pH in a pH range of 3–11.<sup>104</sup> The results of the experiments show the chip is suitable for practical uses and allow the detection of metabolic processes in cells.<sup>104</sup> Qin et al. developed an inkjet printing process to deposit single-wall carbon nanotubes for pH sensing.<sup>78</sup> Their results found that thicker films can be effective sensing materials in potentiometric electrodes.<sup>78</sup> With 5 passes (<20 nm thick film), the sensitivity of the device was only −16.4 mV/pH compared to −48.1 mV/pH for one developed with 200 passes (~700 nm thick film).<sup>78</sup> (Figure 3i).

Moreover, testing has been done on the modification of single-walled carbon nanotubes. Tsai et al. proposed oxygen-plasma-functionalized CNTFs on polyimide substrates as the sensing material for an EGFET sensor.<sup>107</sup> The study demonstrated a sensitivity of −55.7 mV/pH in a pH range of 1–13 for plasma treated CNTF compared to an as-sprayed sensitivity of only −37.6 mV/pH.<sup>107</sup> Gou et al. developed a sensor based on oxidized single-walled carbon nanotubes functionalized with the conductive polymer poly(1-aminoanthracene).<sup>105</sup> Using a chemiresistor, they were able to produce a sensitive pH response that approached the Nernst limit, without the need for a RE.<sup>105</sup>

The development of multiwalled carbon nanotubes is further studied by several researchers. For instance, Jung et al. investigated the pH-sensing characteristics of a multiwalled

Table 4. Summary of the Representative Works on Nanotube-Based pH Sensors

ref	sensing material	reference material	setup	pH range	biocompatibility	response time (s)	sensitivity
Li et al. <sup>104</sup>	single-walled carbon nanotubes (SWCNTs)	Ag/AgCl	open circuit potential (OCP)	3–11	yes	~30	–59.71 mV/pH standard deviation is 1.5 mV/pH
Gou et al. <sup>105</sup>	SWCNTs functionalized with poly (acrylic acid) (PAA)	Ag/AgCl	field effect transistor (FET)	2–12	yes	3–7	
Tsai et al. <sup>107</sup>	oxygen-plasma- treated carbon nanotube thin films (CNTFs)	Ag/AgCl	extended gate field effect transistor (EGFET)	1–13	yes		as-sprayed CNTF: –37.6 mV/pH plasma treated CNTF: –55.7 mV/pH
Qin et al. <sup>78</sup>	Inkjet-printed SWCNTs	Ag/AgCl	OCP	3–11		7	200 passes: –48.1 mV/pH 80 passes: –36.2 mV/pH 20 passes: –22.6 mV/pH 5 passes: –16.4 mV/pH
Jung et al. <sup>106</sup>	multiwalled carbon nanotubes sheet decorated with nickel (MWCNT/Ni)		resistance-based	2–10			

carbon nanotube sheet decorated with nickel.<sup>106</sup> They reported the pH-sensing properties to be highly dependent on the size of the nickel particles.<sup>106</sup> Table 4 summarizes key nanotube developments for pH sensing.

Carbon nanotubes have proven to be a superior material in terms of pH sensing due to their attractive characteristics, including their high surface-to-volume ratio, high mechanical stability, mass production capability, ease of chemical functionalization, and adjustable electrical properties.<sup>78</sup> Additionally, nanotubes can be applied in open circuit potential setups, EGFET testing, electrical resistance test, and chemiresistance testing, making them a versatile sensing material. Their sensitivity has also shown to be improved by both oxidation during the fabrication process, and the incorporation of polymers or nickel particles in the development.<sup>105,106</sup> These developments indicate the possibility of further enhancing the sensing capabilities of nanotubes.

### 3.3. Summary and Conclusions

Thin films and nanostructures provide a precise pH measurement option as the sensing material. Thin film metal oxides have proven to be useful in potentiometric sensors with electrode–electrolyte interfaces. Of the studied metal oxides, IrO<sub>x</sub>, ZnO, and doped ZnO films have displayed the most attractive characteristics for pH sensing due to their high sensitivity, facile fabrication methods, and biocompatibility. Conductive polymers have also served well for potentiometric sensors due to their ion-exchanging properties. The most commonly studied polymer is PANI because of its high conductivity, ease of synthesis, and stability. PANI has also shown to be effective in enhancing the performance of other materials, such as Gr. Nanorods have gained considerable attention due to their higher surface-to-volume ratio. The most popular nanorod material is ZnO considering its chemical stability, nontoxicity, electrochemical activity, fast response, and low cost. Gold nanorods have also been studied, but they require pretreatment, such as HCl, to increase their biocompatibility. However, nanotubes have proven to be a better alternative. The structure of nanotubes allows an extremely high surface-to-volume ratio, almost twice that of nanorods. Nanotubes also demonstrate high mechanical stability, mass production capability, ease of chemical functionalization, and adjustable electrical properties. An oxidation process or incorporating polymers or nickel particles in the development can further enhance the performance of nanotubes. Although various material choices are available, we ultimately select the sensing device material depending on the application and sensitivity requirements.

## 4. pH-SENSING CONFIGURATIONS

The sensing configurations for pH have a wide range from ISFET to resistance-based electrodes. All configurations have their unique advantages and are suited for in vitro and in vivo biomedical applications, given that the dimensions of insertable parts are scaled sufficiently. Although the traditional potentiometric configuration has been widely used in pH sensing for multiple decades, novel configurations have been recently introduced. This section discusses ISFET and EGFET configurations, which are closer in operation principles to traditional potentiometric configurations except for introducing a gating structure (transistor) to modulate current instead of voltage. We then discuss configurations involving interdigitated electrodes (IDEs) where two separate finger-shaped electrodes take on an interdigitated structure to utilize hybrid materials and variation in the capacitances. Furthermore, resistance-based configurations are discussed, where the resistance of the sensing material changes with pH. Finally, we conclude this section by summarizing the discussed configurations and providing remarks.

### 4.1. Ion Sensitive Field Effect Transistor (ISFET)

ISFETs emerged in the 1970s with a milieu of advantages over the glass electrode, including significant durability compared to the more fragile glass electrode, easy storage without many necessary conditions, less measurement bias at extreme pH, and lower temperature dependence, making these sensors ideal for biomedical applications.<sup>108</sup> ISFET devices typically require an RE. On the other hand, ISFETs respond quickly to pH changes, are highly sensitive, and are potentially miniaturizable. The ISFET sensor, consisting of source, gate, and drain terminals, monitors the current flow between the source and drain contacts as it responds to changes in the electric field between the gate and source terminals.<sup>18</sup> The gate material defines the sensitivity and selectivity of the ISFET. For biocompatible sensors, an enzyme membrane can be used to coat the ion-selective gates, or biomolecules may be immobilized on the surface of the gates. Although ISFETs have many advantages, issues arise due to impurities in the semiconductor channel material and instability of the sensing membrane.<sup>109</sup> Another source of variability in ISFET measurements originates from slow responding sites and a hydration effect resulting in a voltage drift.

### 4.2. Extended Gate Field Effect Transistor (EGFET)

In 1983, J. van der Spiegel introduced the EGFET as an alternative to the ISFET for pH sensing.<sup>110</sup> Later, Chi et al. modified Spiegel's EGFET model structure comprising of a RE and a metal oxide semiconductor field effect transistor

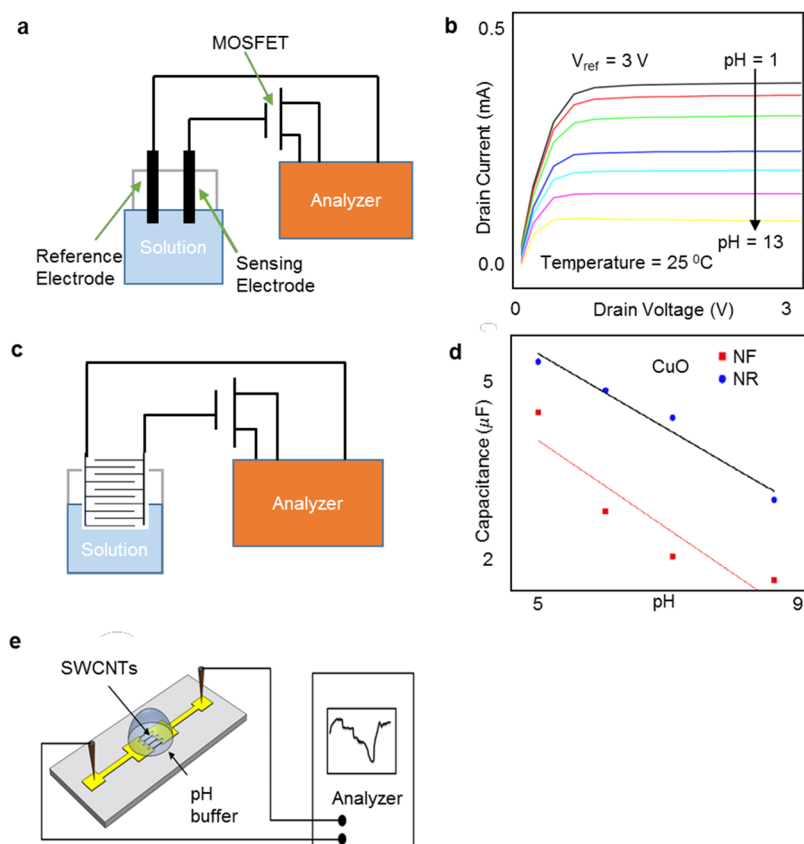


**Figure 4.** Various pH-sensing configurations. (a) Typical extended gate field effect transistor (EGFET) setup. MOSFET stands for metal oxide semiconductor field effect transistor. (b) Plot of the relationship between drain voltage and drain current at a constant reference voltage ( $V_{ref}$ ) of 3 V from ZnO/Si nanowires-based EGFET with a sensitivity of  $-46.25$  mV/pH in the 1–13 pH range.<sup>116</sup> (c) Typical interdigitated electrodes (IDEs) field effect transistor setup. (d) Linear relationship between pH and capacitance for CuO nanoflower (NF) and nanorods (NR) IDEs in the 5–8.5 pH range, with sensitivity of  $0.64$   $\mu$ F/pH for NR at 50 Hz.<sup>117</sup> (e) Schematic of resistance-based pH configuration with single-walled carbon nanotubes (SWCNTs), the sensors had a sensitivity of  $236.3$   $\Omega$ /pH in the 5–9 pH range and response times of 2.26 s at pH 5 to 23.82 s at pH 9.<sup>118</sup> Reproduced with permission from 116, 117, and 118. Copyright 2013 Elsevier. Copyright 2018 Elsevier. Copyright 2011 MDPI (Basel, Switzerland) under CC-BY-3.0 <https://creativecommons.org/licenses/by/3.0/>.

(MOSFET) connected to a sensing electrode.<sup>111</sup> The RE has a stable electric potential, while the sensing electrode has an electric potential that is sensitive to changes in pH. The MOSFET is composed of a gate, source, drain, and body. A voltage, generated by the RE and the interaction of sensing electrode with  $H^+$  in solution, is applied to the gate to create a conducting channel. The conducting channel allows current to flow from the drain to the source (in the case of n-type MOSFET configurations).<sup>112</sup> Figure 4a represents a typical EGFET setup, composed of the RE and the sensing electrode submerged in a solution. The RE is connected to a constant voltage source, while the sensing electrode is connected to a MOSFET configuration.

The site-binding model, in which the surface potential ( $\varphi$ ) at the sensing layer and electrolyte interface is determined by the number of binding sites on the sensing membrane, is used to derive the concentration of the  $H^+$  ions in the solution:<sup>113</sup>

$$2.303(\text{pH}_{\text{pzc}} - \text{pH}) = \frac{q\varphi}{kT} + \sinh^{-1}\left(\frac{q\varphi}{kT} \frac{1}{\beta}\right) \quad (6)$$

where  $\text{pH}_{\text{pzc}}$  is the pH value at the point of zero charge,  $k$  is the Boltzmann's constant,  $T$  is the absolute temperature of the system in Kelvin,  $q$  is charge of the electron, and  $\beta$  is the

sensitivity parameter. The surface sites per unit area,  $N_s$ , is related to  $\beta$ , by the equation:

$$\beta = \frac{2q^2 N_s \left(\frac{K_b}{K_a}\right)^{1/2}}{KTC_{DL}} \quad (7)$$

where  $C_{DL}$  is the electrical double layer's capacitance from the Gouy–Chapman–Stern model,<sup>113</sup>  $K_a$  is the acid equilibrium constant, and  $K_b$  is the base equilibrium constant.<sup>114</sup>

The gate voltage of the transistor is related to the current ( $I_{DS}$ ) between the drain and source by the MOSFET expression. The drain-source voltage ( $V_{DS}$ ) relates to the current linearly before the current saturates. The current saturates when the drain-source voltage reaches the gate-source voltage ( $V_{GS}$ ) minus a threshold voltage ( $V_T$ ), necessary for establishing a conductive channel between source and drain. The complete current equation is given by

$$I_{DS} = K_n \left[ (V_{GS} - V_T)V_{DS} - \frac{1}{2}V_{DS}^2 \right] \quad (8)$$

where  $K_n$  is a technology constant,<sup>114</sup> and for the saturation region, when  $V_{DS} = V_{GS} - V_T$ , the relationship is defined by

$$I_{DS} = \frac{1}{2}K_n[(V_{GS} - V_T)^2] \quad (9)$$

An important factor to consider in the EGFET is the material used in sensing electrode. The material must have a high sensitivity to the activity of  $H^+$  in the solution. An ideal sensing electrode would have a sensitivity of approximately  $-59.2$  mV/pH at room temperature. It is composed of an ion selective sensing membrane and conducting polymer, which converts charge carriers from ions to electrons. Several experiments have been conducted to find materials that are close to the ideal sensitivity for the sensing membrane. Common materials used include ZnO, SnO<sub>2</sub>, and IrO<sub>2</sub>.

Table 5 shows representative EGFET sensors and their key properties, such as the sensing electrode and RE materials, the

**Table 5. Summary of the Representative EGFET pH Sensors**

ref	sensing material	reference material	maximum sensitivity (mV/pH)	pH range
Chiu et al. <sup>113</sup>	passivated ZnO	Ag/AgCl	-49.35	4-12
Batista et al. <sup>114</sup>	ZnO calcinated at 150 °C	Ag/AgCl	-38	2-12
Yang et al. <sup>115</sup>	Al-doped ZnO	Ag/AgCl	-57.95	1-13
Li et al. <sup>116</sup>	ZnO/silicon nanowires (NWs)	Ag/AgCl	-46.25	1-13
Chi et al. <sup>111</sup>	SnO <sub>2</sub>	Ag/AgCl	-56-58	2-12

maximum sensitivity, and the pH range. Figure 4b shows representative results from experiments utilizing ZnO/Si NWs in EGFET configuration at reference voltage ( $V_{ref}$ ) of 3 V, 1-13 pH range, exhibiting  $-46.25$  mV/pH sensitivity.

Compared to other configurations, the EGFET structure has several advantages, such as being easy to fabricate at a low cost, having a disposable gate, and having long-term stability.<sup>113</sup> In addition, EGFET offers the advantage of isolating the electronics part (i.e., the transistor) from the chemical sensing part (i.e., the sensing electrode), in contrast to the ISFET where the transistor's gate is exposed to the solution under test. However, the EGFET structure still poses some limitations. Common materials, such as zinc oxide, used for the sensing membrane of the working electrode, may have low sensitivity to pH due to impurities in the material used for the sensing membrane.<sup>114</sup> Therefore, these materials must be modified through passivation<sup>113</sup> or doping,<sup>115</sup> which may be cost ineffective and time-consuming. In addition, the EGFET configuration also includes a RE, which may be expensive and bulky.

**Table 6. Summary of the Representative IDEs pH Sensors**

ref	setup	sensing material	variable measured	maximum sensitivity	pH range
Ali et al. <sup>121</sup>	interdigitated extended gate field effect transistor (IEGFET)	ZnO thin film	current	-22.4 mV/pH	4-11
Haarindraprasad et al. <sup>126</sup>	IEGFET	ZnO nanostructured thin film	current	3.72 $\mu$ A/pH	2-10
Lakard et al. <sup>122</sup>	interdigitated microarray potentiometric	polypyrrole thin film covered with a plastic polyvinyl chloride membrane	current	-58 to -60 mV/pH	2-11
Manjakkal et al. <sup>117</sup>	interdigitated impedance-metric	CuO nanorods	capacitance	0.64 $\mu$ F/pH at 50 Hz	5-8.5

### 4.3. Interdigitated Electrodes (IDEs)

**4.3.1. Hybrid IDEs.** IDEs are another popular configuration for pH sensing. They were popularized in the 1960s and have since been integrated into various biological sensing devices. IDEs are transducers that consist of two interdigitated electrode structures. IDEs have microgaps, which are gaps between the anode and cathode, allowing the electrode to exhibit sensitivity to changes in pH.<sup>120</sup> In addition to the microgaps, the IDEs also have metal-semiconductor interdigitated extended gates that include "finger" electrodes with a sensitive membrane.<sup>121</sup> Unlike the traditional EGFET, the IDEs configuration does not contain a separate reference electrode.<sup>121</sup> IDEs are usually fabricated by photolithography.<sup>120</sup> Figure 4c shows a typical interdigitated setup, i.e., the interdigitated extended gate field effect transistor (IEGFET).<sup>121</sup> IDEs structures can also be hybrid structures, which contain a mix of organic and inorganic materials, such as a mix of polymers and glass.<sup>122</sup>

In the IDEs configuration, there is a constant voltage connected to a reference interdigitated electrode. The sensing interdigitated electrode is sensitive to the activity of  $H^+$ , which generates a surface potential. The voltage applied to the gate of the MOSFET configuration is the superposition of the reference voltage and sensing electrode's surface potential, allowing current to flow.

IDEs are simple, easy to fabricate, stable, highly sensitive, and have a great potential to be miniaturized. Thus, IDEs offer many of the same benefits as the EGFET configuration, but have the added advantages of making experiments easier to carry out and inexpensive due to the lack of a separate bulky RE.<sup>121</sup> Because of the IDEs' unique features, the IDEs configuration presents itself as a promising alternative to the EGFET and ISFET. However, despite the advantages, IDEs also present some limitations. Like the EGFET configuration, the sensing material must be highly sensitive.<sup>117</sup> Even though some IDEs' materials, like CuO, are biocompatible, they may only have short-term stability and show a sub-Nernstian response.<sup>117</sup> Hence, novel materials must be investigated for longevity and maximum sensitivity.

**4.3.2. Capacitance IDEs.** Capacitance-based interdigitated sensors depend on the changes that occur to the capacitance between the two interdigitated electrodes. Changing the charge distribution, the surface area of the electrodes, the dielectric properties, or conductivity can affect the capacitance between the electrodes.<sup>123</sup> The surface area of the electrodes can be increased by adding interdigitated fingers.

The basis of capacitance ( $C$ ) can be found through the equation:

$$C = \epsilon_R \epsilon_0 \frac{A}{d} \quad (10)$$

Table 7. Summary of the Representative Resistance-Based pH Sensors

ref	sensing material	sensitivity	pH range	repeatability	size of micro-electrodes	size of gap ( $\mu\text{m}$ )	response time (s)
Yang et al. <sup>119</sup>	single-walled carbon nanotube (SWCNTs) on flexible parylene-C substrate		4–10	3 cycles	height: 1 $\mu\text{m}$	4	
Li et al. <sup>118</sup>	dielectrophoresis aligned SWCNTs	236.3 $\Omega/\text{pH}$	5–9	10–15 cycles for 5 devices	width: 6 $\mu\text{m}$	3	pH 5: 2.26 pH 6: 3.08 pH 7: 11.1 pH 8: 17.05 pH 9: 23.82
Copa et al. <sup>131</sup>	ZnO nanorods		4–10		thickness: 100 nm length: 0.25–0.75 mm		10
Chinnathambi et al. <sup>129</sup>	polyaniline functionalized electrochemically reduced graphene oxide (ERGO-PA)	1.71 $\Omega/\text{pH}$	4–9			100	
Nguyen et al. <sup>128</sup>	emeraldine salt polyaniline (ES- PANI) and poly(vinyl butyral) (PVB) blend film	0.28 $\text{M}\Omega/\text{pH}$	1–8	2 cycles	3850–3980 $\mu\text{m}$ (length) $\times$ 20–50 $\mu\text{m}$ (width)	20–120	

where  $\epsilon_0$  is the permittivity of free space,  $\epsilon_R$  is the relative permittivity of dielectric material (i.e., the solution of interest),  $A$  is the surface area of finger electrodes, and  $d$  is the distance between the finger electrodes.<sup>124</sup>

For simplified IDEs, where edge effects can be neglected, the capacitance can be found through the equation:

$$C = \eta \epsilon \frac{lt}{d} \quad (11)$$

where  $\eta$  is the number of interdigitated fingers,  $\epsilon$  is the permittivity ( $\epsilon_R \epsilon_0$ ) of the sensitive coating film,  $l$  is the length of the interdigitated electrodes,  $t$  is the thickness of the electrodes, and  $d$  is the distance between the electrodes.<sup>124</sup> A more complex model must be used to find the capacitance of IDEs larger than the nanoscale.

For valid measurements, the capacitance behavior of the sensing probe must exhibit stability and specificity. Measuring the changes in capacitance is useful because it can detect minute changes in biological systems, which is critical for detecting changes in pH.<sup>123</sup> Capacitance decreases with greater pH values, due to the increasing presence of  $\text{OH}^-$  ions. The  $\text{OH}^-$  ions increase the negative charge in the solution.<sup>125</sup> Figure 4d illustrates this trend in an experiment that investigates the sensitivity of CuO nanoflowers (NFs) and nanorods (NRs) using interdigitated electrodes.<sup>117</sup> The interdigitated NR CuO electrode showed 0.64  $\mu\text{F}/\text{pH}$  at 50 Hz in the 5–8.5 pH range. Table 6 summarizes key IDE sensors, indicating the ability to integrate various structures with the interdigitated configuration, such as the metal oxide nanorods (discussed in Section 3.2.3), metal oxide thin films (Section 3.2.1), and polymeric thin films (Section 3.2.2).

#### 4.4. Resistance Variation

Resistance-based pH sensors are also promising for detecting the activity of  $\text{H}^+$ . Resistance-based sensors have been traditionally used as gas and temperature sensors. However, they have also arisen as a promising alternative to the ISFET and EGFET for accurately measuring pH. Resistance-based sensors are composed of electrodes with a highly sensitive layer. These electrodes are connected, by external wiring, to a semiconductor device analyzer.<sup>118</sup> Figure 4e shows the experimental setup. Common materials used for the sensing layer include metal

oxides, such as zinc oxide and iridium oxide, and carbon materials, such as SWCNTs.<sup>127</sup> In addition, some of these sensors include interdigitated electrodes, as mentioned in the previous subsection, to increase their surface area. The semiconductor device analyzer measures the resistance of the solution.<sup>118</sup> The SWCNTs sensor reported in Figure 4e has a sensitivity of 236.3  $\Omega/\text{pH}$  in the 5–9 pH range with a response time that varies from 2.26 s at pH 5 to 23.82 s at pH 9. Unlike the ISFET and EGFET configuration, resistance-based pH sensors do not require an RE.<sup>105</sup>

It is important to note that resistance increases as pH increases due to the increase of  $\text{OH}^-$  ions in the solution.<sup>119</sup> The  $\text{H}^+$  and  $\text{OH}^-$  interact with the material in the sensing layer, which contributes to a change in resistance that the semiconductor device analyzer measures.<sup>128</sup> Yang et al. provided an example of a time vs resistance plot at 4–10 pH range, specifically using SWNTs on parylene as the sensing membrane material.<sup>119</sup> Linear trend between pH and resistance has also been observed for electrochemically functionalized polyaniline reduced graphene oxide as the sensing membrane material.<sup>129</sup>

To evaluate sensor performance and repeatability, the normalized resistance can be found through the equation:

$$\frac{\Delta R}{R_r} = \frac{R - R_{\min}}{R_{\max} - R_{\min}} \quad (12)$$

where  $\frac{\Delta R}{R_r}$  is the normalized sensor resistance,  $\Delta R$  is the sensor resistance relative to the lowest sensor resistance,  $R_r$  is the sensor resistance range of the pH-sensing test,  $R_{\max}$  is the maximum sensor resistance, and  $R_{\min}$  is the minimum sensor resistance.<sup>118</sup> This equation is used to evaluate resistive sensors' sensitivity, repeatability, and reproducibility from device to device, which is important if the devices are produced on a large scale.

Resistance-based pH sensors provide many advantages that make them ideal for pH sensing over other devices. The materials used, such as SWCNTs, are affordable.<sup>118</sup> These devices also display high sensitivity and long-term stability.<sup>105</sup> In one such experiment with carbon nanotubes, a device exhibited the same performance and calibration 120 days after the initial testing.<sup>105</sup> One of the main advantages is that this sensor does not require a bulky and expensive RE. Furthermore, the small

size of resistance-based pH sensors makes them ideal for miniaturization and optimal for in vivo applications.<sup>129</sup>

Nevertheless, there are still some challenges facing resistance-based pH sensors. Even though a similar fabrication process is followed, it is difficult to replicate the same behavior of sensing material on each electrode.<sup>118</sup> Similar to the disadvantage of the hybrid interdigitated electrode configuration and EGFET setups, the sensing material of the resistance-based sensors must also be carefully selected because not all biocompatible materials have a high sensitivity and long-term stability. Hence, the remaining challenges for resistance-based pH sensors are electrode-to-electrode variability, the poor selectivity to H<sup>+</sup>s (since other ions interacting with the surface can also affect the resistance), and limited material choices. These areas are subject to further research but can, generally, be mitigated through controlling processes variations, doping the material or functionalizing the surface with coatings that are selective to H<sup>+</sup> (usually at the expense of sensitivity), and studying the resistance change behavior of more materials that are biocompatible such as IrO<sub>x</sub> and doped ZnO.<sup>130</sup> Table 7 summarizes representative resistance-based pH sensors. It is worth mentioning that the sensitivity of resistance-based sensors varies significantly based on the choice of materials. For instance, Table 7 shows sensitivities of 1.71 Ω/pH, 236.3 Ω/pH, and 0.28 MΩ/pH for polyaniline functionalized electrochemically reduced graphene oxide (ERGO-PA), dielectrophoresis aligned SWCNTs, and emeraldine salt PANI (ES-PANI) and PVB blend film, respectively. Also, the representative works show the limited pH range of operation, compared to the EGFET (Section 4.2) and IDEs (Section 4.3) configurations.

#### 4.5. Summary and Conclusions

From the ISFET to resistance-based sensors, pH-sensing configurations have evolved to measure pH more accurately, affordably, and efficiently. The ISFET and EGFET configurations both measure the current between the drain and source and are highly sensitive, but use a bulky and expensive RE. Interdigitated electrodes configurations measure the current or capacitance and have interdigitated fingers that increase surface area. Resistance-based sensors measure the resistance of a solution affordably and quickly and have a great potential to be miniaturized with their lack of an RE. Ultimately, these devices offer promising solutions to measuring pH, but many steps need to be taken to improve their selectivity and assess their suitability for biomedical applications, such as surface treatment for selectivity against other common biological ions (i.e., Na<sup>+</sup>, K<sup>+</sup>, Ca<sup>2+</sup>), biocompatibility tests, and long-term stability assessment.

### 5. SENSING STANDARDS AND PROTOCOLS

Given the diverse materials (Section 3) and configurations (Section 4) available for pH sensing as well as the expanding trends in both, standards and protocols are essential. Without standards and common protocols, the impact of research and its usefulness would be limited, and it would not be possible to provide objective contexts where various materials and systems can be accurately benchmarked. Therefore, this section is dedicated to discussing issues pertaining to the inherent properties of the various pH-sensing components, such as REs, buffer solutions, and transistors (in the case EGFET configuration, Section 4.2), and the effect of measuring instrument input resistance ( $R_{in}$ ) on results. Furthermore, surface conditioning is discussed in terms of pre-tests' initial treatments, as well as intermittent cleaning between measure-

ments. We then discuss standardization issues and recommendations for complete and accurate pH-sensing systems' characterization, including the importance of time plots, their analysis, and identifying a convention for determining a critical point for sensitivity, response time, and drift objective assessment. Although this section is generally important for all pH-sensing applications, it has to be emphasized that for clinical biomedical applications, especially in vivo experiments, standards and protocols are indispensable.

#### 5.1. Inherent Properties of Components

Despite the many advantages that the pH-sensing configurations offer, there are some inherent properties of device components that may affect biological systems and pH measurements, either enhancing or diminishing the accuracy for these devices. Although these intrinsic properties are often ignored, they play an important role in determining the performance of devices.

For instance, the RE is a common component of pH-sensing configurations, yet its behavior is often unreported. Whether the RE is solution filled, usually with potassium chloride (KCl), or gel filled, usually with sodium chloride (NaCl), can have an effect on the stabilization time with a response time in the range of tens of seconds or tens of minutes, respectively.<sup>132</sup> Common problems that REs may exhibit are that some electrodes may (i) suffer from leakage of inner electrolytes, (ii) get contaminated,<sup>105</sup> and (iii) require frequent calibration, as some electrodes are less stable, especially ones that are micro-fabricated.<sup>132</sup>

In addition, the inherent properties and behaviors of sensing materials such as thickness, crystallinity, and composition must be considered. Specific sensing materials, such as zinc oxide and iridium oxide, must be nontoxic and biocompatible, especially for in vivo applications.<sup>116</sup> These materials, unfortunately, may also dissolve or react with the solution and become modified on their surfaces with depositions from the test solutions. These depositions may cause sections of the sensing membrane to become insensitive to variations in H<sup>+</sup> activity, due to the deposits blocking direct contact between the sensing material and the electrolyte.<sup>133</sup> Furthermore, it has been determined that increased surface area has improved sensitivity of devices. For example, Chiu et al. determined that EGFETs with ZnO nanorod arrays had a greater sensitivity of 44.01 mV/pH than EGFETs with ZnO thin films (−38.46 mV/pH) in the 4–12 pH range.<sup>113</sup> Moreover, Chen et al. showed that EGFETs with sensing membranes with larger contact areas had a greater sensitivity, using an EGFET device with a tin oxide/indium tin oxide (SnO<sub>2</sub>/ITO) sensing gate.<sup>134</sup> Chen et al. also showed simulation results of the variation in sensitivity with electrode contact area from ~−14 mV/pH at 0.1 mm<sup>2</sup> to −55 mV/pH for areas greater than 0.8 mm<sup>2</sup>. Interestingly, in this experiment, beyond a certain contact area ~0.8 mm<sup>2</sup>, sensitivity seems to saturate at the −55 mV/pH. It is worth mentioning that experimental observations do not back up the simulation results. In fact, higher sensitivity has been commonly attributed to a larger sensing area, even when the area is greater than 0.8 mm<sup>2</sup>.<sup>36,135,136</sup> Additionally, crystallinity and composition of metal oxides also affect sensitivity. Batista et al. concluded that ZnO calcinated at 150 °C is amorphous and its composition also has zinc monoacetate, which yields a sub-Nernstian sensitivity of −38 mV/pH in an EGFET configuration.<sup>114</sup>

Other components that need to be assessed include the characterization instrument, glass electrode, and commercial transistor. The transistor often has drift that may cause the graph

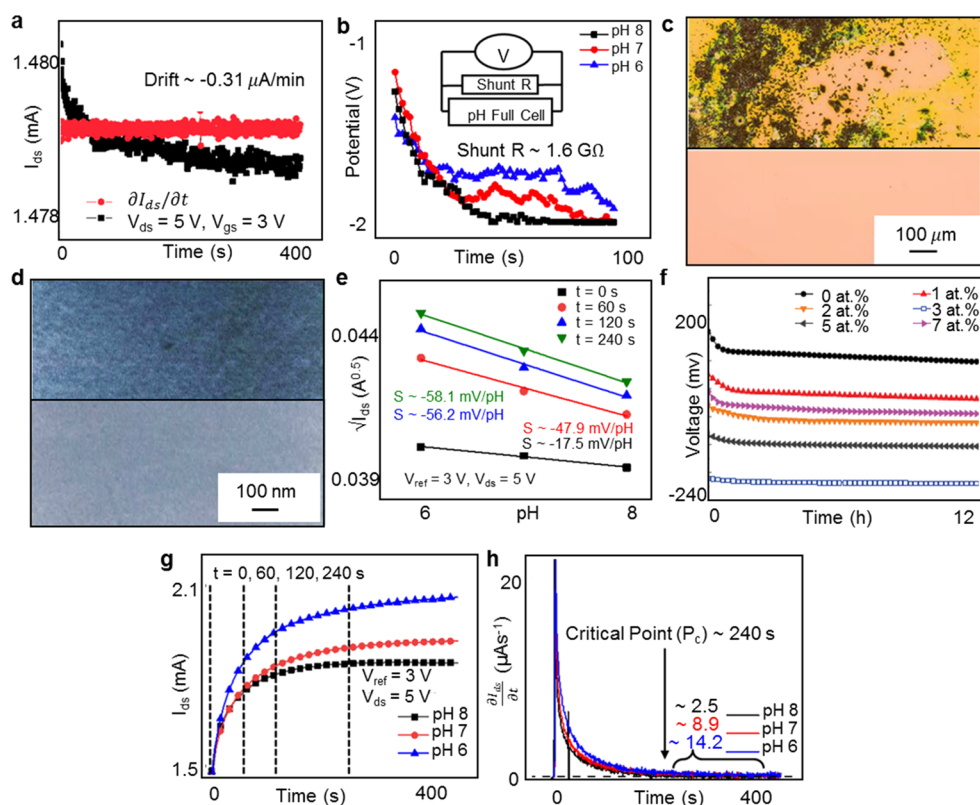


**Figure 5.** Inherent properties of the device components and input resistance of measurement system. (a) The relationship between time, drain to source current ( $I_{ds}$ ) and drift for a commercial CD4007 nMOS commonly used in EGFET, showing a drift of  $-0.31 \mu\text{A}/\text{min}$  at drain to source voltage ( $V_{ds}$ ) of 5 V and gate to source voltage ( $V_{gs}$ ) of 3 V.<sup>132</sup> (b) The relationship between time and potential with shunt resistance ( $R$ ) of  $1.6 \text{ G}\Omega$ .<sup>132</sup> (c) The effect of  $\sim 3$  h cycling tests in pH 6, 7, and 8 on the ZnO surface through (bottom) digital image of pristine ZnO surface and (top) digital image of the ZnO surface after successive testing. (d) Scanning electron microscopy pictures of the  $\text{Ta}_2\text{O}_5$  surface structure (bottom) after 5 and (top) 30 CIP cycles. Neither a visible degradation nor a destruction of the  $\text{Ta}_2\text{O}_5$  films has been observed after CIP procedure.<sup>146</sup> (e)  $\sqrt{I_{ds}}$  vs pH of solution at different time instants at a reference voltage ( $V_{ref}$ ) of 3 V and  $V_{ds}$  of 5 V, and corresponding sensitivity values ( $S = \text{slope of the } \sqrt{I_{ds}} \text{ vs pH plot divided by the slope of the } \sqrt{I_{ds}} \text{ vs } V_{gs} \text{ plot}$ ).<sup>132</sup> (f) Drift characteristics of the undoped ZnO and Al doped ZnO (AZO) with different atomic percentages (atom %) nanostructured pH-EGFET sensors measured within pH = 7 for the duration of 12 h. AZO with 3 atom % Al is the most stable with  $1.27 \text{ mV}/\text{h}$  drift.<sup>147</sup> (g) Actual drain current plot with time for ZnO sensing film vs Ag/AgCl reference electrode (RE) (the dash lines indicate different time instants to highlight the change in relative and absolute current values with time).<sup>132</sup> (h) The first derivative of part (g) with time, highlighting the suggested placement of the critical point ( $P_c$ ) and the estimated drift rates for solutions of different pH values.<sup>132</sup> Reproduced with permission from ref 132, 146, and 147, respectively. Copyright 2018 John Wiley and Sons, Inc. Copyright 2005 Elsevier. Copyright 2013 Hindawi under CC-BY-3.0 <https://creativecommons.org/licenses/by/3.0/>.

to deviate from an ideal Nernstian response. Drift is caused by diffusion of  $\text{H}^+$  and  $\text{OH}^-$  and variations in the sensing surface.<sup>137</sup> Figure 5a shows the relationship between pH and drift for  $\text{SnO}_2/\text{ITO}$  EGFET and the relationship between time, current, and drift for a commercial CD4007 nMOSFET, commonly used as the transistor in EGFET configurations (inherent drift  $\sim -0.31 \mu\text{A}/\text{min}$ ). Interestingly, drift seems to decrease slightly with time. In addition, Chen et al.'s work suggests an increase in drift value with the increase in pH. For instance, drift values of 0.884, 1.58, 1.71, 1.8, and  $2.51 \text{ mV}/\text{h}$  correspond to pH values of 2, 4, 6, 8 and 10, respectively, for the  $\text{SnO}_2/\text{ITO}$  EGFET. On the other hand, drift values of 14.2, 8.9, and  $2.5 \mu\text{A}/\text{min}$  for pH 6, 7, and 8, respectively, for ZnO/Au EGFET, i.e., lower gate voltage drift at higher pH.<sup>132</sup> Hence, the observed trends here cannot be generalized as drift values, and trends would depend on the pH solution constituents as well as the sensing electrode materials. There also may be a leakage current into the gate of the transistor, leading to a loss of a couple of millivolts, but this does not affect sensitivity because it is common in all solutions and should practically cause a systemic error, mainly affecting the standard reduction potential calculations. A MOSFET device,

which is part of the ISFET and EGFET setups, usually has high input resistance (Section 5.2 has further information) and input capacitance. For the EGFET and ISFET devices, the site binding model, discussed in Section 9.4, and electrochemical reactions at the surface of the sensing material affect the measurement of surface potential.<sup>138</sup>

There are many steps that are required in order to characterize components on pH-sensing configurations. The RE must be checked for stability and response time by calibrating it in different test solutions using a specialized instrument such as a digital pH meter with a high input resistance. For a transistor in the EGFET configuration, stability and drift can be determined by an instrument such as a semiconductor device analyzer. The test solutions must also be characterized to ensure that they are stable in their pH values after long periods of time and during exposure to ambient test environments. Exposure to the surrounding air may affect the pH of the solution. As mentioned previously, exposure to carbon dioxide ( $\text{CO}_2$ ) may lead to a decrease in pH. Test solutions are assessed using a traditional and reliable pH-sensing device. After these intrinsic properties

Table 8. Summary of the Common Substrate Cleaning Techniques Used in pH Sensor's Fabrication

ref	sensing material	cleaning method	setup	sensitivity	repeatability	stability	pH range
Li et al. <sup>116</sup>	ZnO/silicon nanowires (SiNW)	(1) Cleaned with sulfuric acid (H <sub>2</sub> SO <sub>4</sub> :H <sub>2</sub> O <sub>2</sub> = 3:1)  (2) Rinsed with deionized water (3) Soaked in dilute hydrofluoric acid (HF:H <sub>2</sub> O = 1:100) (1) Ultrasonically cleaned in acetone deionized water	extended gate field effect transistor (EGFET)	-46.25 mV/pH	hysteresis: 9.74 mV	difference ratios: < 5% in pH = 5–13, 25% in pH = 1, 15% in pH = 3	1–13
Rasheed et al. <sup>155</sup>	ZnO/Ag/ZnO	(2) Dried with nitrogen gas (1) Wafer was precleaned with acetone and isopropanol	EGFET	0.62 $\mu$ A <sup>1/2</sup> /pH	hysteresis: 5.4 mV		2–12
Ding et al. <sup>156</sup>	AlGaIn/GaN	(2) Dried with nitrogen (1) After etching, cleaned in a fuming nitric acid for an hour	high electron mobility transistor (HEMT)	37.17 $\mu$ A/pH	hysteresis: resolution of 0.1 pH		7.0–8.0
Oh et al. <sup>154</sup>	Al <sub>2</sub> O <sub>3</sub> /SiO <sub>2</sub>	(2) Piranha solution (1:1 solution of 97% H <sub>2</sub> SO <sub>4</sub> and 30% H <sub>2</sub> O <sub>2</sub> ), 6:1 buffered oxide etchant, and deionized water rinsing, each for 10 min (1) Ultrasonication in acetone, isopropyl alcohol and deionized water	electrolyte-insulator-semiconductor (EIS)	-60.2 mV/pH	hysteresis: 22.4 mV		4.0–10.0
Huang et al. <sup>136</sup>	ZnO/SiNW	(2) Immersed in a mixture of 5 M aqueous hydrofluoric acid and 0.02 M silver nitrate solution for 1 h at room temperature (3) After etching, immersed in 30 wt % nitric acid solution for 1 min (4) Rinsed with deionized water and air-dried (1) Rinsed with methanol for 5 s	EGFET	-66 mV/pH			2.0–12.0
Coppa et al. <sup>157</sup>	ZnO	(2) Dried in flowing nitrogen (1) Rinse in acetone	Schottky barrier diodes				
Kumar et al. <sup>158</sup>	ZnO	(2) Clean in dimethyl sulfoxide (DSMO) (3) Final clean with toluene (99.9%) (after each step, dried in flowing nitrogen)					
Ali et al. <sup>159</sup>	ZnO	(1) Silicon substrate cleaned with solution consisting of 40% H <sub>2</sub> SO <sub>4</sub> and 60% H <sub>2</sub> O <sub>2</sub>	EGFET	-27.86 mV/pH			

are characterized, pH testing and objective assessment of various configurations can take place.

## 5.2. Input Resistance of Characterization Systems

Along with assessing the inherent properties of components, it is important to assess and characterize the internal resistance ( $R_{in}$ ) of the pH tools. pH full measurement cells (i.e., ones composed of at least a sensing electrode and a RE immersed in an electrolyte) have high impedance. Digital multimeters, semiconductor device analyzers, n-type and p-type commercial transistors, instrumentation amplifiers, electrometer, electrochemical analyzers, and pH meters each have their own input resistance. For instance, digital multimeters usually have a  $R_{in}$  in the range of 10 M $\Omega$  to 10 G $\Omega$ .<sup>139</sup> Semiconductor device analyzers usually have an  $R_{in}$  greater than 1 T $\Omega$ .<sup>140,141</sup>

For OCP measurements, the input resistance of the potentiometer must be orders of magnitude larger than the resistance of the pH full cell. The pH full cell resistance includes the resistance of the glass sensing electrode or other sensing electrodes and the resistance of the RE.<sup>132</sup> Figure 5b illustrates the relationship between time and OCP with a shunt resistance of 1.6 G $\Omega$  showing inaccurate results. The resistance of the pH full cell occurs as a result of the sensing material's resistivity ( $\rho$ ) and sensing geometry. For example, instruments measuring the potential of the glass electrode should have an  $R_{in}$  in the hundreds of G $\Omega$  to T $\Omega$  range, because the membrane resistance of the glass electrode is in M $\Omega$ .<sup>142</sup> An instrument with high input resistance is correlated to smaller error, better stability, and higher and better pH response, because only a small portion of the current would travel through the instrument's resistance.<sup>132,143,144</sup>

Overall, the ability of the pH device to perform successfully is dependent on the resistivity of the sensing material, the resistance of the measuring instrument, and the resistance of the pH cell.

## 5.3. Surface Cleaning

The process of cleaning a sensor is extremely important in order to ensure reusability and confidence in measurement; however, the detailed process is rarely discussed.<sup>148</sup> Often times, the importance of cleaning the sensor is underestimated. In fact, it has been reported that the sensor performance differs by as much as 13% with different cleaning procedures carried out.<sup>148</sup>

Since different cleaning procedures can cause such different results, not using a systematic cleaning process could lead to wrong conclusions. For example, a sensor's high sensitivity might be mistakenly shadowed by undesired deposits if an inefficient cleaning procedure was used. While the cleaning process is rarely discussed, it is extremely important in ensuring sensor's accuracy, quality, and objective reporting. In general, based on the sensor material and setup, three types of cleaning are performed: cleaning the substrate that the sensor is based on (ex situ), cleaning of the sensor material itself (in situ), and cleaning the electrode in between measurements. All three of these cleaning methods should be carried out to ensure maximum quality, reliability, and life span of the sensor.

The initial step of cleaning happens on the substrate that the sensing film is deposited on. For example, silicon wafers are often used to grow silicon nanowire (SiNW) structures. To ensure that no impurities or any contaminant exists on the silicon substrates, steps should be taken to clean the surface of the substrate before growing microstructures. This step is crucial and previous studies have shown that cleaning the surface enhances the quality of the sensing device.<sup>149–152</sup>

In most cases, the substrate surface is submerged in either an alcohol solution (acetone, methanol, etc.) and/or an acid (sulfuric acid, hydrosulfuric acid, piranha solution, nitric acid, etc.) and then rinsed by deionized water. The purpose of using alcohol and acid is to clean organic residues or any impurities off the substrate surfaces. The substrate is then dried either with paper towel, flowing nitrogen, or in air.<sup>153</sup> Additionally, in the case of Ag or other ions assisted etching processes, the wafer is also cleaned in acid to remove silver dendrites and residual ions.<sup>154</sup> Table 8 summarizes common substrate cleaning techniques (ex situ cleaning). The various different cleaning protocols, even for the same substrate material, is indicative of the need for a standard protocol to eliminate variations in sensing film quality due to the conditioning of the underlying substrate.

Additionally, to ensure higher sensitivity and overall quality, it is important that the surface of the sensing material is kept clean of any residues during the manufacturing process of the sensing material and electrode structure. Different types of cleaning vary depending on the specific material and the setup used, but they all have commonalities, such as immersing the surface in acid or alcohol, and plasma treatment. Specifically, for sensors using ZnO, another common cleaning method that is often used is plasma treatment, often under ultrahigh vacuum (UHV) conditions.<sup>157</sup>

An important note on plasma treatment is that under short duration plasma treatment (~2 min), using X-ray photoelectron spectroscopy (XPS) and AFM, the surface composition of the examined sensing material might change. For instance, it has been reported that plasma treatment of AlGaN barrier layer increased the Al–O bonds at the surface. The increase in Al–O bonds is important to an increase in pH sensitivity, while further exposure to plasma treating increases Ga–O over Al–O bonds, and significantly decreases the sensitivity. With this process, a smooth and clean surface with an ultrathin oxide membrane can be obtained, increasing the sensitivity and quality of the sensor.<sup>160</sup> Hence, while short-term exposure to plasma could remove contaminants from the sensing surface, long-term exposure of the film to plasma could result in significantly lower sensitivity.<sup>160</sup> In addition, the temperature, time, and pressure that the film is treated in should change based on many factors, most notably the crystallography of the material. For example, the settings are significantly different for ZnO (0001) and ZnO (000 $\bar{1}$ ).<sup>161</sup> Table 9 summarizes the cleaning methods for a pH-sensing material surface (in situ cleaning). Similar to the observations made on Table 8, cleaning methods differ for the same sensing material. Furthermore, in this case it is the sensing surface itself that is being subjected to varying conditioning techniques. Given the dependence of pH measurements on sensing material's surface quality, the conditioning protocol is critical to report. Similarly, investigating how the conditioning protocol has affected the surface is essential, for consistency in reporting and comprehensibility.

## 5.4. Surface Resetting (Intermittent Cleaning vs In Situ Discussion)

With time, pH electrodes naturally undergo aging effects, which slightly impacts their performance.<sup>145</sup> This is exacerbated with coatings and contamination that occur with frequent use of the sensor (Figure 5c).<sup>132,145</sup> Resetting the surface of sensors is imperative for obtaining reliable results when monitoring pH. However, its method depends on the sensing requirements and

Table 9. Summary of the Intermittent Cleaning Methods for pH-Sensing Materials' Surface

ref	sensing material	cleaning method	setup	sensitivity	repeatability	stability	pH range
Ding et al. <sup>156</sup>	AlGaN/GaN	(1) Treated in a UV/O <sub>3</sub> chamber (400 W, 10 min) (2) Immersed in ethanol solution with 20 μL of 5% 3-aminopropyl triethoxysilane (APTES), by volume, for 2 h with periodic supply of the vaporized solution (3) APTES surface rinsed with deionized water five times	high electron mobility transistor (HEMT)	37.17 μA/pH			7.0–8.0
Wang et al. <sup>160</sup>	AlGaN/GaN	(1) Short-time O <sub>2</sub> plasma treatment (1–5 min)	ion sensitive field effect transistor (ISFET)	–58.7 mV/pH			4.0–9.0
Coppa et al. <sup>157,161</sup>	a-ZnO	Exposure to a 20 W remote 20% O <sub>2</sub> /80% He plasma as follows: i-ZnO (0001): 30 min, 525 °C, and 0.050 Torr ii-ZnO (0001): 60 min, 550 °C, 0.050 Torr	a-Surface studies only b-Schottky barrier diodes				
Zhang et al. <sup>38</sup>	ZnO	(1) ZnO NWs and NW–NF hybrid structures treated with oxygen plasma for 30 s to remove impurities and organic contaminants	extended gate field effect transistor (EGFET)	–43.22 mV/pH	difference between trails <0.01 mV	no degradation in 2 h testing periods	2–9
Kumar et al. <sup>158</sup>	ZnO	(1) Argon sputter cleaning					

given application. The two main methods are intermittent cleaning between each measurement, or in situ solutions.

Intermittent cleaning is the most common form of resetting the surface of a sensor in research studies. Frequent cleaning of the surface minimizes the effects of contamination.<sup>145</sup> This method allows for more consistent and accurate measurements of pH, by ensuring there is little to no residual substance from previously tested materials. A pH-sensing membrane based on an ionic liquid polymer composite developed by Ping et al. performed with a sensitivity of 57.5 mV/pH, close to the Nernstian expected value.<sup>71</sup> In between each measurement, the membrane electrodes were washed with deionized water, and no hysteresis was observed.<sup>71</sup> When testing *p*-aminothiophenol functionalized gold nanorods, they also showed well retained values.<sup>76</sup> In between each of the measurements, the culture dishes were rinsed with phosphate buffer solution three times.<sup>76</sup> Intermittent cleaning can also be applied to some implantable sensors. An implantable, battery-less, and wireless capsule with integrated pH sensors for gastroesophageal reflux monitoring was developed and implanted in the esophagus wall of a pig.<sup>162</sup> Between each measurement, the esophagus was flushed with tap water to reset the sensor.<sup>162</sup> The device consistently performed with sensitivities between –51.1 and –57.7 mV/pH.<sup>162</sup> However, intermittent cleaning is not practical in real-world applications where measurements must be taken continuously and in real-time.

Cleaning-in-place (CIP) is an in situ solution that exposes the sensor to a chemical process before measurements in order to combat hysteresis. Many industries, including biotechnology, food, pharmaceutical, cosmetic, construction and building materials, and water purification, produce a large demand for in-line pH sensors.<sup>146,163,164</sup> Since they cannot utilize glass electrodes due to strict regulations, which happen to be less prone to fouling, they rely on ion-sensitive field-effect transistors.<sup>132,146,163</sup> Schöning et al. developed a “non-glass” pH sensor based on a Ta<sub>2</sub>O<sub>5</sub>-gate electrolyte–insulator–semiconductor structure.<sup>146</sup> Before measurements, the sensor was subjected to cleaning in 4% NaOH solution at 80 °C for 15 min, then in 0.65% HNO<sub>3</sub> solution at 80 °C for 5 min.<sup>146</sup> The hysteresis seen during testing ranged between 1.5 and 9 mV, depending on the sensor type, number of CIP cycles, and the pH value of the buffer.<sup>146</sup> The device performed with a Nernstian value of 57 mV/pH, which showed to be independent of number of CIP cycles, because after 30 cycles no degradation of the sensor surface was observed (Figure 5d). Linkohr et al. investigated the stability of AlGaN/GaN pH sensors that have undergone CIP treatments.<sup>163</sup> They exposed their sensors to 1.5% NaOH at 80 °C for 30 min and then rinsed them with deionized water afterward.<sup>163</sup> The sensor showed hysteresis below 3 mV in the pH range of 2–10, but then jumped to 25 mV with pH 12, indicating a negative effect from alkaline solutions.<sup>163</sup> After 15 cycles, the sensitivity dropped from –57 mV/pH to –30.3 mV/pH, clearly showing how the process of CIP impacted the performance of the sensor.<sup>163</sup> While CIP treatments do well in preventing hysteresis, they heavily impact the lifetime of these sensors, producing a significant challenge for researchers and increased costs.<sup>146,163</sup>

Intermittent cleaning enables researchers to obtain accurate results by diminishing the effect of hysteresis and improving the lifetime of sensors.<sup>145,146,163</sup> CIP produces more realistic results for real-world applications. These treatments applied before measurements help prevent hysteresis, typically seen with cross contamination.<sup>146,163</sup> However, they decrease the lifetime of a

Table 10. Summary of the Surface Resetting Techniques for pH Sensors

ref	sensing material	reference material	resetting method	pH range	sensitivity
Queeney et al. <sup>145</sup>			• Spray-jet		
Ghoneim et al. <sup>132</sup>	ZnO	Ag/AgCl	• Retractable housing • Applying a voltage in reverse direction		
Schöning et al. <sup>146</sup>	Ta <sub>2</sub> O <sub>5</sub>	Ag/AgCl	• Briefly dissipating the charge from the sensing electrode Cleaning in 4% NaOH solution at 80 °C during 15 min and subsequently in 0.65HNO <sub>3</sub> solution at 80 °C during 5 min	3 to 10	• −57 mV/pH, independent of number of CIP cycles  • Hysteresis between 1.5–9 mV dependent on number of CIP cycles and pH value of buffer
Linkohr et al. <sup>163</sup>	AlGaN/GaN	Ag/AgCl	Sensor is exposed to 1.5% NaOH at 80 °C for 30 min and rinsed in DI water afterward.	2 to 12	• After 15 cycles, sensitivity dropped from −57 mV/pH to −30.3 mV/pH • Hysteresis below 3 mV between pH 2 to 10 and 25 mV when pH 12
Ping et al. <sup>71</sup>	poly(vinyl chloride) and <i>n</i> -cetylpyridinium hexafluorophosphate incorporated with quinhydrone	Ag/AgCl	membrane electrodes washed with deionized water	2 to 9.5	• −57.5 mV/pH  • No hysteresis observed
Zong et al. <sup>76</sup>	gold nanorods	<i>p</i> -amino-thiophenol	cell culture dishes were washed with phosphate buffered saline for three times	3 to 8	
Cao et al. <sup>162</sup>	IrO <sub>x</sub>	Ag/AgCl	washed with tap water	1.9 to 12	between −51.1 and −57.7 mV/pH

sensor due to the strong chemicals used.<sup>146,163</sup> Other in situ methods that have been discussed include altering the electrical properties of the sensor, such as by temporarily applying a voltage in the reverse direction of the cell potential.<sup>132</sup> Another method would be to model the equilibrium surface charge density as a function of pH, which could then be related to the measured potential.<sup>132</sup> These approaches still require further investigation, but they open possibilities to improve in situ solutions for accurate pH sensing. Table 10 summarizes the surface resetting techniques discussed in this section. The spray-jet solution utilizes an intermittent jet of air or water directed at the tip of the pH electrode to clean the contamination coating. This is suitable for submersible systems. However, it is not suitable when the dilution of tested solution is an issue, which is definitely the case with biomedical applications. The same applies to all intermittent cleaning methods involving chemical or DI splashing treatment. In that case, the pH probe can be fixed in a retractable housing, where it can be retracted, washed away from the testing environment, and reinserted. This concept is suitable for biomedical applications as the sensing probe can be implanted and retracted at specific intervals for cleaning. However, when the system does not constitute a probe structure, as in wearable pH-sensing patches and systems (Section 8.1), even the retractable housing would be inapplicable. In that case, the most feasible option is either to apply an electrical signal to reverse the reaction that resulted in contamination coating, or periodic discharging of the previous measurements' surface charge.

### 5.5. Time Plots and Analysis

When using a pH sensor, the device will require some time before it can obtain at least 90% of the full response.<sup>132</sup> This time period is referred to as the response time, and it can range anywhere from a few seconds to several minutes depending on a number of factors. The final point after the complete response is defined as the critical point and is used in the calculation of the calibration plot for the device, making it extremely important.<sup>132</sup> Taking the critical point too early or too late can have detrimental effects on the measured sensitivity value. As

depicted in Figure 5e, while in saturation mode, the sensitivity of a ZnO EGFET sensor jumps from −17.5 mV/pH to −58.1 mV/pH just by waiting until the critical point has been reached.<sup>132</sup> In linear mode, the sensitivity jumps from −9.8 mV/pH to −84.8 mV/pH, possibly indicating that an equilibrium was reached earlier.<sup>132</sup> It is necessary to report the time plot in order to determine how long the electrodes must remain in a solution before an accurate measurement can be collected.<sup>132</sup>

Unfortunately, even with their vast importance, many papers utilizing EGFET and ISFET do not include time plots that show a response time in their discussion. Without referring to a time plot for corroboration, performance results are not as reliable as they should be. Nonetheless, several ISFET, EGFET, and potentiometric works include time plots to show stability and drift characteristics of a device; however, they rarely indicate when the critical point has been reached. Thus, the calculation of drift becomes arbitrary. For instance, Figure 5f shows drift values defined as the slope of the output voltage vs time plot between 5 and 12 h.<sup>107,147</sup> The oxygen plasma treated CNTF in pH 7 had a drift value of 1.36 mV/pH,<sup>107</sup> and the drift values for Al doped ZnO films with different Al atomic percentages (atom %) of 0, 1, 2, 3, 5, 7 atom % corresponded to 16.81, 13.59, 4.77, 1.27, 3.38, and 8.79 mV/h in pH 7.147 Although these observations and stating the exact range for calculating the drift are very useful, the lower limit of 5 h is not a common time frame for collecting a pH measurement. Therefore, an earlier time range that is feasible for collecting pH measurements (i.e., several minutes) would be most useful and expectedly would result in higher drift values. On the other hand, a wearable pH sensor using PANI in OCP configuration exhibited a drift of 0.7 mV/h.<sup>68</sup> In the latter case, drift was calculated from an hour of continuous measurement in a 4 h time frame, most likely between the third and the fourth hour. Furthermore, a ZnO pH sensor in OCP configuration with ±3 mV/h drift was reported with no indication of either a time range or the window of calculation (likely within the first 15 min based on the reported stability plot).<sup>37</sup> One solution to determining the critical point is to evaluate the first derivative of the time plot, demonstrated in Figure 5g,h.<sup>132</sup> The point

Table 11. Summary of the Representative EGFET and ISFET Works, Highlighting the Limited Reporting of Time Plots

ref	setup	sensing material	reference material	sensitivity	response time	time plot
Ghoneim et al. <sup>132</sup>	extended gate field effect transistor (EGFET)	ZnO	Ag/AgCl	<ul style="list-style-type: none"> <li>At 240 s: <math>-58.1</math> mV/pH saturated, <math>-84.8</math> mV/pH linear</li> <li>At 0 s: <math>-17.5</math> mV/pH saturated, <math>-9.8</math> mV/pH linear</li> </ul>	240 s	included
Wang et al. <sup>147</sup>	EGFET	aluminum-doped ZnO (AZO)	Ag/AgCl	Al dosage of 3%: $-57.95$ mV/pH		
Li et al. <sup>168</sup>	ion sensitive field effect transistor (ISFET)	indium tin oxide (ITO)/ polyethylene terephthalate (PET)	Ag/AgCl	$-44.86$ mV/pH		
Chen et al. <sup>98</sup>	EGFET	iridium nitride nanorod	Ag/AgCl	<ul style="list-style-type: none"> <li>Current: <math>26 \mu\text{A}/\text{pH}</math></li> <li>Voltage: <math>-22.66</math> mV/pH</li> </ul>		
Lee et al. <sup>99</sup>	ISFET	ZnO-based nanorod/gate-recessed AlGaIn/GaN	Ag/AgCl	$-57.66$ mV/pH		
Tsai et al. <sup>107</sup>	EGFET	oxygen-plasma-treated carbon nanotube thin films	Ag/AgCl	$-55.7$ mV/pH		
Batista et al. <sup>114</sup>	EGFET	ZnO		$-38$ mV/pH		
Ali et al. <sup>121</sup>	EGFET	ZnO		$-22.4$ mV/pH		
Chiu et al. <sup>169</sup>	EGFET	tantalum ZnO (ZnO:Ta)	Ag/AgCl	$-41.56$ mV/pH		
Lin et al. <sup>170</sup>	EGFET	indium-gallium-zinc-oxide nanoparticles/silicon nanowire (IGZO/SiNWs)	Ag/AgCl	$-50$ mV/pH		
Rasheed et al. <sup>171</sup>	EGFET	multilayer ZnO/Pd/ZnO structure	Ag/AgCl	$-52$ mV/pH		
Yang et al. <sup>115</sup>	EGFET	Al-doped ZnO (AZO)		Al-dosage of a-0%: $-35.23$ mV/pH b-1.98%: $-57.95$ mV/pH c-3.35%: $-55.61$ mV/pH d-6.27%: $-53.34$ mV/pH		
Huang et al. <sup>136</sup>	EGFET	zinc oxide/silicon nanowire hybrid	Ag/AgCl	<ul style="list-style-type: none"> <li>SiNWs: <math>-52</math> mV/pH</li> <li>ZnO/SiNW: <math>-58</math> to <math>-66</math> mV/pH</li> </ul>		
Lee et al. <sup>172</sup>	EGFET	ZnO thin films and ZnO nanorods	Ag/AgCl	<ul style="list-style-type: none"> <li>Unpassivated: <math>47.96 \mu\text{A}/\text{pH}</math></li> <li>Passivated: <math>52.58 \mu\text{A}/\text{pH}</math></li> </ul>	10 s	included
Chiu et al. <sup>113</sup>	EGFET	ZnO thin films and nanorods	Ag/AgCl	<ul style="list-style-type: none"> <li>Unpassivated intrinsic-ZnO (i-ZnO) nanorod array: <math>-44.01</math> mV/pH</li> <li>Unpassivated i-ZnO thin film: <math>-38.46</math> mV/pH</li> <li>Passivated iZnO thin-film: <math>-42.37</math> mV/pH</li> <li>Passivated i ZnO nanorod array: <math>-49.35</math> mV/pH</li> </ul>		
Wang et al. <sup>57</sup>	EGFET	Al-doped ZnO nanostructures	Ag/AgCl	$-57.95$ mV/pH		
Thanh et al. <sup>165</sup>	EGFET	ZnO nanorods	Ag/AgCl	$-15.4$ mV/pH		
Maiolo et al. <sup>72</sup>	EGTFT	ZnO nanowalls	Ag/AgCl	$-59$ mV/pH		
Chang et al. <sup>173</sup>	EGFET	ZnO thin films and nanowire array	Ag/AgCl	$48.6 \mu\text{A}/\text{pH}$ $-36.9$ mV/pH		
Fernandes et al. <sup>167</sup>	EGFET	ZnO thin films	saturated calomel	<ul style="list-style-type: none"> <li>Fluorine doped tin oxide substrate with Al % of 0%: <math>-22.3</math> mV/pH 3%: <math>-29</math> mV/pH 7%: <math>-40.1</math> mV/pH 8%: <math>-30.9</math> mV/pH</li> <li>ITO substrate 3%: <math>-23</math> mV/pH 7%: <math>-26.6</math> mV/pH 8%: <math>-33</math> mV/pH 10%: <math>-30</math> mV/pH</li> </ul>		
Rosli et al. <sup>166</sup>	EGFET	ZnO nanostructures/Au/ITO		$-38.2$ mV/pH		

where a constant value begins signifies that the critical point has been reached. Figure 5h indicates the critical point is at 240 s.

It is strongly recommended to report the time plot, which clearly indicates the response time of their device.

Low<sup>98,114,165–167</sup> (or high<sup>57,99,107,115,136</sup>) reported sensitivities can be due to the sensing material used, the fabrication process followed, or an early (or late) extraction of values before (or after) reaching the critical point. This could result in incorrect

**Table 12. Summary of the Various Reports on pH Sensors, Indicating Response Times and Emphasizing the Absence of a Clearly Identified Critical Point**

ref	setup	sensing material	reference material	response time (s)	critical point
Ghoneim et al. <sup>132</sup>	extended gate field effect transistor (EGFET)	ZnO	Ag/AgCl	240	at 240 s
Goldstein et al. <sup>174</sup>	fiber optics	pH sensitive dye contained within a H <sup>+</sup> permeable envelope		42	
Grant et al. <sup>175</sup>	<ul style="list-style-type: none"> <li>• Optoelectronics</li> <li>• Electrochemical</li> </ul>	<ul style="list-style-type: none"> <li>• Silica optical fibers</li> <li>• IrO<sub>x</sub></li> </ul>	<ul style="list-style-type: none"> <li>• N/A</li> <li>• Ag/AgCl</li> </ul>	5400	
Li et al. <sup>104</sup>	open circuit potential (OCP)	single walled carbon nanotubes (SWCNTs)	Ag/AgCl	~30	
Gou et al. <sup>105</sup>	FET	SWCNTs functionalized with poly (acrylic acid) (PAA)	Ag/AgCl	3–7	
Qin et al. <sup>78</sup>	OCP	Inkjet-printed SWCNTs	Ag/AgCl	7	
Korostynska et al. <sup>16</sup>	OCP	120 mg of lithium perchlorate (LiClO <sub>4</sub> ) and 10 μL of pyrrole (PPy) dissolved in 5 mL of acetonitrile	Ag film	<1	
Yoon et al. <sup>72</sup>	OCP	polyaniline (PANI) nanopillar array	Ag/AgCl	<1	
Guinovart et al. <sup>59</sup>	OCP	electropolymerized PANI	polyvinyl butyral polymer (PVB)	<20	
Ping et al. <sup>71</sup>	OCP	poly(vinyl chloride) (PVC) and <i>n</i> -cetylpyridinium hexafluorophosphate (CPPP) incorporated with quinhydrone (QH)	Ag/AgCl	<10	
Rout et al. <sup>100</sup>	FET	ZnO	Au	150	

**Table 13. Summary of the Representative pH Sensors and Their Reported Drift Values**

ref	setup	sensing material	reference material	drift	critical point
Chang et al. <sup>176</sup>	ion sensitive field effect transistor (ISFET)	ZrO <sub>2</sub>	Ag/AgCl	hours 1–7	
				n-channel	
				pH 3 –58.55 mV	
				pH 5 –51.54 mV	
				pH 7 –41.61 mV	
				pH 9 –34.66 mV	
				pH 11 –32.52 mV	
				p-channel	
				pH 3 13.33 mV	
				pH 5 6.04 mV	
				pH 7 –4.91 mV	
				pH 9 –25.92 mV	
				pH 11 –30.82 mV	
Wang et al. <sup>147</sup>	extended gate field effect transistor (EGFET)	aluminum-doped zinc oxide (AZO)	Ag/AgCl	Al dosage of 3% best drift rate at 1.27 mV/h over 12 h	
Rigante et al. <sup>178</sup>	FinFET	HfO <sub>2</sub>	Ag/AgCl	<ul style="list-style-type: none"> <li>• Single wire FinFET: drift time of 0.13 mV/h.</li> <li>• 3-wire FinFET: Drift time of 0.1 mV/h.</li> <li>• 5-wire FinFET: 0.12 mV/h (all over 105 h)</li> </ul>	
Tang et al. <sup>168</sup>	ISFET	indium tin oxide (ITO)/ polyethylene terephthalate	Ag/AgCl	drift rate <1.7 mV/h over ~8.5 h	
Zhou et al. <sup>177</sup>	open circuit potential (OCP)	IrO <sub>2</sub>	Ag/AgCl	<ul style="list-style-type: none"> <li>• Over 86 h: potential drift 0.3 mV/h</li> <li>• First 30 h: potential drift 0.6 mV/h</li> </ul>	

conclusions. Including a time plot indicates the response behavior of the device, makes results and findings more reliable, and enables objective benchmarking of various sensing materials and systems. Table 11 summarizes various EGFET and ISFET works and time plots. An important observation for EGFET and ISFET reports is the necessity of identifying the critical time at which the output or transfer plots of the transistor are collected. This can be identified by collecting the time plots ( $I_{ds}$  vs time) discussed in this subsection and identifying the critical point (discussed in detail in the next section, Section 5.6). In general, sensitivity values for ISFET and EGFET configurations vary widely from –22.4 to –59 mV/pH, and response times range

from tens of seconds to several minutes. In addition, the EGFET configuration (Section 4.2) is gaining popularity because it offers the advantage of separating the electronics part from the sensing part, compared to the ISFET configuration (Section 4.1).

### 5.6. Critical Point ( $P_c$ ) for Response and Drift Determination

In addition to time plots,  $P_c$  in pH sensing is an important characteristic of pH sensors that is often overlooked. The critical point is used to determine the response time, drift, and sensitivity of a device. Each of these ultimately determines the effectiveness of a device, so without knowing the critical point there is no reliable way to evaluate a device.

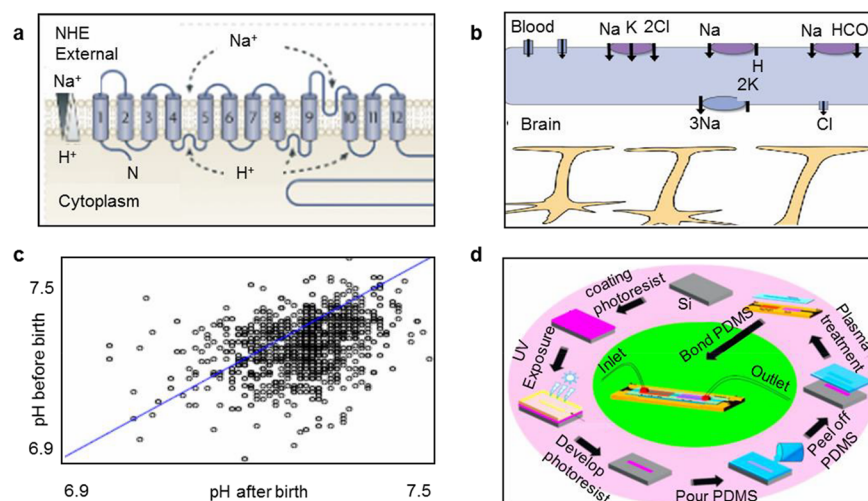


**Figure 6.** pH regulation in the human body. (a) Ion carriers ( $\text{Na}^+\text{-H}^+$  exchanger (NHE)) regulation of cell pH.<sup>179</sup> (b) Blood–brain barrier ion transporters and channels.<sup>191</sup> (c) pH before birth and after birth, showing good correlation between fetal scalp pH value and outcome pH value and used to study the reliability of fetal scalp pH values,<sup>194</sup> (d) Microfluidic device fabrication scheme for ZnO-based pH sensor with open circuit potential (OCP) configuration, with  $-43.71$  mV/pH sensitivity, drift of 3 mV/h, and response times between 26 and 32 s in the 1.68–9.18 pH range.<sup>37</sup> Reproduced with permission from refs 179, 191, 194, and 37, respectively. Copyright 2009 Springer Nature, Ltd. Copyright 2014 Elsevier. Copyright 2016 Springer Nature, Ltd. Copyright 2017 American Chemical Society.

Response time is important for pH sensors because for real-life applications there may only be a small window of time to take a measurement, and thus a device must be able to respond within that time. Although the response time of a device is defined as the time it takes for a device to reach 90% of the full response, or the time it takes for a device to reach the critical point,<sup>132</sup> many reports do not explain how this value was determined.<sup>16,59,71,72,78,100,104,105,174,175</sup> Without reporting how the critical point was found or when it is achieved, there is no way to know if these are correct measurements or just arbitrary values. Table 12 summarizes various reports, indicating response times, and whether the critical point was identified. This table clearly shows the dispersion in response time reporting from <1 s to 90 min. Although that is possible based on the material system; there is 20 times variation for PANI in OCP (from <1 s to <20 s). With an arbitrary point for response calculation, it is highly subjective to compare materials or systems responses across different reports, unless the same work compares two materials or systems using the same subjective methodology. This highlights the need for the critical point convention and its usefulness in identifying proper sensitivity values and separating the full response from the onset of drift.

Drift is another important characteristic of pH sensors; it determines the stability of a device. Over time, most electrodes suffer from potential drift, i.e., the slope of the output after the critical point (full response) has been achieved.<sup>176</sup> Quantifying drift begins at the critical point, so without knowledge of when the critical point of a device occurs, it is difficult to assess drift and accurately determine suitability for long-term monitoring. Various reports<sup>147,168,177,178</sup> show drift values; however, there is no explanation of how it was extracted. Thus, failing to report when or how the critical point was reached makes objective benchmarking of these reports infeasible. Table 13 summarizes representative pH sensors and their reported drift values. Notably, the lack of a common convention for calculating drift results in subjective time frames and ranges for calculating drift. When drift is collected in the first seven hours, the values are in the 4.6–8.4 mV/h range for  $\text{ZrO}_2$  n-channel ISFET and 0.7–4.4

mV/h range for p-channel ISFET. For 12 h, an average drift of 1.27 mV/h was reported for AZO EGFET. For larger time ranges, drift values of 0.1 and 0.3 mV/h have been reported for 3-wire  $\text{HfO}_2$  FinFET and  $\text{IrO}_2$  in OCP configuration. The trend clearly shows that longer time ranges and later time frames exhibit lower drifts, and it would be inaccurate to compare drifts of configurations and materials if time range and time frames are inconsistent.

Evidently, a standardized method for identifying the critical point is essential. The method discussed is to take the first derivative of the time plot and locate the point at which constant values begin, as illustrated in Figure 5g,h. The point at which this occurs is then to be defined as the critical point and used in the sensitivity calculation.

Following standards and protocols for pH measurements is what ensures the validity of the measurement and extends its applicability to future and related works. Traditional pH measurements start with proper calibration of the tested device. This can be done using standardized buffer solutions such as the National Institute of Standards and Technology (NIST) recommended buffers, or in phosphate buffered solutions that mimic biological fluids. This is usually conducted by using a minimum of two calibration pH buffer solutions that cover the expected range of the desired pH measurements. A three-point calibration with three buffered solutions is recommended for a more precise calibration plot. Once calibration is complete, the device is washed in deionized water and used to measure the test solution. A traditional potentiometric measurement would output the voltage difference between the reference electrodes and sensing electrode versus time. The analysis of the plot is straightforward and response time, saturation value, and drift can be extracted. With the advancements in pH sensing and biomedical applications, the actual sensing environment is far more complex than the common standard buffer solutions. Hence, it is more feasible to calibrate in more customized environments that closely match the real one. To this end, arbitrary choices for calibration and testing might be not only acceptable but even more accurate. To cope with the emerging

trends in measurement technologies, providing as much information as possible about calibration, measurement, and analysis is essential, including specifications of characterization instruments. In this section, we highlighted the new aspects that are essential for establishing standards and protocols to cope with current progress. These include (i) accounting for extrinsic components effects, (ii) instrumentation, (iii) initial and intermittent surface conditioning, (iv) collecting and analyzing time plots in all cases, and (v) defining conventions that would enable consistent reporting. Nonetheless, at this stage there is no clear protocol that is widely approved and followed across the pH-sensing community. This highlights the need for careful reporting that includes all possible sources of error (intrinsic and extrinsic to the assessed system). Through proper reporting, various studies can be objectively benchmarked. Only then will patterns emerge for best practices, and new universal standards and protocols can be established.

## 6. pH REGULATION IN THE HUMAN BODY

pH regulation in the human body is crucial for proper functionality and disease prevention. Strict regulation mechanisms exist at the cellular and organ levels. This section focuses on pH regulation in the extra- and intracellular environments as well as the organ level, specifically the kidney and lungs. We also discuss the essential role of blood in pH regulation throughout the body.

### 6.1. Cells

$\text{pH}_i$  must be maintained within a strict range in order for cellular processes to proceed. This balance is regulated both within the membrane of the cell as well as certain organelles. These cellular compartments have inherent pH buffering capacities varied by intracellular weak acids and bases. An additional buffer in most mammalian cells is created by the hydration of  $\text{CO}_2$  and deprotonation of carbonic acid.<sup>179</sup> These two buffering capacities compensate for changes in  $\text{pH}_i$ . Acidification of the cell is prevented by membrane  $\text{H}^+$  pumps or proton coupling (Figure 6a). The energy to force these  $\text{H}^+$  against the electrochemical gradient can be provided by adenosine triphosphate (ATP).<sup>179</sup> To recognize changes in pH and acknowledge the need for  $\text{H}^+$  transfer, membrane recognition proteins are utilized. Individual organelles, such as lysosomes, must also maintain specific pH values to perform. Organelles preserve their pH through similar methods like the cell, i.e., through membrane  $\text{H}^+$  transfer activity.<sup>179</sup> Because of the excellent buffering abilities of the cells, a deviation in cellular pH usually indicates anomalies in functionality.<sup>179,180</sup> For instance, cellular pH can become vitally important in recognizing and treating cancer cells because their pH is different from healthy cells.<sup>181,182</sup> Hence, understanding and monitoring pH can enable recognition of cancerous growth. To this end, extensive recent studies have been carried out to sense both  $\text{pH}_i$  and extracellular pH ( $\text{pH}_e$ ),<sup>180,183,184</sup> including sensing in an in vivo-like 3D environment<sup>185</sup> and in vivo imaging.<sup>186</sup>

### 6.2. Kidneys and Lungs

Regulation of pH levels in internal organs such as the kidneys and lungs are also vital to understand. For instance, kidneys contribute to organismal pH regulation by specific  $\text{H}^+$  buffering and secretory mechanisms. The bicarbonate buffer system entices the kidneys to reabsorb filtered  $\text{HCO}_3^-$  and convert it into excreted products.<sup>187</sup> This reabsorption takes place in the proximal tubule. The distal nephron then excretes acid to be trapped in urine with either filtered anions or ammonia. Overall

acid buffering and excretion by the reclamation of filtered bicarbonate and its regeneration are essential to the renal acid–base balance.<sup>187</sup>

Lungs also function in the excretion of metabolically produced  $\text{CO}_2$ . The lungs control the  $\text{CO}_2$  partial pressure ( $\text{pCO}_2$ ), or the  $\text{pCO}_2$  reflecting the amount of the gas dissolved in the blood, to counteract the influx of  $\text{H}^+$  and resulting acidosis or alkalosis due to the excessive retention or excretion of  $\text{CO}_2$ .<sup>188</sup> This pulmonary regulation of acid–base balance is based on ventilation adjustment. Ventilation, directed by chemoreceptors, afferent and efferent nerves, central nervous connections, and the skeletal muscles, occurs in response to both arterial pH and that of the cerebral spinal fluid (CSF).<sup>189</sup> Worth mentioning, this ventilation must balance the need to control the pH and also the need for oxygenation. Arterial response is observed to be more rapid than CSF response.  $\text{CO}_2$  functions in these processes alongside its combination and dissociation products to eliminate acid waste and regulate extracellular pH ( $\text{pH}_e$ ).<sup>189</sup> The lungs, by excreting carbonic acid, contribute to the buffer system, which controls blood pH.<sup>190</sup> Blood pH varies inversely with  $\text{pCO}_2$  concentration. The pH of CSF differs from arterial pH in that carbonic acid among other molecules diffuses easily. This results in a direct effect of  $\text{pCO}_2$  through the blood–brain barrier and the necessity for constant action of the bicarbonate pump to maintain a normal pH.<sup>189</sup> With a sudden increase or decrease in  $\text{pCO}_2$ , respiratory acidosis or alkalosis occurs, severely changing CSF pH and possibly causing delirium or even a coma.<sup>188</sup>

### 6.3. Blood

Given the important role of blood pH and its effect on CSF, blood pH is tightly regulated in the human body, fluctuating between 7.35 and 7.45. The bicarbonate buffer system in the kidneys and the respiratory function of the lungs are the main regulatory functions for blood pH. Other methods for pH regulation include ion transporters and channels across different barriers, such as across the blood–brain barrier (Figure 6b).<sup>191</sup> Specifically, the chloride–bicarbonate exchanger and the sodium–hydrogen ion channel found on the blood–brain barrier help regulate the pH level in both the blood and the brain. Changes in blood pH can be attributed to several things, including strenuous activity, environmental changes, and health complications. However, these mechanisms allow the blood pH to drop or rise outside that range for short periods of time without fear of complications.

When participants were subjected to a short interval of high intensity exercise, their average pH dropped to 7.11.<sup>192</sup> After five intervals of high intensity exercise, their average pH decreased to as low as 6.94.<sup>192</sup> This continuous drop during exercise was due to the increase of  $\text{CO}_2$  in the blood. Once participants had longer time to rest, their respiratory function was allowed to increase their pH level back up to normal levels.<sup>192</sup> Coso et al. investigated whether this result was affected by the physical condition of the person, i.e., trained versus untrained.<sup>195</sup> This experiment showed that physical condition of individuals has little effect because the blood pH of both trained and untrained groups were remarkably similar.<sup>195</sup>

Although there are normal cases when blood pH drops out of the regulated range for short periods of time, concerns arise when the blood pH is not able to return to the safe range. This is a clear indication that there is some anomaly inside the body. Dangerous environmental changes significantly affect blood pH levels. Osborn investigated the effects of cardiac function on the

Table 14. Summary of the Representative Studies Correlating pH to Physical Conditions

ref	testing condition	blood sample	lowest average pH
Coso et al. <sup>195</sup>	bicycle exercise	capillary blood taken from finger	7.207 ± 0.051 for trained and 7.182 ± 0.080 for untrained individuals
Hermansen et al. <sup>192</sup>	treadmill or bicycle exercise	capillary blood taken from fingertips	after one exercise interval (1 min workout and 4 min rest): 7.11, and after five exercise intervals: 6.94
Momiyama et al. <sup>196</sup>	out-of-hospital cardiac arrest		unfavorable outcome: 6.93 ± 0.19
Kuehnle et al. <sup>194</sup>	pregnancy	fetal scalp blood and umbilical artery	before birth: 6.98, and after birth: 6.90
Osborn et al. <sup>193</sup>	hypothermia	arterial blood	light anesthesia and no artificial respiration: 7.16
Mani et al. <sup>37</sup>	cancer		

respiratory performance and blood pH by subjecting dogs to low temperatures and inducing hypothermia. Osborn showed hypothermia effect on pH under light anesthesia for an 11 kg dog with no artificial respiration.<sup>193</sup> The results showed that when temperatures dropped, the respiratory function plummeted, and with that the arterial pCO<sub>2</sub> increased.<sup>193</sup> The rise in arterial pCO<sub>2</sub> was assumed to be the cause of the drop in pH level, having an inverse relation with one another.<sup>193</sup>

Health complications are another important factor in blood pH levels. Momiyama et al. investigated the prognostic values of blood pH levels in patients resuscitated from out-of-hospital cardiac arrest and found that pH levels were much higher with an average of 7.26 in patients with favorable outcomes compared to those with unfavorable outcomes with an average of 6.93.<sup>196</sup> A pH level of 7.05 was found to be the optimal cutoff level for favorable outcome in patients and the pH level of a patient with a favorable outcome never dropped below 6.95.<sup>196</sup> Blood pH level is such a key factor in evaluating health that obstetricians use it to inform their decisions on their delivery method for pregnancies.<sup>194</sup> When the fetal scalp blood pH was 7.20 or lower, a doctor would have to make the decision to perform a c-section or an instrumental vaginal delivery in order to avoid complications (Figure 6c shows good correlation between fetal scalp pH value and outcome umbilical pH value, used to study the reliability of fetal scalp pH values).<sup>194</sup> However, results may not always be reliable and can be false at times. It was recommended to take at least two samples before making a decision as close to the time of delivery as possible.<sup>194</sup> There is also direct correlation between pH and the presence of cancer cells in the blood (tumor cells). Mani et al. developed a working ZnO-based microfluidic pH sensor as a tool to examine circulating tumor cells (Figure 6d).<sup>37</sup> The device achieved a Nernstian response of -43.71 mV/pH along with a high stability and drift of 3 mV/h, and a short response time between 26 and 32 s in the 1.68–9.18 pH range.<sup>37</sup>

When blood pH drops below 7.35, it is an important warning sign of functional anomalies inside the body. There are many causations for a drop in pH, such as strenuous activity that does not allow the blood to get enough oxygen, dangerous drops in body temperature that cause a rise in pCO<sub>2</sub> levels, and health problems like cardiac arrest and pregnancy complications. The human body regulates this as much as possible with the help of the bicarbonate buffer system in the kidneys and the respiratory function of the lungs, so short-term drops in pH are usually normal. However, when a rise back to normal levels is not seen, concerns arise. Table 14 shows a summary of studies correlating pH to physical conditions. The importance of pH sensing in blood is evident through its myriad biomedical applications, which ranges from monitoring simple physiological changes such as exercising to more serious conditions as cardiac arrest,

pregnancy, hypothermia, and cancer. The next section discusses the expanding biomedical applications of pH sensing for both ex vivo (Section 7.1) and in vivo (Section 7.2) experiments.

## 7. pH SENSING IN BIOMEDICAL APPLICATIONS

Among other pH applications, those of biomedical ones ranging from ex vivo to in vivo are numerous. This section discusses progress in pH sensors for both ex vivo and in vivo applications. Examples of ex vivo applications include the common urine and saliva tests, and the recent tooth decay assessment tests. On the other hand, the in vivo applications discussed include glioblastoma detection (the most frequent brain tumor), pH<sub>i</sub> and pH<sub>e</sub> sensing, oral hygiene assessment, monitoring of ischemic episodes, and sweat analysis.

### 7.1. Ex Vivo

**7.1.1. Urine Tests.** pH sensing of excreted bodily fluids is used to assess the condition of the patient. In particular, urine pH testing is a popular method, given the convenience of large sample collections and usefulness for assessing the treatment needs of a patient. The pH of the fluid acts as a biochemical marker, which is analyzed most commonly in two ways. Dipstick testing utilizes single-use test strips which report pH, presence of glucose, presence of certain proteins, and other important variables.<sup>197</sup> Though cheap and easy to use, dipsticks demonstrate significant pH measurement variability at more extreme values. Alternatively, urine pH can be found using a pH meter, which demonstrates more accuracy but requires personnel training and frequent calibration.<sup>197</sup> Though the pH meter is ideal for guiding patient treatment decisions, the dipstick remains a valuable, if less precise, tool for patient use. Another factor to consider is that the pH of urine samples is unstable at higher temperatures, thus, affecting the results of analysis on tampered and old samples.<sup>198</sup> This is relevant to the drug testing applications of urine pH testing.

**7.1.2. Saliva Tests.** Similar to urine tests, the pH of saliva is also often tested either as a medical guide or drug testing method. Difficulties arise in saliva pH testing because of the limited sample size and collection issues.<sup>199</sup> Saliva is generally collected by spitting or stimulation by chewing or sucking. Once the sample is procured, a filtration device is often used to reduce the viscosity, making it easier to analyze later. Given that unstimulated saliva pH may range from 5 to 7, differences in these values can be quantified to indicate medical changes in the patient.<sup>200</sup> Since these supplementary steps increase cost, while only providing a short window of sample viability, saliva testing is less common than urine testing.

**7.1.3. Tooth Decay.** Recently, applications of miniaturized pH sensors have gained increasing attention, especially in oral hygiene, due to its noninvasive nature, its small size, and its ability to quantify pH. For example, one of the common

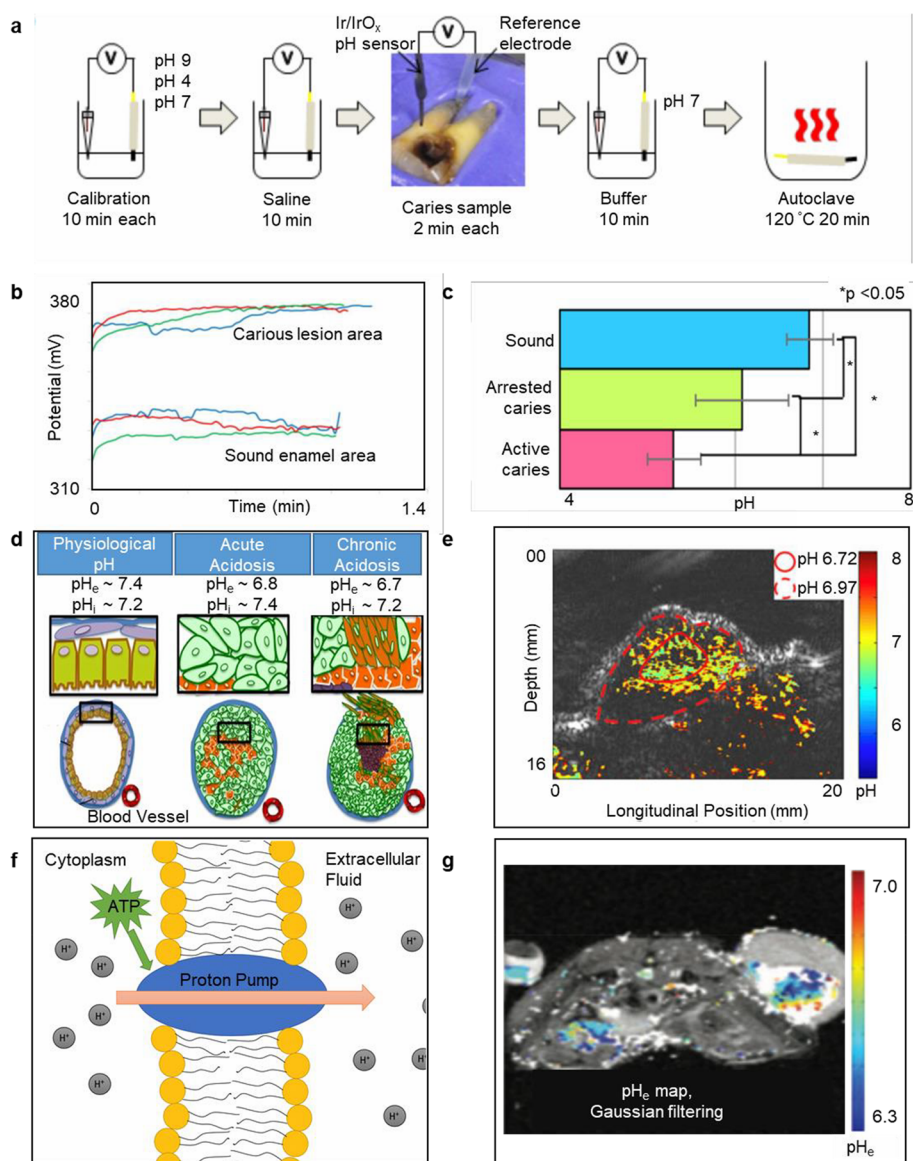


**Figure 7.** pH sensing in biomedical applications (ex vivo tooth decay and in vivo glioblastoma and intra- and extracellular tests). (a) Experimental protocol for measuring pH of dental caries. The pH 7 buffer used after tooth measurement is to check the agreement of all measured points to ensure reproducible results. The final step is for sterilization before new measurements are taken.<sup>204</sup> (b) Corresponding plot for carious (pH 6.16) vs healthy enamel (pH 6.99).<sup>201</sup> (c) Data representation showing pH variation between healthy root (pH 6.85), arrested caries (pH 6.07), and active caries (pH 5.3). Statistically significant differences were accepted when the *P*-value is <0.05.<sup>204</sup> (d) The reverse pH gradient evident within cancerous cells through multiple stages of acidosis (physiological extracellular pH (pH<sub>e</sub>) ≈ 7.4, acute acidosis pH<sub>e</sub> ≈ 6.8, and chronic acidosis pH<sub>e</sub> ≈ 6.7). pH<sub>i</sub> stands for intracellular pH.<sup>182</sup> (e) The tumor itself can be identified by its acidic pH via nanosonophore assisted multispectral photoacoustic imaging.<sup>210</sup> (f) Transport of protons from cytoplasm to extra-cellular fluid via a proton pump. ATP stands for adenosine triphosphate. (g) pH<sub>e</sub> map using chemical exchange saturation transfer (CEST) magnetic resonance imaging (MRI) in a subcutaneous Michigan Cancer Foundation-7 (MCF-7) mouse model with a Gaussian filter.<sup>211</sup> Reproduced with permission from ref 204, 201, 204, 182, 210, and 211, respectively. Copyright 2018 American Chemical Society. Copyright 2016 Elsevier. Copyright 2018 American Chemical Society. Copyright 2013 Damaghi, Wojkowiak, and Gillies under CC-BY-3.0 <https://creativecommons.org/licenses/by/3.0/>. Copyright 2017 Springer Nature, Ltd. under CC BY 4.0 <https://creativecommons.org/licenses/by/4.0/>. Copyright 2015 John Wiley & Sons, Inc.

applications of pH sensors is in detecting dental erosion. Dental erosion is defined as the loss of tooth structure by acid dissolution.<sup>201</sup> The main cause of dental caries is due to the lack of oral hygiene, causing bacteria to grow on the teeth surface, and creating an acid as a byproduct.<sup>201</sup> Figure 7a shows the sensing setup, where sensing and REs are both attached to the tooth.<sup>202</sup> For the case of enamel cavities, the main clinical diagnosis is done by the visual cues and human judgment. However, this method is prone to human error and depends highly on the dentist's experience and skill.<sup>203</sup> There are other

ways to assist a dentist in evaluating dental caries, such as radiographic examination. However, early stages of teeth erosion cannot be detected using this method, due to its low sensitivity and high rate of false positives and negatives.

Since dental caries are fairly common, a quantitative method to evaluating them would be highly beneficial; especially since early diagnosis would improve oral health, minimize tooth loss, and ultimately improve overall health and quality of life.<sup>204</sup>

Under normal conditions, the salivary pH is maintained around 6.7–7.3.<sup>205</sup> When the pH of the saliva, specifically on

dental plaque or in dental cavity, is below a critical value of 5.5, it is an indicator of potential dental decay. Therefore, pH measurement can be used to assist the diagnosis of dental caries. Indeed, multiple papers reported that the sensors were able to detect significant pH differences between sound enamel (pH 6.99) and carious enamel (6.16) as well as healthy root (pH 6.85), arrested caries (pH 6.07), and active caries (pH 5.30) (Figure 7b,c).<sup>201,204</sup> Other studies have shown that irregular salivary pH could be a sign of diseases such as anxiety disorder and gingivitis, besides tooth decay.<sup>206–209</sup>

In general, there is great interest in developing a miniaturized pH sensor that works reliably on different areas of the mouth. However, there are numerous obstacles to this development. First, while the sensing surface of most sensors is extremely small (0.015 mm long and 0.75 mm wide<sup>204</sup>), the overall footprint of the pH sensor device is huge, and unsuitable for fine oral measurements. In addition, the rough surface of human teeth may also provide challenges to sensors with flat sensing surface.<sup>203</sup>

Researchers were able to overcome these issues by taking advantage of iridium oxide's (Ir/IrOx) unique properties, of being mechanically strong and chemically inert. Ir/IrOx was utilized in a needle-like shape pH sensor. The probe diameter was 300  $\mu\text{m}$ , and was capable of measuring the pH on all types of surfaces—even in deep cavities.<sup>201</sup> Moreover, due to the sensor's size, it is able to measure in between teeth, which has traditionally been the hardest. Using an Ir/IrOx needle as the sensing material effectively solved the issues of the sensor being too large and measuring on rough surfaces.

In fact, the pH sensors that adopted IrOx as the sensing material have all shown relative success (near Nernstian sensitivity and very high repeatability) in ex vivo testing.<sup>201,204</sup> As a result, iridium oxide is recommended for oral pH-sensing applications. Other sensing materials used, though less common, include tantalum oxide ( $\text{Ta}_2\text{O}_5$ ) and carbon microfiber.

Most reported pH sensors for monitoring tooth decay use the ISFET configuration (Section 4.1). Currently, most studies test teeth samples externally (ex vivo), before moving to in vivo testing, since the ex vivo testing environment is relatively more stable.

While a lot of progress has been made on oral pH sensors, there is much work to be done to develop a model that can work in clinical situations, as the environment becomes more complicated as pH sensors are moved from an external tooth to within the mouth. Within the mouth, other factors may interfere with the pH sensor's reading. For example, the effect of saliva on the pH sensor has not been fully investigated. Human saliva has numerous components, including many charged proteins. This may interfere with proper functionality of the pH sensor.<sup>204</sup> Also, the effect of oxygenated saliva on the sensors has not been fully explored.<sup>205</sup> Table 15 summarizes key works on tooth decay ex vivo measurements. For tooth decay applications, a sufficient pH range is 5–7 with calibration ranges usually extending farther on both sides, with ISFET configuration (Section 4.1) and metal oxides (Section 3.2.1), such as  $\text{Ta}_2\text{O}_5$  and IrOx.

## 7.2. In Vivo

**7.2.1. Glioblastoma.** Given that the  $\text{pH}_e$  of solid tumors is known to be acidic, as shown in Figure 7d,e, the measurement of pH in this region is essential to monitoring and treating cancerous growth (physiological  $\text{pH}_e \approx 7.4$ , acute acidosis  $\text{pH}_e \approx 6.8$ , and chronic acidosis  $\text{pH}_e \approx 6.7$ ).<sup>181,182,214</sup> Current in vivo

Table 15. Summary of the Key Works on Tooth Decay Ex Vivo Measurements

ref	testing surface/ environment	setup	sensing material	sensitivity	pH range	repeatability
Fujii et al. <sup>202</sup>	enamel teeth used For enamel samples	ion sensitive field effect transistor (Isfet)	tantalum oxide ( $\text{Ta}_2\text{O}_5$ )		4.8–6.8	standard error <0.3 pH
Ratanaporncharoen et al. <sup>204</sup>	18 extracted human tooth samples	Isfet	Ir/Irox	–56.96 Mv/Ph	3–9	relative standard deviation (RSD) among eight measurements were 0.09 and 1.67% in the first cycle, 0.06 and 1.09% in the second cycle, and 0.03 and 0.57% in the third cycle
Tabata et al. <sup>201</sup>	21 extracted human teeth (different types of cavities at different sites)	Isfet	Ir/Irox	–57.4 Mv/Ph	4–8	standard error for sound enamel area is 0.05 pH, for carious lesion area is 0.01 pH
Murakami et al. <sup>203</sup>	20 extracted carious tooth (divided into active/arrested)	Isfet	$\text{Ta}_2\text{O}_5$		5.3–6.8	each sample tested three times using different methods
Kaneto et al. <sup>212</sup>	on the surface of teeth (6 subjects, age 25–28)	Isfet	silicon microelectrode	–54 Mv/Ph	3.77–7.27	standard error up to 0.6 pH
Chaisiwamongkhon et al. <sup>205</sup>	commercial synthetic saliva and authentic human saliva		carbon microfiber		2–8	max standard error 0.08 pH
Gashti et al. <sup>213</sup>	attachment surface of a biofilm of the oral bacteria, <i>Streptococcus salivarius</i>		$\text{Ag}/\text{SiO}_2^+$ fluorescein isothiocyanate (FITC) nanoparticles		4.3–7.3	

Table 16. Summary of the Representative  $\text{pH}_e$  Sensing Works

ref	sensing material	experimental setup	sensitivity	pH range
Chung et al. <sup>22</sup>	$\text{IrO}_x$	potentiometric	$-69.9 \pm 2.2 \text{ mV/pH}$	4–10
Munteanu et al. <sup>222</sup>	carbon fiber modified with reduced graphene oxide and syringaldazine	voltammetric pH microsensor	$-60 \pm 2.5 \text{ mV/pH}$	
Marzouk et al. <sup>226</sup>	$\text{IrO}_x$	potentiometric	$-63.5 \pm 2.2 \text{ mV/pH}$	2–10
Das et al. <sup>227</sup>	palladium oxide thin film	extended gate field effect transistor (EGFET)	$-62.87 \text{ mV/pH}$	2–12

tumor pH measurement is largely performed by pH-sensitive positron emission tomography (PEmT) radiotracers, magnetic resonance spectroscopy (MRS), magnetic resonance imaging (MRI), and optical imaging.<sup>215</sup> PEmT uses radiolabeled DMO to determine the pH gradient, but is largely inaccurate and imprecise. MRS and MRI monitor metabolic and physiologic processes. MRS uses chemical shifts between pH-dependent and -independent resonances to determine pH.<sup>216</sup> Overall there is room for development in in vivo pH measurement of cancerous cells, and the methods available require consideration of their respective drawbacks and advantages.

**7.2.2. Intracellular and Extracellular  $\text{pH}_i$ .**  $\text{pH}_i$  is also another useful biomedical indicator to suggest the conditions within a cell, and thus the health of that cell. In vivo measurement of  $\text{pH}_i$  ideally should be sensitive and not affect the subject. There are a number of methods to obtain this pH, including nuclear magnetic resonance spectroscopy, pH microelectrodes, and pH-sensitive fluorescent reporters.<sup>217</sup> One can determine  $\text{pH}_i$  from the negative logarithm based 10 of the acid dissociation constant ( $\text{pK}_a$ ) and  $\text{pH}_e$  of a weak acid or base exposed to the cell. Nuclear magnetic resonance uses the ratio between protonated and deprotonated phosphate groups to determine the pH with great accuracy. Once pH-sensitive microelectrodes are prepared and calibrated, they act as miniaturized pH meters and are best applied to larger cells to provide accurate results. Fluorescent indicator dyes can measure varying pH within a cell by close monitoring of the cell under a microscope. There are also pH-sensitive fluorescent proteins which act similar to the dye but can be coded within the cell itself.<sup>217</sup> Consideration of each method's sensitivity and accuracy and set up is necessary to determine the ideal intracellular sensor for a particular application.

$\text{pH}_e$  is the pH of the extracellular fluid outside of the cell. Many mechanisms exist that export  $\text{H}^+$  ions, produced by oxidative metabolism and fermentation, into the extracellular fluid.<sup>211</sup> Figure 7f is a simplified schematic of  $\text{H}^+$  ions being transported to the exterior of the cell from the interior by a proton pump, establishing a concentration gradient.

Acid–base homeostasis plays a vital role in maintaining physiological and cellular responses.<sup>218</sup> Healthy cells maintain a normal  $\text{pH}_e$  of around 7.4 by biological buffers.<sup>219</sup> In a highly acidic or basic  $\text{pH}_e$ , cellular functions, such as enzyme activity and DNA synthesis, are greatly diminished or ceased completely.<sup>218</sup> Thus, a deviation from the normal  $\text{pH}_e$  may be an indication of a disease or a physiological abnormality.

Another example is that deviation from the normal  $\text{pH}_e$  can impair the immune response, especially in acidic environments, due to inhibition of lymphocyte activity.<sup>218</sup> An instability of  $\text{pH}_e$  can also be an indication of metabolic abnormalities.<sup>22</sup> Furthermore, insulin resistance in skeletal muscle cells may be correlated to the lowered  $\text{pH}_e$ , as the insulin receptor's phosphorylation level, also known as activation, was diminished.<sup>220</sup> Interestingly,  $\text{pH}_e$  is found to range from 5.7 to 6.1

during the early stages of wound healing. In addition, cancer cells have been found to have a lower  $\text{pH}_e$  than a normal cell (which in turn promotes drug resistance and increases invasiveness<sup>221</sup>). While these cancer cells maintain a close to normal  $\text{pH}_i$ , their  $\text{pH}_e$  is found to be more acidic, ranging from 6.2 to 6.9,<sup>219</sup> than the surrounding blood and tissues, which have a pH of 7.4.<sup>222</sup> This acidity is caused by the dependency on anaerobic metabolism where an excess amount of lactic acid is produced by glycolysis, due to insufficient removal from tumor vasculature.<sup>223</sup> The acidity is also caused by a large amount of  $\text{CO}_2$ .<sup>223</sup>  $\text{pH}_e$  can also have an effect on the uptake of anticancer drugs and how tumor cells respond to therapy.<sup>223</sup> Because the maintenance of  $\text{pH}_e$  plays a key role in physiological and cellular functions, it is important to have an accurate, precise, and reliable device that will determine the  $\text{pH}_e$  value in vivo.

There are many devices that are used for detecting  $\text{pH}_e$ , including microelectrodes, radionuclide imaging, MRI relaxometry, and MRS.<sup>211</sup> Microelectrodes are miniaturized electrodes with ion-selective membranes that are sensitive to changes in  $\text{pH}_e$ .<sup>224</sup> One configuration that uses electrodes is the potentiometric pH sensor, which uses an ion-selective sensing electrode and RE to determine  $\text{pH}_e$ . ISFET and EGFET configurations can also be used, but they require a transistor in their configurations.<sup>112</sup> In addition, microelectrodes can be interdigitated to increase surface area.<sup>121</sup> Radionuclide imaging uses PEmT to detect pH-sensitive radiolabeled probes.<sup>211</sup> Fluorescence utilizes the properties of dyes to measure  $\text{pH}_e$  optically.<sup>211</sup> MRI relaxometry examines the pH-dependent relaxation rates.<sup>225</sup> Figure 7g shows an example of a  $\text{pH}_e$  map, using MRI and a Gaussian filter. MRS is a noninvasive technique that analyzes changes in  $\text{pH}_e$ .<sup>211</sup> These techniques and devices for measuring  $\text{pH}_e$  must be highly sensitive, be highly selective, display long-term stability, and have the ability to be used in vivo. Table 16 shows different experimental set-ups to measure  $\text{pH}_e$  and their sensitivities. In most cases, metal oxide (Section 3.2.1) sensing films are utilized in different configurations (Section 4) due to their biocompatibility and facile deposition methods. Although the reported pH ranges are relatively wide,  $\text{pH}_e$  variation is usually within less than 1 pH unit around the neutral value (i.e., pH 7).

**7.2.3. Oral Hygiene.** Salivary pH marks an important biological marker for many bodily diseases, including periodontal disease such as gingivitis, and dental caries, which was discussed in Section 7.1.2. Due to saliva's noninvasiveness and ease of collection, storage, and shipping, saliva has great potential for pH testing.<sup>206</sup>

While, in recent years, physical monitoring systems—such as heart rate monitors and temperature sensors—have evolved, developing an accurate pH sensor is still a challenge in health monitoring. Overcoming this challenge would enable additional biomedical sensing applications and lead to a more personalized medical care.<sup>228,229</sup>

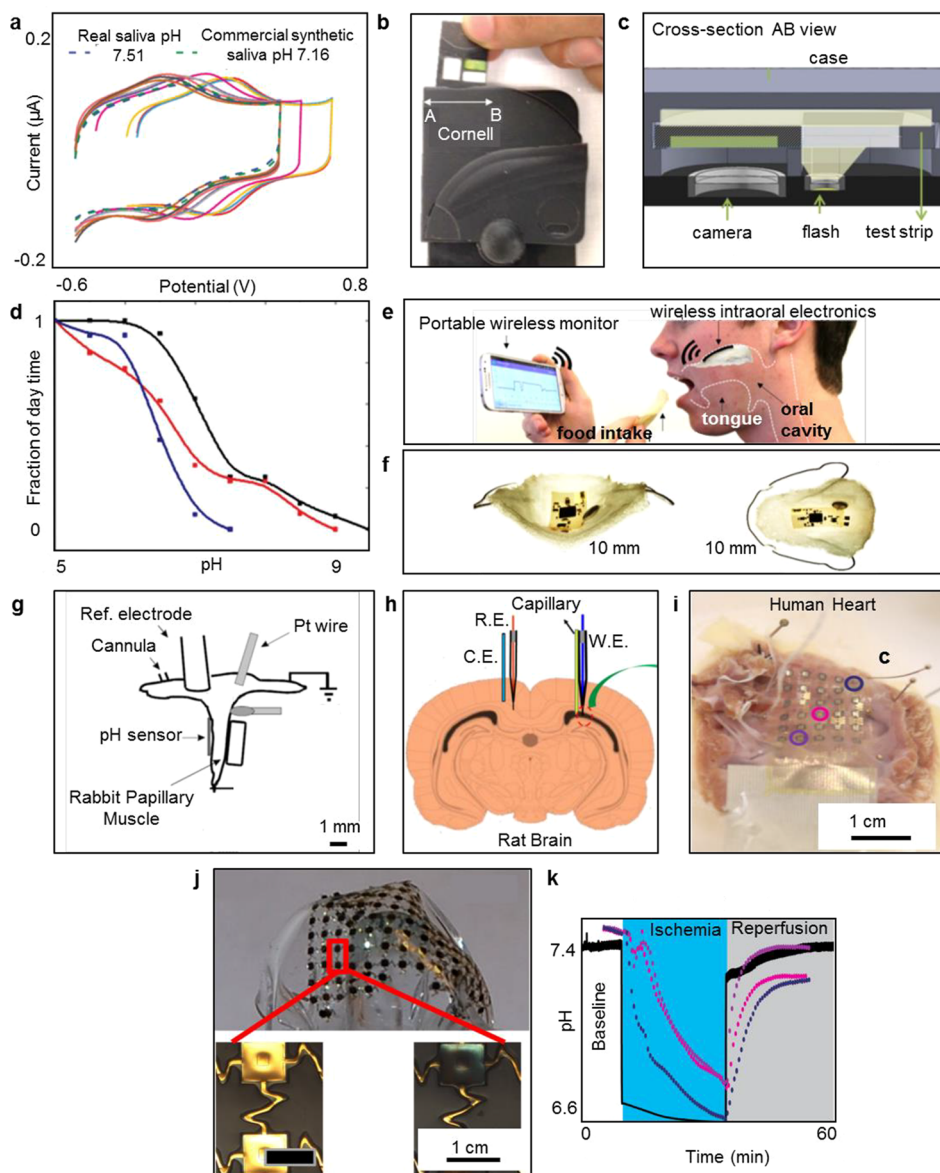


**Figure 8.** pH sensing in biomedical applications (in vivo oral hygiene and ischemia tests). (a) pH readings from commercial synthetic saliva with actual saliva.<sup>205</sup> The green dotted line represents measurement from commercial synthetic saliva sample, and the blue dotted line represents the real saliva sample's results, having pH values of 7.16 and 7.51 respectively. The cyclic voltammetry scan rate is 4 V/s to remove the influence of any oxygen reduction reaction, and the solid lines represent results from prepared synthetic saliva samples of various pH values. (b) A digital image and a (c) cross-section of the phone case setup that is used for colorimetric analysis of pH strips,<sup>231</sup> and (d) test result from three male individuals (aged 25–37) during 16 h of regular day time, showing variation in pH.<sup>231</sup> (e, f) An overview of the sodium and pH-sensing system, with Na<sup>+</sup> sensitivity of 60 mV/decade vs Ag/AgCl reference electrode (RE), long-term stability of 1 week, and low detectability limit of 10<sup>−4</sup> mol/L.<sup>228</sup> (g) Different components of the sensor inserted into the papillary muscle of the rabbit heart used to indicate pH drop with ischemic episodes.<sup>232</sup> (h) 1,2-Naphthoquinone (1,2-NQ) pH sensor insertion into the rat brain for in vivo ischemia testing. The results showed a normal pH of 7.21, 7.13, and 7.27 in the striatum, hippocampus, and cortex regions, respectively, and a decreased pH upon global cerebral ischemia of 6.75, 6.52 and negligible change in the striatum, hippocampus, and cortex regions, respectively. R.E., W.E., and C.E. stand for reference, working, and counter electrodes, respectively.<sup>233</sup> (i) IrOx pH sensors array tested on the right ventricle of a human heart in OCP configuration, with a response time as low as 0.5 s and a sensitivity of 69.9 mV/pH. The results indicated a drop in pH from 7.4 to 6.55 during ischemic episodes. Location of pH sensors specified by colored circles (navy, pink, purple).<sup>234</sup> (j) An overview and a zoom in on the same pH sensors array in part (i) on a flexible surface.<sup>234</sup> (k) Time vs pH during ischemia periods, for a human heart showing a drop in pH from 7.4 to 6.6.<sup>234</sup> Reproduced with permission from refs 205, 231, 228, 232, 233, and 234, respectively. Copyright 2017 Royal Society of Chemistry. Copyright 2013 Royal Society of Chemistry. Copyright 2018 National Academy of Sciences. Copyright 2002 Elsevier. Copyright 2016 American Chemical Society. Copyright 2013 John Wiley and Sons, Inc.

Many different factors are in play for oral and salivary pH, including the human's diet and time of the day during measurement. Having a pH sensor that can closely monitor pH variations may enable more targeted studies, for example,

studying the corrosiveness and effects of different sugary beverages on oral pH.<sup>230</sup>

pH measurement can either be done within the mouth, or the saliva can be collected in a test tube. In vivo testing is harder than ex vivo testing, since the uneven surface within the oral cavity

Table 17. Summary of the Representative Oral pH Sensing Works

ref	testing environment	setup	sensing material	pH range	sensor abilities
Watanabe et al. <sup>236</sup>	inside the test subject's mouth		IrO <sub>x</sub>	5.0–9.0	operating time: 19 h, maximum error of 0.15 pH
Oncescu et al. <sup>231</sup>	human subjects	an indicator strip, a reference strip and a flash diffuser	pH strip	5.0–9.0	repeatability depends greatly on phone model (i.e., camera quality)
Lee et al. <sup>228</sup>	in human subjects, and in solutions	sensor placed on a flexible film			
Baliga et al. <sup>206</sup>	test subjects with different level of periodontal conditions	single electrode digital pH meter	single electrode digital pH meter		maximum standard error is 0.11 pH
Chaisiwamongkho et al. <sup>205</sup>	commercial synthetic saliva and authentic human saliva	in vitro		2–8 pH	max standard error 0.08 pH
Hans et al. <sup>230</sup>	collected human saliva	glass type electrode	digital pH meter		standard error lower than 0.3 pH for coffee, Pepsi, fruit drink, but up to 1.25 pH for milk

proves to be a challenge, as current rigid sensors and plastic boards are not suited for oral insertion.

As a result, there are not many reported cases where actual sensors are attached on the inside of the oral cavity, most likely due to the convenience of ex vivo testing. Developing a sensor that is compatible to work inside the human mouth requires extensive research, since the environment within the mouth (uneven surface, different temperatures, and disturbance from mouth-movement) can lead to inaccuracy and repeatability issues in the measurements. Meanwhile, carrying out tests on saliva outside of human body does not change its pH, and greatly increases the accuracy of measurement. Unlike tooth testing, where it is necessary to test directly on the tooth surface (since removing the tooth from the body is not plausible), saliva can be easily collected into a test tube.

Thus, in most cases, commercial pH sensors are used to measure the pH externally for several reasons. For instance, although commercial pH sensors offer great consistency and accuracy, they are usually bulky and not easily implantable. Since a wide pH range is not needed (the normal pH of saliva is 6.7–7.4), most sensors used in this application operate between a range of 5.0–9.0.<sup>230</sup> As a result, during these ex vivo tests, it is simply easier and more efficient to use a commercial pH sensor instead of developing a new sensor, since a commercial pH sensor can accomplish the same purpose and is readily available for purchase. Developing pH sensors that can operate under the unique environment of the mouth still faces challenges. For example, the oxygenated environment of the mouth has an effect on pH measurement. Researchers were able to successfully combat this challenge, as shown in Figure 8a, as the carbon fiber-based pH sensor showed comparable results from commercial synthetic saliva and real saliva samples, where both are oxygenated biological samples with pH values of 7.16 and 7.51 respectively. This means that the sensor was able to overcome the interference caused by an oxygenated environment, using cyclic voltammetry with a scan rate of 4 V/s to remove the influence of any oxygen reduction reaction.<sup>205</sup> Another example is studying the role that the physical state of food plays in its cariogenic potential. The longer the sugar is stuck to the teeth, the longer the bacteria act on sugars and produce acid, leading to development of dental caries. In this case, liquid sugars has lower cariogenic potential than solid and sticky sugars, as they tend to stick to the teeth surface due to their property of adherence.<sup>230</sup>

While many researchers focused on developing a miniaturized pH sensor that is flexible and insertable, Oncescu et al. overcame this challenge with a rather simple solution: the researchers developed a system that uses a smart-phone application to

measure the pH of a testing strip in a self-designed case, by taking a picture and analyzing the color through a phone's application.<sup>231</sup> However, the accuracy of this system can be questionable, as many different factors (such as temperature and humidity) can alter the results. The case is shown in Figure 8b, and the exact design is shown in Figure 8c. The study showed great variation between different test subjects. Figure 8d shows test results from three male individuals (aged 25–37), during 16 h of regular day time, showing great variation in pH. Moreover, the smart-phone model and camera could greatly change the results. As a result, the system's accuracy needs further improvements.

Worth mentioning, sodium sensors also prove to be a good indicator of personal health. In addition, they can monitor sodium intake for people who have high blood pressure, hypertension, diabetes, and obesity. Thus, it could prove valuable to develop a system that integrates both a pH sensor and sodium sensor to monitor a wide range of different conditions. Lee et al. incorporated sodium sensors onto a stretchable plastic film, and then attached it onto a retainer.<sup>228</sup> Figure 8e shows the how the sensor is attached, and Figure 8f shows the sensing platform, showing sensitivity for Na<sup>+</sup> ions of –60 mV/decade concentration vs Ag/AgCl RE, long-term stability of 1 week, and low detectability limit of 10–4 mol/L.

Overall, oral and salivary pH levels are accurate indicators of oral and overall body health. In most cases, the saliva is collected and tested externally, due to the ease of the procedure. While sensors that can be orally inserted can be a good alternative, there are only few research studies in this area. Finally, the use of sodium sensors should be considered and integrated with the pH sensor for both expanding applications and validation of sensor readings. Table 17 summarizes key works on oral pH sensors. Commercial and research quality pH sensors have been reported for oral pH studies, and the results indicate the validity of the investigated pH systems for oral pH assessment. Saliva pH lies in the 6–7 pH range with temporary perturbations taking place based on what is being eaten or drunk. An extended lower pH (~5.3–6.16 pH) value is indicative of tooth decay (Section 7.1.3).

**7.2.4. Ischemia.** Out of the numerous biomedical applications pH sensors have, ischemia is certainly among the most important ones. Ischemia is defined as an inadequate blood supply to an organ or part of the body, especially the heart muscles. When oxygen supply is cut off to the cells, the cells are only able to create ATP through glycolysis, and produce H<sup>+</sup> as a byproduct. As of now, ischemia is very hard to detect, and a sensor that can detect ischemic metabolism can result in

individualized treatment and improve patient's overall condition.<sup>237</sup> In addition, pH variation is known to indicate metabolic function abnormality, and accurate monitoring of the pH can greatly assist clinicians by giving them valuable information about the condition of the organ, resulting in more accurate diagnosis and better treatment.<sup>234</sup>

Specifically, in the case of heart ischemia, researchers believed that both the magnitude of the pH shift and the duration of ischemia are important in the heart's ability to resume normal function.<sup>237</sup> In the brain, having an accurate pH sensor can allow scientists to gain a better understanding of the role pH plays in brain diseases.<sup>233</sup>

During ischemia periods before an Ischemic stroke,<sup>238</sup> an inadequate blood supply prevents the accumulation of extracellular potassium ions, and cuts off the oxygen supply, therefore triggering the anaerobic metabolism that produces lactic acid. Most importantly, pH in the affected area usually experiences notable decrease. Since these events happen simultaneously, pH value and ion concentrations, such as potassium ( $K^+$ ), lactate ( $C_3H_5O_3^-$ ) or sodium ( $Na^+$ ), are good indicators and early detectors of ischemia.

In fact, during ischemic episodes, potassium ions' concentration can increase up to four times its normal level.<sup>238</sup> As a result, an integrated sensor, which has pH,  $K^+$ , and other ion detectors integrated onto one sensor could be beneficial. Doing so would provide higher confidence in the data, due to the potential of validation of sensor readings.

There is still much work to be done in order to develop a sensor that is suitable for biomedical use. As shown in previous works,<sup>238,239</sup> the sensors developed all performed well in salt and buffer solutions, with high sensitivity and repeatability. However, when sensors are tested under in vivo conditions in living animal tissues, the measurements are less accurate and tend to fluctuate, with significantly lower sensitivity and repeatability. In addition, there are many other difficulties involving manufacturing miniaturized pH sensors used for in vivo testing. For example, glass electrode sensors are currently most commonly used; however, these electrodes are large and bulky, easy to break, and difficult to be miniaturized for implants.<sup>233</sup> Moreover, the complex environment within the heart requires the sensor to have certain qualities, such as flexibility. The continuous movement, complex curved structure, low stiffness, and heterogeneous surfaces pose substantial engineering challenges for mapping the heart's pH.<sup>234</sup>

In addition, due to the invasive nature of inserting a sensor into the body, the specific procedure is important. Also, the placement of the sensor may have an effect, due to the uneven surfaces of the human body. Figure 8g shows the configuration of the pH sensor tested on the rabbit's heart papillary muscle. The device was used to observe drops in pH with ischemic episodes. Figure 8h shows the 1,2-naphthoquinone (1,2-NQ) pH sensor tested in a rat brain. The results showed a normal pH of 7.21, 7.13, and 7.27 in the striatum, hippocampus, and cortex regions, respectively, and a decreased pH upon global cerebral ischemia of 6.75, 6.52 and negligible change in striatum, hippocampus, and cortex regions, respectively. Figure 8i shows an array of IrOx pH sensors tested on the right ventricle of a human heart in OCP configuration, with a response time as low as 0.5 s and a sensitivity of  $-69.9$  mV/pH. The results indicated a drop in pH from 7.4 to 6.55 during ischemic episodes.

Researchers who used traditional methods mostly opted to use IrOx as the sensing material, citing its high sensitivity and

stability, wide range of pH detection, rapid response times, minimal drift, outstanding chemical selectivity, and high durability.<sup>234</sup> The sensing setup consists of a RE and a miniaturized sensing electrode or array. The size of the sensing surface on the sensing node is 1 mm, making it suitable for in vivo testing. Arrays of sub-millimeter-scale and precision pH sensors distributed on thin elastic membranes were also reported for in vivo testing.<sup>234</sup> The structure and zoom-in view of the individual sensors is shown in Figure 8j. On the other hand, several studies used a nontraditional photometric sensor for ischemic pH measurements<sup>235</sup> and achieved successful real-time monitoring. Using the photometric pH sensor, the severity of the episode is correlated with a decrease in pH and restricting the blood flow. In addition, it was found that during ischemic episodes, there is a noticeable decrease in the pH of the surrounding tissues. In Figure 8k, time (in minutes) is plotted against pH, and showed significant reduction in pH during ischemia for a human heart from a pH of 7.4–6.6.

In conclusion, there are many obstacles facing the development of an accurate sensor for use in detecting ischemia, including the flexibility and ability of the sensor to work in the heart's environment. The available studies suggest that traditional ways of pH analysis do not work well given the obstacles, and newer ways of pH sensing could result in better implantable sensors with higher sensitivity, repeatability, lower drift, and overall better quality. Table 18 summarizes works on pH sensors for monitoring ischemia. The physiological pH range for monitoring ischemia is pH 6–8, and, similar to  $pH_e$  (Section 7.2.2), metal oxides (especially IrOx) are commonly used as the pH-sensing material.

**7.2.5. Sweat Analysis.** Sweat, a fluid produced by the body to reduce body temperature, is also a common external bodily fluid for measuring pH and is critical to assess the physiological health of an individual. Sweat is secreted by the sweat gland. Sweat has a pH range between 5 and 7, which is acidic in comparison to a neutral pH in blood. It is composed of different substances, both organic and inorganic.<sup>240</sup> The substances include amino acids, minerals, lactic acid, urea, salts, fatty acids, and trace elements.<sup>241</sup> Despite these many compounds in sweat, approximately 99% of sweat is composed of water.<sup>242</sup> Since sweat includes cations such as sodium, potassium, and magnesium, it is important that the sensor to be used is selective for  $H^+$ , so that the cations are not falsely accounted for while determining the measurement of pH. Sweat is a useful bodily fluid because it can be stored for the long-term, is easy to measure noninvasively, and is less prone to alterations compared to other body fluids.<sup>242</sup> In fact, humans perspire at a rate between 300 and 700 mL/day, and during exercise, may perspire at a rate of 1.4 L/h. Thus, sweat is a plentiful source for pH measurements.<sup>243</sup>

Assessing the pH and analytes of sweat is important as it can be used for early detection of diseases in the human body, as it is correlated to the blood. One such disease is diabetes. Diabetes often causes more acidic pH levels in the body. With diabetes, an individual often develops diabetic ketoacidosis, a condition in which many ketones are produced, causing a very acidic blood pH.<sup>244</sup> Another is cystic fibrosis, a condition that affects the digestive system and lungs. A basic pH ( $\sim 9$ ) can be an indicator of cystic fibrosis, due to the lack of reabsorption of bicarbonate ions.<sup>245,245–247</sup> In addition to being a useful way to detect diseases, sweat can also be used to detect drugs. According to the pH partition theory, bases are likely to accumulate in acidic

Table 18. Summary of the Representative Works on pH Sensors for Monitoring Ischemia

ref	issue investigated	tested medium	sensing material	setup	sensitivity	pH range	repeatability
Rai et al. <sup>238</sup>	myocardial ischemia (heart)	pH buffer solutions	tantalum oxide	ion sensitive (ISFET)	0.07 $\mu$ A/pH	6.5–8.0	
Marzouk et al. <sup>239</sup>	ischemic heart	ischemic rabbit papillary muscle	Ir/IrO <sub>x</sub>			6.4–7.4	standard error $\pm$ 0.2 pH
Zhou et al. <sup>233</sup>	in vivo monitoring meter for pH	rat brain (in vivo)	1,2-naphthoquinone	ratiometric microelectrochemical meter		5.8–8.0	max standard error 0.09 pH
Soller et al. <sup>237</sup>	develop a sensor which could detect ischemic metabolism	dog heart					mean pH at 2 h: standard error around 0.09 pH
Anastasova et al. <sup>239</sup>	develop a flexible sensor that can detect pH, K <sup>+</sup> , Na <sup>+</sup> ions to assess ischemia	salt solutions	IrOx membrane	miniature glass electrode/photometric sensor	–24.2 mV/pH to –73.4 mV/pH	6.8–7.8	relative standard deviation of 0.9–3.4% $\pm$ 0.05 pH
Steward et al. <sup>235</sup>	evaluate effectiveness of the miniature glass electrode and the photometric sensor for ischemia	dog heart					
Chung et al. <sup>234</sup>	thin, stretchable sensor for monitoring ischemia	explanted rabbit hearts and a donated human heart	IrO <sub>x</sub>	open circuit potential (OCP)	–69.9 $\pm$ 2.2 mV/pH	4.0–10.0	

fluids such as sweat.<sup>248</sup> Therefore, basic drugs usually accumulate in the individual's sweat.<sup>242</sup>

Devices that measure the pH of sweat include fabric/flexible plastic-based sensors, and epidermal-based sensors. They can be worn during exercise and could be used for real-time monitoring of the sweat from an individual.<sup>249</sup> The fabric/flexible plastic-based sensors have textiles and fabrics with special properties, and are in constant contact with the skin.<sup>250</sup> Epidermal-based sensors (i.e., elastomeric stamps and tattoos) are usually printed directly on the skin.<sup>251</sup> Table 19 summarizes works on pH sweat monitoring. Potentiometric (i.e., OCP) configuration is the most widely used in sweat analysis, due to the simplicity of the setup.

Table 19. Summary of the Representative Works on pH Sweat Monitoring

ref	setup	pH range	sensitivity	response time (s)
Caldara et al. <sup>243</sup>	optical pH sensor	2–10	205 Hz/lux	110
Dang et al. <sup>247</sup>	potentiometric	5–9	–11.13 $\pm$ 5.8 mV/pH	<8
Guinovart et al. <sup>252</sup>	potentiometric	3–11		<60
Guinovart et al. <sup>251</sup>	potentiometric	3–7	$\sim$ –54 mV/pH	<25
Guinovart et al. <sup>253</sup>	potentiometric	3–9	–90 mV/pH	$\sim$ 50
Yin et al. <sup>68</sup>	potentiometric	4–7	–63.7 mV/pH	
Curto et al. <sup>254</sup>	barcode pH sensor microfluidic platform	1–12		<20
Curto et al. <sup>249</sup>	optical pH sensor	4.5–8		

## 8. STATUS QUO

Complementing the discussed sections on various pH-sensing biomedical applications, from the ex vivo (Section 7.1) to the in vivo (Section 7.2), this section focuses on notable progress and the status quo for wearable and implantable pH-sensing systems.

### 8.1. Wearable pH-Sensing Systems

Wearable electrochemical sensors are promising for a variety of biomedical applications, due to their noninvasiveness and ease of use. Examples include detecting hormone levels, oxygen concentration, ion concentration, and pH levels. Their non-invasiveness gives these devices a potential for large-scale use. Their ease of use makes them accessible to the general population. An ideal wearable electrochemical pH sensor would be miniaturized, while still preserving high performance, high reliability, and a Nernstian response.<sup>247</sup> They should also have low manufacturing costs and great flexibility, to follow the contours of the human body.<sup>240</sup> Examples of wearable sensors are illustrated in Figure 9. Figure 9a shows the conceptual design of a band-aid wearable pH sensor on a human model, utilizing cotton yarns dyed with carbon nanotube ink, with a response time <60 s, and sensitivity of –59 mV/pH in potentiometric configuration vs a Ag/AgCl RE in the 3–11 pH range.<sup>252</sup> Figure 9b shows the structure of an ISFET pH sensor configuration for wound monitoring, using Al<sub>2</sub>O<sub>3</sub> gate dielectric and sensitivity of –50 mV/pH in the 3.3–11.4 pH range.<sup>255</sup> These pH sensors are useful for early detection of a disease, assessing human performance, and other useful applications.<sup>250</sup> These pH sensors often measure pH from sweat, wounds, and saliva. Since there

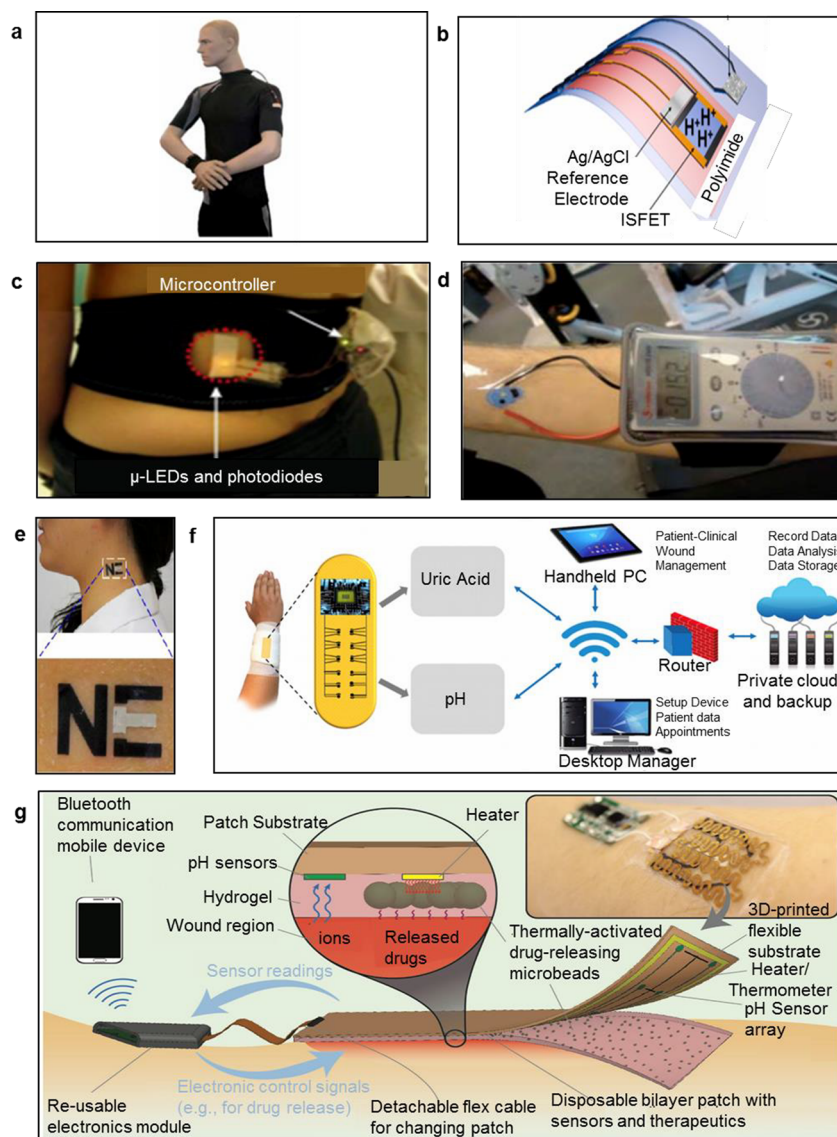


**Figure 9.** Wearable pH sensors. (a) Illustration of band-aid sensor on human model. The sensor utilized cotton yarns dyed with carbon nanotubes ink and showed a response time  $<60$  s, and a sensitivity of  $59$  mV/pH in potentiometric configuration vs Ag/AgCl reference electrode (RE) in the 3–11 pH range.<sup>252</sup> (b) Schematic of a wearable device integrating the ion sensitive field effect transistor (ISFET) configuration, with an  $\text{Al}_2\text{O}_3$  gate dielectric and a sensitivity of  $-51.2$  mV/pH in the 3.3–11.4 pH range.<sup>255</sup> (c) Representative application of wearable pH electrochemical sensor.<sup>265</sup> (d) Entire epidermal tattoo pH sensor experimental setup attached to the wrist to measure pH of human perspiration.<sup>251</sup> (e) Wearable example of a tattoo epidermal-based sensor for biomarkers (such as lactate) assessment of sweat.<sup>250</sup> (f) Schematic of a smart wound care pH sensor integrated with a uric acid sensor.<sup>263</sup> (g) Schematic of a full-setup of a smart bandage, including an integrated pH sensor, temperature sensor, drug loaded hydrogel, and an electronic heater to release drugs on-demand.<sup>264</sup> Reproduced with permission from refs 252, 255, 265, 251, 250, 263, and 264, respectively. Copyright 2013 Royal Society of Chemistry. Copyright 2017 American Chemical Society. Copyright 2014 MDPI (Basel, Switzerland) under CC-BY-3.0 <https://creativecommons.org/licenses/by/3.0/>. Copyright 2013 Royal Society of Chemistry. Copyright 2014 Elsevier. Copyright 2018 Electrochemical Society. Copyright 2018 John Wiley and Sons.

are other substances in sweat and other outer bodily fluids, the device must be highly selective and only measure the activity of  $\text{H}^+$ . In addition, some of these sensors may be wireless or stretchable to allow for ease of movement and portability,<sup>247</sup> and may integrate other sensors as well, such as temperature and glucose sensors,<sup>256</sup> as the integrated disposable sweat monitoring strip. The integrated sensors include pH, glucose, and temperature sensors. The pH sensor included a PANI sensing electrode in OCP configuration vs Ag/AgCl RE and showed nonlinear voltage dependence of pH in the 4–7 pH range.<sup>256</sup>

A common application of these wearable sensors is measuring the pH in sweat. As mentioned in Section 7.2.5, sweat is a very

popular body fluid to measure due to its ease of measurement. However, it does contain other substances, both organic and inorganic, such as sodium ions and glucose.<sup>240</sup> Sweat usually has a normal physiological pH on the more acidic side, ranging from 5 to 7 due to its composition of minerals, lactic acid, and urea.<sup>241</sup> Measuring analytes in sweat—since it is correlated to blood—can be an indicator for diseases, such as diabetes and hypochloremia.<sup>247</sup> Wearable sweat sensors can be categorized into two types: fabric/flexible plastic-based sensors, and epidermal-based sensors. Fabric/flexible plastic-based sensors have constant contact with the skin.<sup>250</sup> Textiles, which are tough, flexible, and react to external stimuli,<sup>257</sup> are printed on the fabric

Table 20. Summary of the Representative Wearable pH Sensor Developments

ref	setup	sensitivity	response time (s)	sensing material	pH range	sensed medium
Dang et al. <sup>247</sup>	potentiometric	$-11.13 \pm 5.8$ mV/pH	<8	graphite-polyurethane composite	5–9	sweat
Guinovart et al. <sup>252</sup>	potentiometric	$-59$ mV/pH	<60	cotton yarns dyed with carbon nanotubes ink	3–11	sweat
Bandodkar et al. <sup>251</sup>	potentiometric	$\sim -54$ mV/pH	<25	poly(aniline) (PANI) associated with the reversible emeraldine salt (ES)–emeraldine base (EB) transition	3–7	sweat
Karyakin et al. <sup>253</sup>	potentiometric	$-90$ mV/pH	$\sim 50$	PANI	3–9	sweat
Nyein et al. <sup>68</sup>	potentiometric	$-63.7$ mV/pH		PANI	4–7	sweat
Curto et al. <sup>249</sup>	optical pH sensor			methyl red, bromocresol green, bromocresol purple and bromothymol blue dyes	4.5–8	sweat
Guinovart et al. <sup>262</sup>	potentiometric	$-58 \pm 0.3$ mV/pH	<20	electropolymerized PANI	4.35–8	wounds
Nakata et al. <sup>255</sup>	ion sensitive field effect transistor (ISFET)	$-51.2$ mV/pH		Al <sub>2</sub> O <sub>3</sub>	3.3–11.4	sweat
Giachet et al. <sup>266</sup>	textile-based optical sensor			curcuma-dyed cotton/curcuma-dyed polyamide	curcuma dyed cotton: 6.5–8.5; curcuma dyed polyamide: 8.5–13.0	buffer solutions
Rahimi et al. <sup>267</sup>	potentiometric	$-53$ mV/pH	58	PANI	4–10	wounds
Bandodkar et al. <sup>251</sup>	potentiometric	$-50$ mV/pH	25	PANI	3–7	sweat

plastic-based sensors. These textiles must not affect the pH of the skin where the sensor is measuring.<sup>258</sup> Fabrics that are often used include wool, cotton, and nylon, since they have the chemical and physical properties for an optimal electrochemical pH sensor. A representative wearable pH sensor is provided in Figure 9c. Epidermal-based PANI pH sensors in potentiometric configuration vs Ag/AgCl ink electrode, as shown in Figure 9d, measure pH by having conformal contact with the skin.<sup>251</sup> These sensors exhibited a sensitivity of  $-50.1$  mV/pH (increased with stretching up to  $-59.6$  mV/pH), a response time between 10 and 25 s, and a batch- to-batch relative standard deviation of 4.63% ( $n = 4$ ) in the 3–7 pH range. Similarly, elastomeric stamps and tattoo sensors (Figure 9e) printed directly onto the skin have been reported for detection of other biomarkers in sweat, such as lactae.<sup>250</sup> These types of sensors use various pH-sensing configurations, such as potentiometric, ISFET and EGFET configurations (discussed in Section 4). Epidermal pH-sensing hydrogel fibers have also been reported for detecting wound healing and skin disorders, thus, overcoming the susceptibility to long-term degradation, as in the case of electrochemical electrodes exposed to sweat.<sup>259</sup>

Interestingly, wearable sensors are especially applicable for monitoring infant physiological health and, more importantly, are useful for early detection of potential life-threatening health conditions. Due to an infant's inability to communicate verbally, sensors must provide clinicians and parents with critical health information at home or in a neonatal intensive care unit (NICU), while avoiding irritation, interruption of sleep, or causing stress to the infant.<sup>260</sup> Another application of wearable pH sensors is measuring a wound's pH. Wounds are particularly costly to a patient and may fail to heal properly.<sup>261</sup> Whereas the pH of healthy skin tends to be more acidic, in the range 5–5.5, wound pH tends to be more basic, typically having a pH ranging from 7 to 8.5.<sup>262</sup> There is a correlation between pH values and wound healing. The healing process may also be affected by the pH value beneficially, or detrimentally.<sup>262</sup> Therefore, it is important to have tools that can accurately monitor a wound's pH. Figure 9f,g shows schematics of different smart wound

monitoring systems that are integrated with uric acid sensors,<sup>263</sup> temperature sensors, drug loaded hydrogel, and an electronic heater to release drugs on-demand.<sup>264</sup> Table 20 summarizes key wearable pH sensor developments. Despite the many advantages that these wearable, noninvasive pH sensors present, these wearable pH sensors still have serious limitations and challenges. With normal body movement, epidermal-based pH sensors may show mechanical malfunctions. Some pH sensors also may not have long-term stability and may not be sensitive to highly acidic or highly basic solutions.<sup>250</sup> In addition, wearable sensors are often not worn over a long period of time, due to the physical discomfort it may cause for the user.<sup>260</sup> Therefore, many improvements need to be made on these wearable devices in order to promote large-scale public use and accessibility.

## 8.2. Implantable pH Sensing Systems

While wearable pH sensors may offer a noninvasive, easy-to-use option for users, they are limited to measuring only substances found outside of the body. This mainly includes fluids produced by the body, such as sweat, saliva, urine, and open wounds. Implantable sensors, on the other hand, allow for wider opportunities of application. Though significant work must still be done, development of a miniaturized, implantable sensor presents the opportunity to monitor real-time pH levels anywhere in the human body, including blood, the esophagus, and brain tissue. pH is an effective parameter in the blood for many circumstances, as discussed in Section 6.3. In these circumstances, such as for sickle cell disease, it is beneficial to determine pH measurements in vivo.<sup>174</sup> A miniature fiber optic pH sensor was produced for physiological use and was tested in the jugular vein of a sheep.<sup>174</sup> Utilizing fiber optics, a pH-sensitive dye contained within a H<sup>+</sup> permeable envelope is implanted in the area of interest, in this case the vein, and the optical density of the dye is then measured by illuminating the dye through a single strand fiber and sensing the back scattered light through another optic fiber strand that is connected to a remote light detector.<sup>174</sup> The sensor functioned within the physiological pH range of 7.0–7.4, and when tested in vivo, the

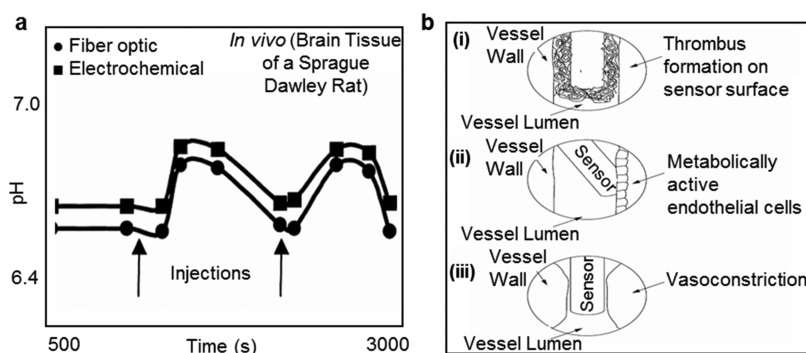


**Figure 10.** Implantable pH sensors. (a) Silica-based fiber optic (●) and IrO<sub>x</sub> electrochemical (■) measurements of tissue pH in response to injections of sodium bicarbonate into the peritoneal cavity at 3 and 18 min, showing a reasonable response time of ~5 s, sensitivity of  $-57.9$  mV/pH after 85 min, and a drift of  $0.4$  mV/h.<sup>175</sup> (b) Analytical performance of intravascular sensors can be influenced by (i) thrombus formation on the sensor surface, (ii) “wall effect” caused by positioning the sensor near metabolically active endothelial cells, and (iii) vasoconstriction around the sensor.<sup>268</sup> Reproduced with permission from refs 175 and 268. Copyright 2001 Elsevier. Copyright 2002 Elsevier.

**Table 21.** Summary of the Representative Implantable pH Sensors

ref	sensing material	reference material	setup	location	response time	pH range	sensitivity
Frost et al. <sup>268</sup>	(1) Copolymer of <i>n</i> -butylmethacrylate and 2-methacryloxyloxyethyl phosphorylcholine. (2) pH indicator reagent dyes (e.g., phenol red).		(1) Fiber optics (2) Microdialysis catheter, sensors	blood vessels			
Goldstein et al. <sup>174</sup>	pH sensitive dye contained within a H <sup>+</sup> permeable envelope		fiber optics	jugular vein of a sheep	42 s	7.0–7.4	
Cao et al. <sup>162</sup>	IrO <sub>x</sub>	Ag/AgCl	frequency sensing	esophagus wall of a pig		1.9–12	$-51.1$ to $-57.7$ mV/pH
Grant et al. <sup>175</sup>	● Silica optical fibers ● IrO <sub>x</sub>	Ag/AgCl	● Optoelectronics ● Electrochemical	brain tissue of a rat	5 s	6.6–7	$-57.9$ mV/pH
Hao et al. <sup>269</sup>	polyvinylchloride (PVC) matrices onto carbon fiber electrodes	Ag/AgCl	potentiometric	brain tissue of a rat	<1 s	6–8	$-58.4$ mV/pH
Wencel et al. <sup>270</sup>	8-hydroxypyrene-1,3,6-trisulfonic acid (HPTS) encapsulated in sol-gel matrix		fiber optics	human tissue	<2 min	6–8	

results were comparable, if not better than a commercial glass electrode, with a response time of 0.7 min.<sup>174</sup> Implantable pH sensors can also help with the treatment of patients that had traumatic brain injury.<sup>175</sup> Grant et al. developed silica-based fiber optic and IrO<sub>x</sub> potentiometric sensors to monitor the pH of brain tissue.<sup>175</sup> When tested *in vitro* in blood, the fiber optic sensor demonstrated a Nernstian value of  $-57.9$  mV/pH, and the electrochemical sensor showed similar results at  $-57.8$  mV/pH vs Ag/AgCl RE, with a response time of 5 s and a drift of  $0.4$  mV/h.<sup>175</sup> Both were implanted in the brain of a Sprague–Dawley rat model, and sodium bicarbonate was injected into the peritoneal cavity of the rat to change the pH of the brain tissue.<sup>175</sup> Both sensors reacted similarly; however, they displayed different results, due to a calibration issue (Figure 10a).<sup>175</sup> The test ran for 50 and 165 min—thrombus formation may occur for longer durations.<sup>175</sup>

Although miniature fiber optic pH sensors show promise in monitoring the pH *in vivo*, results are vastly affected by biological responses.<sup>268</sup> Some of these responses include thrombus formation due to the absorption of proteins on the sensor’s surface, the “wall effect” caused by placing the sensor near metabolically active endothelial cells, and reduced blood flow from vasoconstriction around the sensor (Figure 10b).<sup>268</sup> These responses are reduced when implanting in larger blood vessels.<sup>268</sup>

Implantable sensors can also be used in different organs. Cao et al. developed an implantable, battery-free, and wireless

capsule with pH sensors in order to monitor gastroesophageal reflux disease (GERD).<sup>162</sup> The pH sensor utilized iridium oxide as the sensing material vs Ag/AgCl RE, and demonstrated Nernstian values between  $-51.1$  and  $-57.7$  mV/pH in the pH range 1.9–12.<sup>162</sup> When tested in the esophagus wall of a pig and compared to a commercial pH sensor, it showed comparable results and performed better when introduced to an alkaline solution of pH 11.<sup>162</sup> Unlike the commercially available sensors, this device has no limit on monitoring duration and is a suitable option for monitoring real time pH.<sup>162</sup>

Table 21 summarizes key implantable pH sensors. With significant advantages seen in implantable pH sensors, the most important is the wide range of application possibilities. Several studies successfully monitored in real-time the pH level in blood, the esophagus, and the brain. However, the biological response of the body and the lack of reliable performance of the implanted devices pose substantial challenges.<sup>268</sup> Hao et al. demonstrated a viable route to address the fouling of the sensing membrane due to biological deposits.<sup>269</sup> This is done using an H<sup>+</sup> selective membrane with polyvinyl chloride (PVC) matrices onto carbon fiber electrodes in a potentiometric setup. The sensor exhibited improved antifouling property and reversible and repeatable results, even after three hours *in vivo* (inside rat’s brain, with response time <1 s and  $-58.4$  mV/pH sensitivity). Furthermore, Wencel et al. demonstrated a robust ratiometric fiber optics-based pH sensor in human tissue.<sup>270</sup> The sensor used a 8-hydroxypyrene-1,3,6-trisulfonic acid (HPTS) in hydrogel matrix

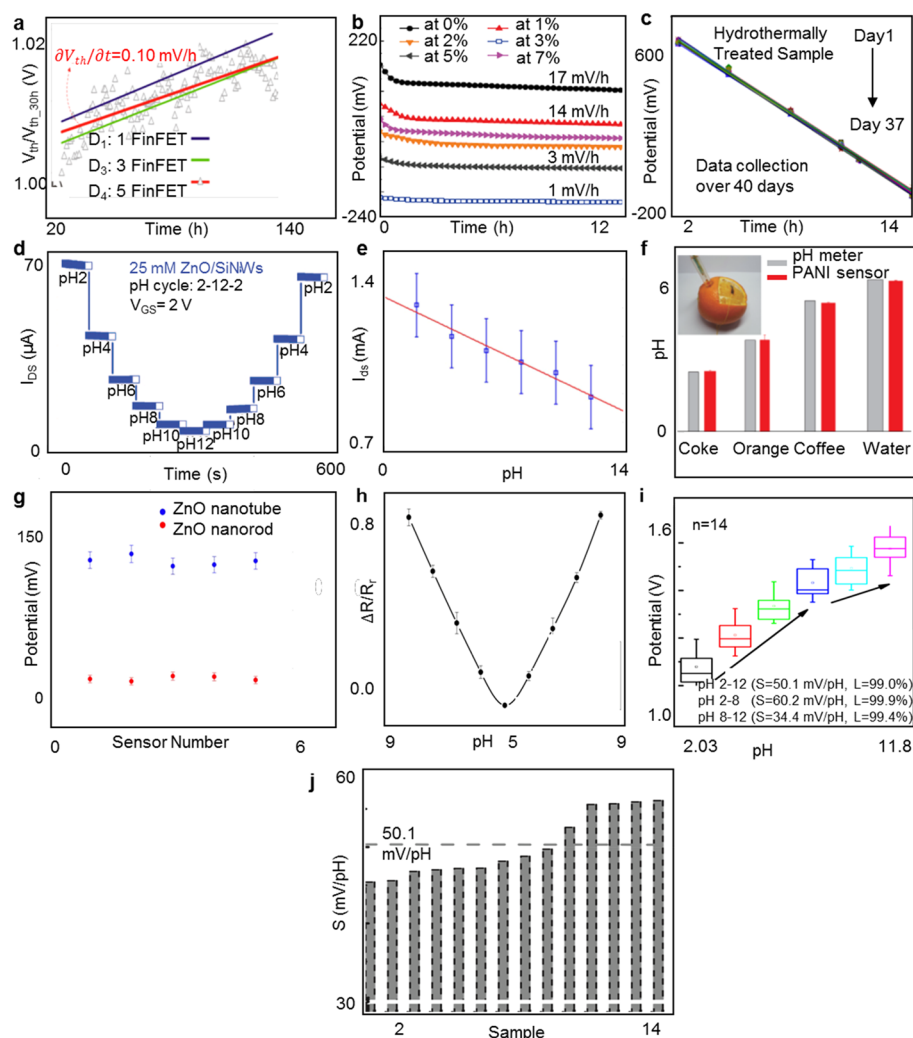


**Figure 11.** Stability, repeatability, and reproducibility assessment of pH sensors. (a) Drift at pH 6 with time for three different fin field effect transistor (FinFET) in liquid gate configuration devices normalized at the initial  $V_{th}$  at time (h) = 30: D1 (single wire with fin thickness (TFin) = 30 nm), D3 (three wire FinFET with TFin = 20 nm), and D4 (five wire FinFET with TFin = 30 nm). The device used  $HfO_2$  as gate dielectric and sensing material and silicon nanowire channels, showed a sensitivity of  $-57$  mV/pH vs Ag/AgCl reference electrode (RE), and excellent stability when tested for 105 h. The single wire FinFET (D1) showed a drift of  $0.13$  mV/h, a 3-wire FinFET (D3) showed a drift time of  $0.1$  mV/h, and a 5-wire FinFET (D4) showed  $0.12$  mV/h.<sup>178</sup> (b) Drift characteristics of the undoped ZnO and aluminum doped ZnO (AZO) nanostructured pH-EGFET sensors measured within pH = 7 for the duration of 12 h, with drift values ranging from 1 to 17 mV/h.<sup>58</sup> (c) Fitting curves of 13 tests after 24 h of hydrothermal hydration of Ir/IrO<sub>2</sub> at 220 °C, recorded over 40 days. Measured cell potentials were carried out against a commercial Ag/AgCl (saturated KCl) RE; the device sensitivity range is  $-59$  to  $-70.5$  mV/pH.<sup>271</sup> (d) Hysteresis of  $\sim 5$   $\mu$ A measured in ZnO/SiNWs-based pH sensor in extended gate field effect transistor (EGFET) configuration, as a time vs drain source current, with sensitivity of  $-66$  mV/pH.<sup>136</sup> (e) pH plotted against drain source current for CuS-based pH sensor in EGFET configuration, with error bars typically representing standard deviation through pH 7–4–7–10–7 cycle and sensitivity of  $-23.3$  mV/pH. The sensor exhibited repeatability with a relative standard deviation (RSD) of 0.04%, 0.02%, and 0.38% for glass, tungsten and Si substrates, respectively.<sup>274</sup> (f) Test results in Coke, orange, coffee, and water from a commercial pH sensor and a flexible polyaniline (PANI) nanopillars-based pH sensor in OCP configuration vs Ag/AgCl RE, showing good repeatability. The columns represent average values from five readings, and the error bars typically represent the standard deviation of the measurements. The sensor has sensitivity of  $-60.3$  mV/pH, drift of  $0.64$  mV/h in pH 5, drift of  $0.49$  mV/h in pH 7, response time of 1 s, and sustained performance over 1000 mechanical bending cycles.<sup>60</sup> (g) Reproducibility test of five ZnO nanotube electrodes and five ZnO nanorod electrodes vs Ag/AgCl RE in OCP configuration, with a sensitivity of  $-45.9$  and  $-28.4$  mV/pH, respectively, showing excellent reproducibility, with error bars representing relative standard deviation of 5%.<sup>36</sup> (h) Plot of normalized resistance and pH value across five single-walled carbon nanotube (SWNTs) sensors in resistance-based configuration with response time varying from 2.26 s in pH 5 to 23.82 s in pH 9 and sensitivity of  $236.3$   $\Omega$ /pH. A droplet has been placed and removed 10–15 times before the sensor showed the depicted stable response. The dots show the average values, and the error bars represent standard deviation from the five devices.<sup>118</sup> (i) Plot showing pH value and output voltage of 14 indium tin oxide (ITO)/polyethylene terephthalate (PET)-EGFET electrode samples and (j) Their sensitivity (S) (average of  $-50.1$  mV/pH).<sup>143</sup> Reproduced with permission from refs 178, 58, 271, 136, 274, 60, 36, 118, and 143, respectively. Copyright 2015 American Chemical Society. Copyright 2013 Hindawi under CC-BY-3.0 <https://creativecommons.org/licenses/by/3.0/>. Copyright 2017 Springer Nature, Ltd. Copyright 2013 Electrochemical Society. Copyright 2017 Elsevier. Copyright 2017 Elsevier. Copyright 2009 MDPI (Basel, Switzerland) under CC-BY-3.0 <https://creativecommons.org/licenses/by/3.0/>. Copyright 2011 2009 MDPI (Basel, Switzerland) under CC-BY-3.0 <https://creativecommons.org/licenses/by/3.0/>. Copyright 2012 Elsevier.

Table 22. Summary of the Stability Results of Various pH Sensors

ref	setup	pH range	sensing material	reference material	stability
Wang et al. <sup>272</sup>	open circuit potential (OCP)	1–13	IrO <sub>2</sub>	Ag/AgCl	average of 10 calibration curves over period of 2.5 years: <i>k</i> and slope = −58.4 mV/pH
Wang et al. <sup>271</sup>	OCP	1.68–12.47	Ir/IrO <sub>2</sub>	Ag/AgCl	<ul style="list-style-type: none"> <li>• E2 had a stable, gradual, negative potential drift</li> <li>• E3 remained relatively constant without much potential drift over 40 days</li> </ul>
Wang et al. <sup>147</sup>	extended gate field effect transistor (EGFET)	1–13	aluminum-doped ZnO (AZO)	Ag/AgCl	Al dosage of 3% best drift rate at 1.27 mV/h over 12 h
Rigante et al. <sup>178</sup>	FinFET	3–10	HfO <sub>2</sub>	Ag/AgCl	<ul style="list-style-type: none"> <li>• Single wire FinFET: drift time of 0.13 mV/h.</li> <li>• 3-wire FinFET: drift time of 0.1 mV/h</li> <li>• 5-wire FinFET: 0.12 mV/h (all over 105 h)</li> </ul>
Li et al. <sup>168</sup>	ion sensitive Field effect transistor (ISFET)		indium tin oxide (ITO)/ polyethylene terephthalate (PET)	Ag/AgCl	drift rate <1.7 mV/h over ~8.5 h
Kurzweil et al. <sup>20</sup>	ISFET	1.6–12.2	Ru/RuO <sub>2</sub>	Ag/AgCl	0.13 mV/pH (pH 4) 0.38 mV/pH (pH 7) 7.31 mV/pH (pH 10) (over 13 min)
Zhou et al. <sup>177</sup>	OCP	2.22–11.81	IrO <sub>2</sub>	Ag/AgCl	<ul style="list-style-type: none"> <li>• Over 86 h: potential drift 0.3 mV/h</li> <li>• First 30 h: potential drift 0.6 mV/h</li> </ul>
Vanamo et al. <sup>273</sup>	OCP	1–9	poly(3,4-ethylenedioxy thiophene) doped with poly(styrenesulfonate) anions (PEDOT/PSS) film	Ag/AgCl	<ul style="list-style-type: none"> <li>• After overnight short-circuiting, measured for 30 min: −3.24 mV/h and +4.08 mV/h</li> </ul>

on an optical fiber tip and exhibited reliable performance, indicated by the low drift (0.003 pH in 22 h in lab setup and 0.004/h in vivo). These studies highlight the rapid advancements in pH sensing, and collectively, show the importance of pH sensing in biomedical applications.

## 9. CHALLENGES

Evidently, throughout Sections 4–8, there are common challenges that persist, mainly those pertaining to the reliability of pH-sensing measurements. This section discusses reliability issues, such as stability, repeatability, and reproducibility. All these issues are critical milestones for a pH-sensing system to be suitable for biomedical applications and mass production. Furthermore, the modeling and theoretical aspects of pH-sensing mechanisms are discussed, and the challenges facing accurate predictions that comply with experimental results are highlighted.

### 9.1. Stability of pH-Sensing Devices

Although significant progress has been made on the improvement of pH-sensing systems, stability is still a challenge. Electrodes suffer from potential drift over time which makes it practically difficult to obtain consistent values. This phenomenon is known to be influenced by a number of factors including the testing setup, sensing electrode material, RE material, and fabrication method.

Most glass electrodes and ISFET configurations show poor long-term stability.<sup>20,147</sup> The EGFET, on the other hand, has shown better results.<sup>147</sup> A less commonly used setup is the FinFET in liquid gate configuration. The device had critical features of 20 nm, used HfO<sub>2</sub> as gate dielectric and sensing material, and used a silicon nanowire channel. This device showed a sensitivity of −57 mV/pH vs Ag/AgCl RE and had excellent stability when tested for 105 h. The single wire FinFET showed a drift of 0.13 mV/h, a 3-wire FinFET showed a drift

time of 0.1 mV/h, and a 5-wire FinFET showed 0.12 mV/h (Figure 11a).<sup>178</sup>

Results of different testing set-ups show further improvements based on the type of material used for the sensing electrode. IrOx shows the promise of being a superior material for pH sensing in biological media. It demonstrated a fast and stable response in aqueous, nonaqueous, nonconductive, and corrosive media.<sup>20</sup> When used as the pH-sensing material for a miniature multiparameter sensor chip, it demonstrated a drift value of 0.3 mV/h over 86 h, with a rate of 0.6 mV/h for the first 30 h.<sup>177</sup> Research has also been done on the pH sensing and drift characteristics of hydrothermal AZO nanostructured sensors.<sup>147</sup> With 20 measured samples, Al dosage of 3% has the best drift rate at 1.27 mV/h for 12 h (Figure 11b).<sup>147</sup>

Alternative RE materials have also been investigated. For instance, a solid state thin-film RE composed of titanium/gold/silver/silver chloride (Ti/Au/Ag/AgCl) has been assessed for effectiveness as a RE.<sup>168</sup> This fabricated RE performed comparably with the standard silver/silver chloride (Ag/AgCl) RE, at a drift rate of 1.7 mV/h over 8.5 h.<sup>168</sup>

Table 22 summarizes stability results of key pH-sensing reports. A popular method for fabricating oxide thin films for sensing electrodes is thermal oxidation. However, the dry films produced exhibit significant aging effects.<sup>271</sup> Sufficient hydration during fabrication and preparation of electrodes has proven to be a key factor in reducing the amount of potential drift.<sup>271</sup> One method studied was high-temperature hydrothermal hydration treatment where Ir/IrO<sub>2</sub> electrodes were subjected to hydration at 220 °C for 24 h and then soaked in deionized water. Tested within a pH range of 1.68–12.47, electrodes that underwent this method exhibited good stability over the course of 40 days, attributed to the more orderly crystal arrangement and high content of OH<sup>−</sup> groups as shown in Figure 11c.<sup>271</sup> Measured cell potentials were carried out against a commercial Ag/AgCl (saturated KCl) RE in OCP configuration, and the device

Table 23. Summary of the Repeatability Assessments of Various pH Sensors

ref	sensing material	reference material	repeatability	setup
Huang et al. <sup>136</sup>	ZnO/Si nanowires (NWs)	Ag/AgCl	The sensor is slightly more sensitive to acidic than basic solutions	extended gate field effect transistor (EGFET)
Sabah et al. <sup>274</sup>	CuS/glass CuS/W CuS/Si	Ag/AgCl	hysteresis: CuS/glass: 0.48 mV CuS/W: 11.72 mV CuS/Si thin film: 11.05 mV	EGFET
Huang et al. <sup>283</sup>	Si NWs	Ag/AgCl	hysteresis: about 0.8 mV hysteresis: relative standard deviation (RSD) of less than 2% in the 3–13 pH range	EGFET
Wu et al. <sup>284</sup>	touch panel film (TPF)	Ag/AgCl	deviation (RSD) of less than 2% in the 3–13 pH range	ISFET
Yoon et al. <sup>60</sup>	polyaniline (PANI) nanopillar	Ag/AgCl	hysteresis: 1.9 mV compared to initial voltage of 473.1 mV	open circuit potential (OCP)
Prats-Alfonso et al. <sup>282</sup>	IrO <sub>x</sub>	AgCl	hysteresis: 1.5–0.5 mV	OCP
Nguyen et al. <sup>275</sup>	IrO <sub>x</sub>	AgCl	Standard deviation is 0.2 pH units in 4–7 pH range and 0.4 pH units in pH 2	OCP
Salvo et al. <sup>285</sup>	graphene oxide (GO)	AgCl	Repeatability from three trials showed a standard deviation of ±0.2 pH units	OCP

sensitivity range is  $-70.5$  mV/pH with a constant intercept at 0 pH (standard reduction potential difference between sensing and RE) of 800.5 mV over the 40 days. When the same device was hydrated in DI water at room temperature for 24 h, a significant drift in the intercept at 0 pH from 901 to 563 mV was observed. Another method studied is referred to as the carbonate melt oxidation. A uniform iridium oxide film is coated on the surface of an iridium metal wire through oxidation of the wire in a carbonate melt.<sup>272</sup> In another study, using an Ir/IrO<sub>x</sub> electrode, 10 calibration curves were obtained in pH 1–13 over the span of 2.5 years for a long-term stability test. The results showed a stable linear response with the calibration curves overlapping, eliminating the need for frequent calibration.<sup>272</sup> Short circuiting has also been proven to reduce the need for frequent calibration, increasing the stability of electrodes.<sup>273</sup> After short circuiting two identical solid-contact ion-selective electrodes overnight, both drifted slightly toward their original potentials, one at  $-3.24$  mV/h and the other at 4.08 mV/h.<sup>273</sup>

## 9.2. Repeatability of pH-Sensing Devices

Like stability, repeatability is one of the biggest challenges facing pH sensors. Repeatability of a pH sensor means that it behaves the same way and outputs similar results every time it is in a similar solution. Although perfect repeatability is almost impossible to achieve, minimizing deviation is necessary in order to have confidence in the pH sensor's measurement.

This issue becomes especially important as the precision of the data increases, especially in critical applications, such as biomedical sensors.

Factors that contribute to the repeatability of a sensor include the sensor setup, sensing and RE's material, and fabrication process. Normally, the repeatability is measured by carrying out multiple trials of pH measurement in the same buffer solution, and calculating the standard deviation between trials. In this case, the quantitative measure of a sensor's repeatability is its deviation (in pH units), i.e., the lower the deviation, the better the repeatability.

Another route to evaluate repeatability is hysteresis, defined as a measure of how much the pH sensor is impacted by its previous reading (i.e., history). In EGFET, hysteresis is, typically, measured via a series of ( $I_{ds}$  vs time) curves, where the drain-source current ( $I_{ds}$ ) is plotted against time. Cycles of pH measurements were carried out between pH values 2 and 12, for 1 min each. The exact pH for the buffer solutions and time submerged in each buffer could change based on the particular experiment. The relative standard deviation

( $RSD = \frac{\text{standard deviation}}{\text{mean}} \times 100$ ) for the first and second pH measurements is then calculated. The repeatability is obtained by taking the difference between the RSD values at the same pH values. Figure 11d shows a representative hysteresis plot for ZnO coated SiNWs sensing electrode in EGFET configuration with a sensitivity of  $-66$  mV/pH and a hysteresis value of  $\sim 5$   $\mu$ A.

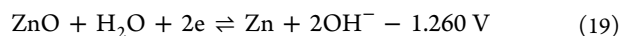
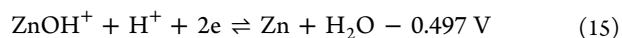
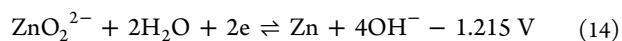
Another example for assessing pH sensors' repeatability is by calculating standard deviations for repeated measurements. Figure 11e,f shows an example of a repeated plot from pH 7–4–7–10–7 cycle, and multiple measurements in various environments, respectively, with error bars typically representing standard deviation from multiple runs (not explicitly defined in reports).<sup>60,274</sup> Figure 11e shows pH plotted against drain source current for CuS-based pH sensor in the EGFET configuration, with standard error bars showing repeatability through pH 7–4–7–10–7 cycle and sensitivity of  $-23.3$  mV/pH. The sensor exhibited repeatability with RSD of 0.04%, 0.02%, and 0.38% for glass, tungsten and Si substrates, respectively, and Figure 11f shows test results in Coke, orange, coffee and water from a commercial pH sensor and a flexible PANI nanopillars-based pH sensor in OCP configuration vs Ag/AgCl RE, showing good repeatability. The columns represent average values from five readings, and the error bars typically represent the standard deviation. The sensor has sensitivity of  $-60.3$  mV/pH, drift of 0.64 mV/h in pH 5, drift of 0.49 mV/h in pH 7, and a response time of 1 s. The flexible PANI pH sensor sustained performance over 1000 mechanical bending cycles, making it suitable for integration with other high performance flexible electronic components that have been demonstrated to survive such bending behavior for mechanically dynamic applications.<sup>276–281</sup> Nguyen et al. showed three measurement runs overlaid as another route for displaying pH sensor's repeatability, indicating acceptable repeatability from an IrO<sub>x</sub>-based pH sensor in OCP configuration vs Ag/AgCl RE with sensitivity of  $\sim -60$  mV/pH and response time of 30 s.<sup>275</sup>

Materials used for the sensor play a significant role in the sensor's repeatability. While most materials show relatively good repeatability, as shown in Table 23 (RSD of 2% for hysteresis, and pH standard deviation of less than 0.2 pH units across multiple trials), those that have a sensing electrode made of IrO<sub>x</sub> showed slightly lower repeatability. In an IrO<sub>x</sub> sensor, the residual standard deviation of the slopes (sensitivity) from 10 independent measurements is 3.4%.<sup>282</sup> Similarly, Nguyen et al.<sup>275</sup> utilized IrO<sub>x</sub> sensors and reported maximum pH standard

deviation across three trails of 0.4 pH units, significantly higher than the average of 0.2 pH units for graphene oxide. The reasoning given for this behavior is the subtle differences of nanoscale pore sizes in the iridium oxide film, quality, and uniformity of Ag/AgCl REs.<sup>275</sup> Hence, repeatability might especially be an issue when using IrOx-based pH sensors. On the other hand, pH sensors using Si NWs have consistently shown relatively better repeatability. A possible reason for Si NW's good repeatability is that the single crystal Si NWs structure is more reliable and stable.<sup>283</sup> Furthermore, a hybrid of Si NW and ZnO sensor exhibited a larger surface area and more binding sites than the pristine Si NWs for adsorbing additional ions, thus improving overall quality of the sensor.<sup>136</sup> Sabah et al. compared different kinds of copper sulfide hybrid sensors.<sup>274</sup> The hybrid material also played an essential role in the sensor's stability. While the method of fabrication, loop cycle, and loop length are all kept the same, changing the sensor's material from CuS/W to CuS/glass decreased the sensor's hysteresis from 11.78 mV to 0.48 mV.<sup>274</sup>

Finally, the setup of a sensor does not seem to have a significant correlation with its repeatability. Similar setups had sensors that exhibited both good and poor repeatability. Overall, while many details factor into the repeatability of the pH sensor, the most important one is the material used in the sensor. Another insight regarding repeatability is that sensors with good overall quality, such as high sensitivity, rapid response time, and low drift, have higher repeatability.

**9.2.1. Mixed Versus Specific Reactions.** A set of chemical reactions with associated standard reduction potential needs to be accounted for when extracting values for surface potential and pH. In the case of ZnO, for example, eqs 13–19 below are all possible chemical reactions that can take place at the sensing surface.<sup>132</sup> These reactions are included to demonstrate the fact that all possible reactions involving Zn ion redox reactions have negative potential, contrary to the typically reported positive values. This indicates competing mixed reactions where Zn ion redox is not a dominant reaction. However, during pH measurement, many different reactions (some expected, some unexpected) can happen between the sensing surface and the solution. Solution tested is not always pure and may contain ions that can also react with the sensing surface and cause unwanted exchanges. Under ideal conditions, only a few specific reactions happen during pH measurement and the sensor follows the Nernstian behavior (−59.18 mV/pH).



In their paper, Ghoneim et al.<sup>132</sup> explained ways to test if multiple reactions are taking place. The actual measured full cell potential is the difference between the two half-cell reactions, varying depending on the pH of tested solution given by eq 20:

$$E_{\text{cell}} = E_{\text{sense}} - E_{\text{ref}} - 59.18 \text{ mV} \cdot [\text{pH}] \quad (20)$$

In the equation,  $E_{\text{cell}}$  represents the measurement voltage difference,  $E_{\text{sense}}$  the standard reduction potential of the sensing

electrode, and  $E_{\text{ref}}$  the standard reduction potential of the RE. The chemical reaction that takes place at the RE is shown below in eq 21, and has a reduction potential of around 220 mV



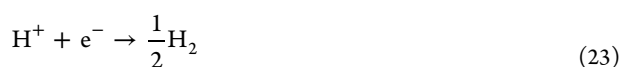
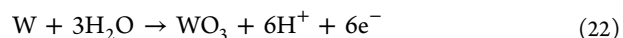
The reduction potential for REs are known, Ag/AgCl electrodes (which are used in almost all pH sensor setups) is known to be around 220 mV. Following the slope calculated from tests, the standard reduction potential (in mV) can be calculated at pH 0. At pH 0, the pH term in eq 20 equates to zero, the potential of RE is around 220 mV, and the voltage difference is the measurement of the pH sensor. Worth mentioning, this is a simplified example, whereas in practical cases there are other elements in the pH cell that consume portions of the observed voltage measurements. For instance, reference electrodes structure includes a porous or semipermeable membrane that allows ionic exchanges between the reference solution and the solution under test. The difference in ions' mobilities and concentrations within the reference electrode (such as 3 M KCl) and the outside solution (i.e., calibration buffers or test solutions) creates a concentration gradient and potential barrier. This is referred to as the liquid junction potential (LJP). The LJP cannot be directly measured and typically consumes a fraction millivolt to few millivolts across, resulting in  $\pm 0.01$  to 0.05 pH error in the pH measurement.

If sensing electrode's reduction potential is close to one of the known equations, then it can be reasonably concluded that the specific reaction is dominant. And expect a stable and repeatable performance. Sometimes, the effect of mixed potential can be obvious. In their paper, Ghoneim et al.<sup>132</sup> calculated the standard reduction potential at the ZnO electrode to be +869 mV, while eqs 13–19 all have negative values, indicating clear mixed potential in this particular case.

The involvement of mixed potential could result in many different unwanted consequences. For example, the sensitivity of the sensor will deviate from the ideal Nernstian response (higher or lower depending on the exact reactions that are happening on the surface). In addition, because the mixed potential reactions can lead to ions accumulating on the surface and ions dissolving in the solution, mixed potential could lead to corrosion and passivation of the sensing surface.<sup>132</sup>

In their paper, Meruva et al.,<sup>286</sup> it was stated that the mixed potential was correlated to the partial pressure level of oxygen ( $\text{pO}_2$ ). The reason behind it is that under higher  $\text{pO}_2$ , more oxygen resides on the sensing surface and interacts with the sensing surface more readily than in normal  $\text{pO}_2$  conditions.<sup>286</sup>

In another case, Macdonald et al.<sup>287</sup> developed a W/WO<sub>3</sub> pH sensor to test the pH under high temperature and pressure. The sensor showed lower values compared to the Nernstian sensitivity. The reduced sensitivity is attributed to a mixed potential. The provided explanation was that this behavior is expected because the W/WO<sub>3</sub> sensor is not an equilibrium system, but rather displays a mixed potential resulting from a balance between a partial anodic process (eq 22) and a partial cathodic reaction (e.g., eq 2).<sup>287</sup>



As shown, it is usually hard to identify what mixed potential reactions are taking place. Most of the time, it is a speculation. Hence, it is essential to understand that sometimes the

Table 24. Summary of the Representative pH-Sensing Works and the Likely Associated Reactions

ref	sensing material	standard reduction potential (mV)	reported potential	likely reaction
Macdonald et al. <sup>287</sup>	W/WO <sub>3</sub>		W+3H <sub>2</sub> O → WO <sub>3</sub> + 6H <sup>+</sup> + 6e <sup>-</sup> H <sup>+</sup> + e <sup>-</sup> → $\frac{1}{2}$ H <sub>2</sub>	mixed potential
Meruva et al. <sup>286</sup>	ionophore tridodecylamine (TDDA)	+465		mixed potential
Chung et al. <sup>234</sup>	IrO <sub>x</sub>	+922	Ir(OH) <sub>3</sub> ⇌ IrO(OH) <sub>2</sub> + H <sup>+</sup> + e <sup>-</sup> Ir(OH) <sub>3</sub> ⇌ Ir(OH) <sub>2</sub> O <sup>-</sup> + H <sup>+</sup> IrO(OH) <sub>2</sub> ⇌ IrO(OH)O <sup>-</sup> + H <sup>+</sup>	IrO <sub>x</sub> dominant reactions
Yang et al. <sup>288</sup>	IrO <sub>x</sub> reduced graphene (rGO)	+676	2[IrO <sub>2</sub> (OH) <sub>2</sub> ·2H <sub>2</sub> O] <sup>2-</sup> + 3H <sup>+</sup> + 2e <sup>-</sup> ⇌ [Ir <sub>2</sub> O <sub>3</sub> (OH) <sub>3</sub> ·3H <sub>2</sub> O] <sup>3-</sup>	mixed potential involving multiple oxidation states of Ir and/or reactions with negative standard reduction potential
Lonsdale et al. <sup>289</sup>	RuO <sub>2</sub>	+611	Ru <sup>(IV)</sup> O <sub>2</sub> + e <sup>-</sup> + H <sup>+</sup> ⇌ Ru <sup>(III)</sup> O(OH)	RuO <sub>2</sub> dominant reactions
Batista et al. <sup>114</sup>	ZnO	+636		mixed potential involving oxygen evolution
Ghoneim et al. <sup>132</sup>	ZnO	+869	oxygen evolution reactions	mixed potential involving oxygen evolution

Table 25. Summary of the Representative Reports on pH Sensors and Their Reproducibility Results

ref	setup	reproducibility	sensitivity	sensing material	pH range
Fulati et al. <sup>36</sup>	potentiometric	5 ZnO nanotube electrodes/5 ZnO nanorod electrodes	ZnO nanotube: -45.9 mV/pH ZnO nanorod: -28.4 mV/pH	ZnO nanotubes/ZnO nanorods	4–12
Voigt et al. <sup>290</sup>	ion sensitive field effect transistor (ISFET)	pH cycles	-54–59 mV/pH	diamond-like carbon (DLC) and Ta <sub>2</sub> O <sub>5</sub>	1–12
Bartic et al. <sup>291</sup>	interdigitated electrodes (IDEs)	sampling experiments of the drain current in time	-62 mV/pH	poly (3-hexylthiophene) semiconducting polymer	2–10
Li et al. <sup>118</sup>	resistance-based	5 sensors	236.3 Ω/pH	single-walled carbon nanotubes (SWNTs)	5–9
Lue et al. <sup>143</sup>	extended gate field effect transistor (EGFET)	30 samples in 3 different runs	-47.2, -48.6, and -51.0 mV/pH	indium tin oxide (ITO) thin films	2–12

speculation can result in wrong conclusions about what is actually happening at the sensing surface.

One potential way to is to scan the surface to see if there are structural changes to deduce the possible mixed potential reactions. It is reasonable to deduce that corrosion and passivation of the sensing surface may indicate the occurrence of mixed potential.

Another challenge is that it is not only hard to understand the exact reactions, but also no empirical solution exists. There are major difficulties to control specific reactions that occur on the sensing surface, and such methods are rarely discussed in recent reports. When mixed potential is interfering with the pH sensor's proper functionality, it may be helpful to change the sensing material.

In conclusion, mixed potential happens when certain ions in the solution/environment react with the sensing surface in an undesired way. A mixed potential artifact might show up as an unexpected standard reduction potential value or serious repeatability and stability issues. Further research is needed in order to accurately determine mixed potentials and suggest solutions to circumvent its effects. Table 24 summarizes representative works and the likely associated reactions. Although there are always competing mixed reaction, a relatively higher stability is correlated with a dominant reaction involving the ions at the sensing surface, pertaining to their reversible oxidation–reduction reactions.

### 9.3. Reproducibility of pH-Sensing Devices

Reproducibility, in which the same response to the same stimuli is given from device to device, is not to be confused with repeatability, in which the same response is given by the same device multiple times to the same stimuli, as shown in the previous subsection. Reproducibility of the response across multiple devices is important because devices often need to be replaced due to deterioration of materials and due to hygienic reasons.<sup>243</sup> In pH reproducibility tests, multiple devices are usually evaluated in specific buffer solutions. Ideally, devices should be reproducible in terms of sensitivity, stability, drift, and response time.

Fulati et al. reported a great example of reproducibility measurements across 10 pH potentiometric sensor electrodes (5 ZnO nanotube sensing electrodes and 5 ZnO nanorod sensing electrodes) at pH 6. In their paper, tests of 5 ZnO nanotube electrodes and 5 ZnO nanorod electrodes vs Ag/AgCl RE in OCP configuration, with sensitivity of 45.9 and 28.4 mV/pH, respectively, showed excellent reproducibility, relative standard deviation of 5%.<sup>36</sup> Figure 11g shows the results from the reproducibility test by Fulati et al. Diamond-like carbon thin films (DLC)- and Ta<sub>2</sub>O<sub>5</sub>-ISFET reproducibility and pH response for low pH values are also shown.<sup>290</sup> Another example of good reproducibility is in Bartic et al.'s experiment, using interdigitated electrodes with organic semiconductors.<sup>291</sup> In Li et al.'s experiment of SWNTs sensors, in resistance-based configuration with response time varying from 2.26 s in pH 5 to 23.82 s in pH 9 and sensitivity of 236.3 Ω/pH, reproducibility

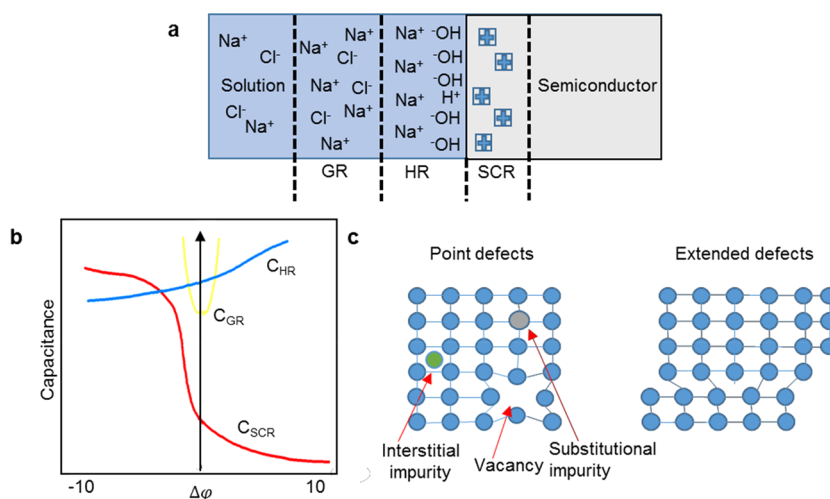


**Figure 12.** Modeling of pH sensors. (a) A simplified schematic of the space charge region (SCR), Helmholtz region (HR), and Gouy region (GR). (b) Dependence of potential on capacitance components at the semiconductor/electrolyte interface.<sup>300</sup> (c) Schematic of examples of point defects and extended defects. Reproduced with permission from ref 300. Copyright 2009 MDPI (Basel, Switzerland) under CC-BY-3.0 <https://creativecommons.org/licenses/by/3.0/>.

was reported across five sensors, finding the normalized resistances, as provided in Figure 11h, with a standard deviation of less than 5%.<sup>118</sup> Noteworthy, a droplet has been placed and removed 10–15 times before the sensor showed the depicted stable response.

To test the reproducibility of an ITO/PET electrode on EGFETS in the wide pH range between 2 and 12, Lue et al. reported on testing 14 ITO/PET electrodes. These 14 electrodes showed an average sensitivity of 50.1 mV/pH with a standard deviation of  $\pm 4.1$  mV/pH. Figure 11i shows the output voltage response of the samples at different pH, and Figure 11j shows the variation in sensitivity across the 14 samples.<sup>143</sup> In addition, Lue et al. prepared 30 samples in 3 different runs, reporting sensitivities of  $-47.2$ ,  $-48.6$ , and  $-51.0$  mV/pH across the runs.<sup>143</sup> These samples were also evaluated in solutions of different temperatures of 25, 40, and 50 °C. At high temperatures, sensitivity dramatically decreases to  $-21.8$  mV/pH. Lastly, these samples were evaluated over a long period of time (55 days) and still showed a sensitivity of higher than  $-45$  mV/pH and had linearity above 98.5%, which shows that these electrodes have both great stability and reproducibility.<sup>143</sup> Table 25 summarizes representative reports on pH sensors and their reproducibility results. Although few examples of good reproducibility have been reported, reproducibility discussions and results are rarely reported in most pH-sensing works.

#### 9.4. Modeling of pH-Sensing Devices

Many models have been developed to understand the mechanism of how pH is measured from the pH-sensing configurations. Devices, which measure the electrical potential, have sensing materials that are sensitive to changes in the activity of  $H^+$ .<sup>292</sup> An ideal device would be highly selective to  $H^+$  and has an ideal Nernstian sensitivity of  $-59$  mV/pH.

To understand how pH is found through electrical potentials, the following equation is used:

$$pH = pH_S + (E - E_S) \left( \frac{F}{2.30RT} \right) \quad (24)$$

where  $pH_S$  is the pH of the standard reference solution,  $E$  is the cell potential of the solution,  $E_S$  is the potential of the standard reference solution,  $F$  is Faraday's constant,  $R$  is the universal gas

constant, and  $T$  is the temperature in Kelvin.<sup>292</sup> Another important model to consider is the Nernst equation:

$$E = \frac{RT}{zF} \ln \frac{[X]_{out}}{[X]_{in}} \quad (25)$$

where  $E$  is the reduction potential,  $R$  is the universal gas constant,  $T$  is the temperature in Kelvin,  $F$  is Faraday's constant,  $z$  is the number of electrons,  $[X]_{out}$  is the concentration of ions outside the cell,  $[X]_{in}$  is the concentration of ions inside the cell.<sup>293</sup>

Particularly for the glass electrode, many models for the potential response have been developed. One model is the Donnan boundary potential model, stating that  $H^+$  and sodium ion diffusion through the glass membrane and the potential generated was caused by the difference of the diffusion rates of different ions.<sup>292</sup> However, later, it was discovered that  $H^+$  ions do not diffuse into the glass membrane.<sup>292</sup> Nikolsky, in 1937, theorized the ion exchange equilibrium theory, whereby establishing that the exchange of the protons by a sodium ion on a glass site leads to a potential difference.<sup>294</sup> Later, in 1967, Durst presented the idea that adsorption of  $H^+$  on the glass surface leads to a potential response.<sup>295</sup> In 1994, Bauke's ideas were published, which stated that the glass surface groups and the ions in aqueous solution are in dynamic equilibrium. The potential on the glass membrane and the potential difference between the glass and solution is caused by a dissociation mechanism.<sup>292,296</sup> A negative potential on the glass membrane is produced by a net-charge density by negatively charged groups.<sup>292,296</sup>

Cheng also proposed his hypothesis for the potential mechanism, whereby an electrode is a double-layer capacitor-based on the Guoy-Chapman model and Poisson–Boltzmann equation.<sup>292,297</sup> Interestingly, this viewpoint does not consider the potential difference to be caused by redox reactions. Instead, a potential is generated through the equation:

$$E_{capacitance} = E_{indicator} + E_{reference} \quad (26)$$

The sensing electrode and RE derive their potentials from the capacitance law,  $E = q/C$ , where  $q$  is the charge density and  $C$  is the capacitance.<sup>297</sup> This model considers how  $H^+$  and  $OH^-$

absorb to the electrode surface in acidic and basic solutions, respectively.<sup>297</sup>

Since Cheng's proposal was drawn from the Gouy–Chapman model, it is important to consider how this model explains a double layer of a surface. At the electrical interface, Helmholtz proposed that charges at the interface formed two layers of opposite charges.<sup>298</sup> However, this model did not account for adsorption of ions on the surface and diffusion of ions, and Guoy and Chapman determined there is a Gouy–Chapman diffuse double layer composed of an uneven distribution of anions and cations.<sup>299</sup> Because this model did not account for highly charged double layers, the Gouy–Chapman model was later modified by Stern to create the Gouy–Chapman–Stern model of what occurs at the metal/electrolyte interface to consider the finite size of an ion. It establishes that there is a Stern layer of ions adsorbing to the electrode surface along with the Gouy–Chapman diffuse layer.<sup>299</sup> These concepts are important because the electrode that measures pH interacts with H<sup>+</sup> and other ions at the metal/electrolyte interface, thus creating a capacitance, which is used to find the potential.

Overall, there are three regions in the model on the metal oxide/electrolyte solution interface where capacitance is measured: the space charge region in the semiconductor, the Helmholtz region, and Gouy diffuse layer, as mentioned earlier. A simplified schematic is provided in Figure 12a of the regions for reference. The total capacitance is found through the equation:

$$\frac{1}{c} = \frac{1}{c_{SC}} = \frac{1}{c_H} = \frac{1}{c_G} \quad (27)$$

where  $C_{SC}$  is the capacitance of the space charge region,  $C_H$  is the capacitance of the Helmholtz region, and  $C_G$  is the capacitance of the Gouy region.<sup>300</sup> Correspondingly, the potential is found through:

$$V = V_{SC} + V_H + V_G \quad (28)$$

Figure 12b shows the relationship between potential and capacitance components at the electrolyte/semiconductor interface.

The space charge region in the semiconductor, between the semiconductor surface and the electrode bulk, is where the majority carriers are depleted and an associated electric field arises.<sup>300</sup> The equation for capacitance ( $C_{SC}$ ) in this region can be found through the equation:

$$C_{SC} = \frac{\partial Q_S}{\partial U} = \left[ \frac{2}{q\epsilon_0\epsilon_S N_D} \left( V - V_{fb} - \frac{kT}{q} \right) \right]^{-1/2} \quad (29)$$

where  $Q_S$ , the space charge, is given by

$$Q_S = qN_D W = \left[ 2q\epsilon_0 N_D \left( V - V_{fb} - \frac{kT}{q} \right) \right]^{1/2} \quad (30)$$

$q$  is the elementary charge,  $\epsilon_0$  is the permittivity of a vacuum,  $\epsilon_S$  is the semiconductor dielectric constant,  $N_D$  is the density of an electron donor,  $V$  is the electrode potential,  $V_{fb}$  is the flat band potential,  $W$  is the width of the space charge layer,  $k$  is the Boltzmann's constant, and  $T$  is the temperature in Kelvin.<sup>300</sup> Specifically, for a n-type semiconductor electrode at open circuit, there is usually a positive charge and the band edges are upwardly bent by an energy of VSC due to the transfer of

electrons from electrode to solution as the redox potential of the electrolyte is lower than the Fermi level.<sup>300</sup>

The Helmholtz region is adjacent to the semiconductor surface and is a result of the adsorption of ions or of surface bonds between the solution species and surface.<sup>300</sup> Whereas the capacitance of the space charge region is considerably dependent on potential, the capacitance in the Helmholtz region has a little dependence. It is important to note that the potential in this region is entirely dependent on the interactions between semiconductor and electrolyte solution.<sup>300</sup> The concentration of H<sup>+</sup> near the solid surface [ $H_S^+$ ] is found through the following equation:

$$H_S^+ = [H_b^+] \exp\left(-\frac{e\psi_0}{kT}\right) \quad (31)$$

where [ $H_b^+$ ] is the Boltzmann distribution bulk concentration. Counter ions could also neutralize the surface charge by adsorbing to the surface. In this region, the capacitance, which is assumed to be constant, is found through the equation:

$$C_H = \frac{\sigma_0}{\psi_0 - \psi_\beta} \quad (32)$$

where  $\sigma_0$  is the surface charge and  $\psi_0$  and  $\psi_\beta$  is the surface potential of the solid and mean potential of adsorbed counterions at the plane, respectively.<sup>300</sup>

For pH devices in general, one model used to explain the mechanism is the site-binding model, which examines the chemical and electrical interactions on the surface of an oxide and solution. Based on the Gouy–Chapman–Stern model, an oxide surface, which contains a surface charge from H<sup>+</sup> and OH<sup>-</sup>, has two layers of constant capacitance and also includes an outer diffuse layer, as mentioned previously.<sup>138</sup> The model states that the changes in the surface potential voltage (i.e., at the sensing layer and electrolyte interface) is a function of the number of binding sites on the sensing membrane.<sup>113</sup> The Site-Binding Model is given by eq 33.

$$2.303(\text{pH}_{pzc} - \text{pH}) = \frac{q\psi}{kT} + \sinh^{-1}\left(\frac{q\psi}{kT\beta}\right) \quad (33)$$

where  $\text{pH}_{pzc}$  is the pH value at the point of zero charge,  $k$  is the Boltzmann's constant,  $T$  is the absolute temperature of the system in Kelvin, and  $q$  is charge of the electron, and  $\beta$  is the sensitivity parameter (defined in eq 34).<sup>301</sup>

$$\beta = \frac{2q^2 N_S (K_a K_b)^{1/2}}{KTC_{DL}} \quad (34)$$

where  $N_S$  is surface sites per unit area, where  $C_{DL}$  is the electrical double layer's capacitance,  $K_a$  is the acid equilibrium constant, and  $K_b$  is the base equilibrium constant.<sup>113</sup> When

$$\beta \gg \frac{q\psi}{kT} \quad (35)$$

then the surface potential can be simplified into

$$\psi = 2.303 \frac{kT}{q} \frac{\beta}{\beta + 1} (\text{pH}_{pzc} - \text{pH}) \quad (36)$$

On the other hand, the exact eq 33 has to be used when:

$$\beta \ll \frac{q\psi}{kT} \quad (37)$$

Table 26. Summary of the Extracted Electrode Potentials for Representative ZnO and IrO<sub>x</sub> pH Sensors

ref	material/structure	standard reduction potential (mV)	reported reaction	likely reaction
Chung et al. <sup>22</sup>	IrO <sub>x</sub>	+922	IrO <sub>x</sub> redox reactions (mixed oxidation states)	dominant IrOx redox reactions (multiple oxidation states)
Yang et al. <sup>288</sup>	IrOx-rGO	+676	$2[\text{IrO}_2(\text{OH})_2 \cdot 2\text{H}_2\text{O}]^{2-} + 3\text{H}^+ + 2\text{e}^- \rightleftharpoons [\text{Ir}_2\text{O}_3(\text{OH})_3 \cdot 3\text{H}_2\text{O}]^{3-}$	dominant IrOx redox reactions and other mixed potentials
Batista et al. <sup>306</sup>	ZnO	+636	For acid: $\text{ZnO} + 2\text{OH}^- + \text{H}_2\text{O} \rightleftharpoons \text{Zn}(\text{OH})_4^{2-}$	mixed potential involving oxygen evolution
Mani et al. <sup>37</sup>	ZnO	+746	For base: $\text{ZnO} + 2\text{H}_3\text{O}^+ + 3\text{H}_2\text{O} \rightleftharpoons \text{Zn}(\text{H}_2\text{O})_6^{2+}$	mixed potential involving oxygen evolution
Fulati et al. <sup>36</sup>	ZnO nanorods/nanotubes	+428.6/+627.2	$\text{ZnO} + \text{H}^+ \rightleftharpoons \text{ZnOH}^+$	mixed potential involving oxygen evolution
Ghoneim et al. <sup>132</sup>	ZnO	+869	mixed potential	mixed potential

For this site binding model, it is important to note that it falls short when considering the crowding effect, low selectivity, and defects, which is mentioned later in this subsection. In the EGFET configuration, there is a MOSFET, which allows a current to flow. A voltage is generated by the activity of H<sup>+</sup> in the solution and the reference voltage. The voltage of the transistor is related to the current ( $I_{\text{DS}}$ ) between the drain and source by the MOSFET expression. The drain-source voltage ( $V_{\text{DS}}$ ) relates to the current linearly before the current saturates. The current saturates when the drain-source voltage reaches the difference between the gate-source voltage ( $V_{\text{GS}}$ ), which is related to the voltage of the RE, and modified threshold voltage ( $V_{\text{T}}$ ). For the linear region, the relationship is defined by the equation:

$$I_{\text{DS}} = K_{\text{n}} \left[ (V_{\text{GS}} - V_{\text{T}}) V_{\text{DS}} - \frac{1}{2} V_{\text{DS}}^2 \right] \quad (38)$$

and for the saturation region, when  $V_{\text{DS}} = V_{\text{GS}} - V_{\text{T}}$ , the relationship is defined by

$$I_{\text{DS}} = \frac{1}{2} K_{\text{n}} [(V_{\text{GS}} - V_{\text{T}})^2] \quad (39)$$

where  $K_{\text{n}}$  is the conduction parameter.<sup>114</sup>

Despite the usefulness of these models, there are some limitations and defects that occur at the interface that interfere with the accuracy of the models. One such effect is the crowding effect. Above a critical electrical potential, ion concentration saturates and causes the potential profile for the electrolyte diffusion layer to change, repelling counterions, which in turn reduces the ion concentration at the surface and causes a lower capacitance.<sup>302</sup> In this case, the pH is underestimated. However, the opposite can also occur, and there can be a greater pH sensitivity due to the crowding effect of counterions in buffer solutions, causing larger H<sup>+</sup> concentrations at the sensor surface. As a result, the models mentioned earlier do not accurately predict pH as they fail to take the crowding effect into account.

In addition, the sensor must be selective to H<sup>+</sup>. Possible cations, such as sodium, could affect the measurement by being accounted for in the model instead of H<sup>+</sup>.<sup>303</sup> Due to a lack of selectivity, the pH predicted by these models can be greatly overestimated because the models account for other cations in the electrolyte solution.

Defects are also a factor to consider in these models. There may be point defects, defective with either a vacancy, interstitial impurity, or substitutional impurity at a single atom, or extended defects, defective at multiple atoms or lattice sites,<sup>304</sup> that may affect the accuracy of the models. As mentioned previously, the site binding model predicts that the number of binding sites affects the potential. Thus, any defect can affect the number of

binding sites and can either overestimate or underestimate the potential, depending on the defect polarity.<sup>305</sup> Common defects are shown in Figure 12c.

## 10. FUTURE OUTLOOK ON PH SENSING IN BIOMEDICAL APPLICATIONS

Throughout the review, we have discussed available materials for pH and structures for pH sensing (Section 3), common configurations for pH-sensing systems (Section 4), sensing standards and protocols (Section 5), pH regulation in the human body (Section 6) and relevant biomedical applications (Section 7), progress in wearable and implantable pH sensors for biomedical applications (Section 8), and the challenges facing pH-sensing systems and measurements (Section 9). In this section we summarize the learnings from the extensive knowledge base on pH sensing for biomedical applications and provide a future outlook on the field.

The strict pH balance maintained by efficient regulation in biological systems makes pH sensing for biomedical applications highly advantageous. Minor deviations in pH can be used as an early indication of malfunction or disease as well as an alarming signal before the rise or propagation of other diseases. As a result, research on pH sensing for biomedical applications has gained sustained interest for decades. For instance, implantable pH sensors (in vivo) have been reported since the 1980s (details can be found in Section 8.2). With advancement in microfabrication technology and nanotechnology manipulation capabilities, new pH-sensing materials, structures, and techniques have emerged.

Among the investigated polymeric materials, PANI repeatedly exhibited desired properties with reliable and stable results, especially for wearable pH-sensing applications. IrOx exhibited extraordinary low drift values, Nernstian sensitivity, fast response time, biocompatibility, and repeatable and reproducible results. It is one of the most investigated materials for pH sensors and the fact that multiple reports from various research groups across the globe repeatedly reported its excellent pH-sensing properties is a testament to its potential. The reliable performance of IrOx pH sensors can be attributed to the stable reaction at its surface as compared to other materials such as ZnO. Table 26 shows extracted electrode potentials for representative ZnO and IrOx pH sensors. The calculated standard electrode reduction potentials for IrOx are relatively closer to the reduction potential of redox reactions involving iridium ions than the case of calculated standard reduction potentials for ZnO electrodes versus the reduction potential of redox reactions involving zinc ions. This indicates that the reactions in the case of IrOx electrodes are likely dominated by the iridium ion redox reactions. However, in the case of ZnO

electrodes, the discrepancy indicates a mixed potential likely dominated by other reactions instead of the zinc ion's redox. This might explain the relative higher stability of IrOx and its wider use as a pH-sensing material.

With the expanding investigated materials library for pH sensing and their various nanostructures, the different sensing configurations and testing instruments, and the myriad biomedical applications demonstrated in implantable and wearable pH sensors, standards and protocols become crucial. Furthermore, the complexity of the sensing mechanism modeling and the stability and repeatability challenges require further investigations. Table 27 shows a representative list of

**Table 27. Summary of the Recommendations for Standardizing and Benchmarking pH Sensing Materials and Systems using EGFET Configuration.**<sup>1,32</sup>

category	description	
intrinsic characterization system properties	input resistance	
	intrinsic time constant	
	stability	
	Of all commercial components:	
	(a) characterization instrument (b) commercial transistor (c) glass electrode (d) reference electrode (RE)	
intrinsic sensing film properties	<ul style="list-style-type: none"> <li>• composition</li> <li>• crystallinity</li> <li>• thickness</li> <li>• resistivity</li> </ul>	
	buffers and solutions properties	<ul style="list-style-type: none"> <li>• compositions</li> <li>• concentrations</li> </ul>
		experimental techniques

recommended reporting parameters for the EGFET pH-sensing configuration. For biomedical applications, another important criterion is biocompatibility (acute and long-term tests) of the materials, especially in the case of implantable pH sensors. A complete systematic reporting would help highlight common issues, benchmark materials and reports, and provide an extensive knowledge base for more informed studies. This is critical in the pursuit for empirical solutions to challenges such as modeling, hysteresis, stability, and repeatability. Similar protocol approaches for piezoelectric energy harvester characterization were reported.<sup>307,308</sup>

Evidently, the integration of various pH sensors with advanced electronics has provided a new platform for the development of novel pH-sensing technologies for disease diagnostics and prevention. Moving forward requires not only expanding available materials and techniques but also addressing the key challenges affecting the reliability and repeatability of pH measurements, reproducibility of sensors, and establishing a convention for standards and protocols for systematic and comprehensive reporting.

Finally, sensitivity, accuracy, and precision requirements of pH sensors for biomedical applications vary widely based on the targeted application. For instance, differentiating tumors from healthy cells requires detecting a difference of less than 0.7 pH units in the range of 6.7–7.4, with probes in the micro-/nanometer diameter range to access the external cell environ-

ment, in a timely fashion (~ few minutes). If a similar application is targeting the immediate response to therapeutic drugs, higher sensitivity and resolution would be necessary with faster response times (~ few seconds). On the other hand, monitoring mouth pH can accommodate fairly larger systems that can detect variations of ~0.2 pH units in the 5.5–7 pH range, and a response time of a few minutes can be accommodated too. Therefore, as pH-sensing systems evolve toward higher sensitivities and detectability, smaller dimensions, faster responses, and long-term reliability and biocompatibility, new biomedical applications would become possible, helping to diagnose and prevent more diseases.

## AUTHOR INFORMATION

### Corresponding Author

\*E-mail: [canand@media.mit.edu](mailto:canand@media.mit.edu).

### ORCID

M. T. Ghoneim: 0000-0002-5568-5284

C. Dagdeviren: 0000-0002-2032-792X

### Notes

The authors declare no competing financial interest.

### Biographies

Mohamed T. Ghoneim is currently pursuing his postdoctoral training at the Conformable Decoders group at Massachusetts Institute of Technology (MIT), Media Lab. He earned his Ph.D. degree in Electrical Engineering from King Abdullah University of Science and Technology. His research interests include electrochemistry, reliability, microfabrication, flexible electronics, and biomedical applications.

Canan Dagdeviren is Assistant Professor of Media Arts and Sciences and LG Career Development Professor of Media Arts and Sciences at MIT, where she leads a research group called Conformable Decoders. Prof. Dagdeviren earned her Ph.D. in Materials Science and Engineering from the University of Illinois at Urbana–Champaign. Her collective research aims to design and fabricate mechanically adaptive electromechanical and electrochemical systems to convert the patterns of nature and the human body into beneficial signals and energy.

Athena Nguyen is currently an undergraduate at MIT, Department of Biological Engineering. In Summer of 2018, she became an undergraduate researcher under the supervision of Prof. Canan Dagdeviren of the MIT Media Lab. She is interested in nanosensors and other devices for biomedical applications.

Naomi Dereje is an undergraduate student at MIT pursuing a bachelor's degree in mechanical engineering with a minor in statistics and data science. In Summer, 2018, she worked with and Conformable Decoders group at the Media Lab under the supervision of Prof. Canan Dagdeviren. She has also worked in the Biomedical Engineering Department at the Catholic University of America in Washington D.C. Her research interests include product design and development.

Jiayao (Kyle) Huang is a current undergraduate student at MIT majoring in aerospace engineering. He previously worked in the Space Systems Lab under Professor David Miller, and Conformable Decoders in MIT's Media Lab under the supervision of Prof. Canan Dagdeviren. His research interests include materials and structures, and propulsion.

Grace C. Moore is currently pursuing an undergraduate degree in materials science and engineering at MIT. In Spring 2018, she worked with Prof. Canan Dagdeviren at the MIT Media Lab as an undergraduate researcher. She has also performed undergraduate research in convection batteries with Prof. Fikile Brushett. Her research

interests include electrochemistry, convection chemistry, electrochemical energy storage, and biomedical applications.

Philip J. Murzynowski is a current undergraduate student at MIT majoring in computer science and electrical engineering. He previously worked in the Space Systems Lab under Prof. David Miller, and Conformable Decoders in MIT's Media Lab under the supervision of Prof. Canan Dagdeviren. His research interests include cyber security, signal processing, and computer architecture.

## ACKNOWLEDGMENTS

The authors thank David Sadat for assisting with the manuscript preparation and the MIT Media Lab for financial support.

## REFERENCES

- (1) Lesney, M. S. A Basic History of Acid- From Aristotle to Arnold. *Am. Chem. Soc.* **2003**, *12*, 47–50.
- (2) Khan, M. I.; Mukherjee, K.; Shoukat, R.; Dong, H. A Review on pH Sensitive Materials for Sensors and Detection Methods. *Microsyst. Technol.* **2017**, *23*, 4391–4404.
- (3) Myers, R. J. One-Hundred Years of pH. *J. Chem. Educ.* **2010**, *87*, 30–32.
- (4) Salis, A.; Monduzzi, M. Not Only pH. Specific Buffer Effects in Biological Systems. *Curr. Opin. Colloid Interface Sci.* **2016**, *23*, 1–9.
- (5) Salek, S. S.; Van Turnhout, A. G.; Kleerebezem, R.; Van Loosdrecht, M. C. M. pH Control in Biological Systems Using Calcium Carbonate. *Biotechnol. Bioeng.* **2015**, *112*, 905–913.
- (6) Tannock, I. F.; Rotin, D. Acid pH in Tumors and Its Potential for Therapeutic Exploitation. *Cancer Res.* **1989**, *49*, 4373–4384.
- (7) Kilpatrick, M.; Kilpatrick, M. The Teaching of the Theory of the Dissociation of Electrolytes. II. The Definition of pH. *J. Chem. Educ.* **1932**, *9*, 1010–1016.
- (8) MacInnes, D. A. Criticism of a Definition of pH. *Science* **1948**, *108*, 693–693.
- (9) Covington, A. K.; Bates, R. G.; Durst, R. A. Definition of pH Scales, Standard Reference Values, Measurement of pH and Related Terminology. *Pure Appl. Chem.* **1985**, *57*, 531–542.
- (10) Barron, J. J.; Ashton, C.; Geary, L. The Effects of Temperature on pH Measurement. *Tsp* **2011**, *1*, 1–7.
- (11) Chiang, J. L.; Jan, S. S.; Chou, J. C.; Chen, Y. C. Study on the Temperature Effect, Hysteresis and Drift of PH-ISFET Devices On the basis of Amorphous Tungsten Oxide. *Sens. Actuators, B* **2001**, *76*, 624–628.
- (12) Rosenthal, T. B. The Effect of Temperature on the pH of Blood and Plasma in Vitro. *J. Biol. Chem.* **1948**, *173*, 25–30.
- (13) Huang, W.-D.; Cao, H.; Deb, S.; Chiao, M.; Chiao, J. C. A Flexible pH Sensor Based on the Iridium Oxide Sensing Film. *Sens. Actuators, A* **2011**, *169*, 1–11.
- (14) Zhang, W.; Abou El-Reash, Y. G.; Ding, L.; Lin, Z.; Lian, Y.; Song, B.; Yuan, J.; Wang, X. A Lysosome-Targeting Nanosensor for Simultaneous Fluorometric Imaging of Intracellular pH Values and Temperature. *Microchim. Acta* **2018**, *185*, 533.
- (15) Pietsch, C.; Hoogenboom, R.; Schubert, U. S. Soluble Polymeric Dual Sensor for Temperature and pH Value. *Angew. Chem., Int. Ed.* **2009**, *48*, 5653–5656.
- (16) Korostynska, O.; Arshak, K.; Gill, E.; Arshak, A. Review on State-of-the-Art in Polymer Based pH Sensors. *Sensors* **2007**, *7*, 3027–3042.
- (17) Ahmed, N. M.; Kabaa, E. A.; Jaafar, M. S.; Omar, A. F. Characteristics of Extended-Gate Field-Effect Transistor (EGFET) Based on Porous n-Type (111) Silicon for Use in pH Sensors. *J. Electron. Mater.* **2017**, *46*, 5804–5813.
- (18) Lee, C. S.; Kyu Kim, S.; Kim, M. Ion-Sensitive Field-Effect Transistor for Biological Sensing. *Sensors* **2009**, *9*, 7111–7131.
- (19) Rajapaksha, R. D. A. A.; Hashim, U.; Fernando, C. A. N. Design, Fabrication and Characterization of 1.0 Mm Gap Al Based Interdigitated Electrode for Biosensors. *Microsyst. Technol.* **2017**, *23*, 4501–4507.
- (20) Kurzweil, P. Metal Oxides and Ion-Exchanging Surfaces as pH Sensors in Liquids: State-of-the-Art and Outlook. *Sensors* **2009**, *9*, 4955–4985.
- (21) Wei, A.; Pan, L.; Huang, W. Recent Progress in the ZnO Nanostructure-Based Sensors. *Mater. Sci. Eng., B* **2011**, *176*, 1409–1421.
- (22) Chung, H. J.; Sulkin, M. S.; Kim, J. S.; Goudeseune, C.; Chao, H. Y.; Song, J. W.; Yang, S. Y.; Hsu, Y. Y.; Ghaffari, R.; Efimov, I. R.; et al. Stretchable, Multiplexed pH Sensors with Demonstrations on Rabbit and Human Hearts Undergoing Ischemia. *Adv. Healthcare Mater.* **2014**, *3*, 59–68.
- (23) Yuqing, M.; Jianrong, C.; Keming, F. New Technology for the Detection of pH. *J. Biochem. Biophys. Methods* **2005**, *63*, 1–9.
- (24) Glab, S.; Hulanicki, A.; Edwall, G.; Ingman, F. Metal-Metal Oxide and Metal Oxide Electrodes as pH Sensors. *Crit. Rev. Anal. Chem.* **1989**, *21*, 29–47.
- (25) Santos, L.; Neto, J. P.; Crespo, A.; Nunes, D.; Costa, N.; Fonseca, I. M.; Barquinha, P.; Pereira, L.; Silva, J.; Martins, R.; et al. WO<sub>3</sub> Nanoparticle-Based Conformable pH Sensor. *ACS Appl. Mater. Interfaces* **2014**, *6*, 12226–12234.
- (26) Zaman, S.; Asif, M. H.; Zainelabdin, A.; Amin, G.; Nur, O.; Willander, M. CuO Nanoflowers as an Electrochemical pH Sensor and the Effect of pH on the Growth. *J. Electroanal. Chem.* **2011**, *662*, 421–425.
- (27) Manjakkal, L.; Cvejic, K.; Kulawik, J.; Zaraska, K.; Szwagierczak, D.; Socha, R. P. Fabrication of Thick Film Sensitive RuO<sub>2</sub>-TiO<sub>2</sub> and Ag/AgCl/KCl Reference Electrodes and Their Application for pH Measurements. *Sens. Actuators, B* **2014**, *204*, 57–67.
- (28) Chen, M.; Jin, Y.; Qu, X.; Jin, Q.; Zhao, J. Electrochemical Impedance Spectroscopy Study of Ta<sub>2</sub>O<sub>5</sub> Based EIOS pH Sensors in Acid Environment. *Sens. Actuators, B* **2014**, *192*, 399–405.
- (29) Lee, I.-S.; Whang, C.-N.; Lee, Y.-H.; Hwan Lee, G.; Park, B.-J.; Park, J.-C.; Seo, W.-S.; Cui, F.-Z. Formation of Nano Iridium Oxide: Material Properties and Neural Cell Culture. *Thin Solid Films* **2005**, *475*, 332–336.
- (30) Ges, I. A.; Ivanov, B. L.; Schaffer, D. K.; Lima, E. A.; Werdich, A. A.; Baudenbacher, F. J. Thin-Film IrOx pH Microelectrode for Microfluidic-Based Microsystems. *Biosens. Bioelectron.* **2005**, *21*, 248–256.
- (31) Yamanaka, K. Anodically Electrodeposited Iridium Oxide Films (AEIROF's) from Alkaline Solutions for Electrochromic Display Devices. *Jpn. J. Appl. Phys.* **1989**, *28*, 632–637.
- (32) Bezbaruah, A. N.; Zhang, T. C. Fabrication of Anodically Electrodeposited Iridium Oxide Film pH Microelectrodes for Micro-environmental Studies. *Anal. Chem.* **2002**, *74*, 5726–5733.
- (33) Spătaru, T.; Roman, E.; Spătaru, N. Electrodeposition of Cobalt Oxide on Conductive Diamond Electrodes for Catalytic Sensor Applications. *Rev. Roum. Chim.* **2004**, *49*, 525–530.
- (34) Lee, W. H.; Lee, J.-H.; Choi, W.-H.; Hosni, A. A.; Papautsky, I.; Bishop, P. L. Needle-Type Environmental Microsensors: Design, Construction and Uses of Microelectrodes and Multi-Analyte MEMS Sensor Arrays. *Meas. Sci. Technol.* **2011**, *22*, 042001.
- (35) Al-Hilli, S. M.; Al-Mofarji, R. T.; Klason, P.; Willander, M.; Gutman, N.; Sa'Ar, A. Zinc Oxide Nanorods Grown on Two-Dimensional Macroporous Periodic Structures and Plane Si as a pH Sensor. *J. Appl. Phys.* **2008**, *103*, 014302.
- (36) Fulati, A.; Usman Ali, S. M.; Riaz, M.; Amin, G.; Nur, O.; Willander, M. Miniaturized pH Sensors Based on Zinc Oxide Nanotubes/Nanorods. *Sensors* **2009**, *9*, 8911–8923.
- (37) Mani, G. K.; Morohoshi, M.; Yasoda, Y.; Yokoyama, S.; Kimura, H.; Tsuchiya, K. ZnO-Based Microfluidic pH Sensor: A Versatile Approach for Quick Recognition of Circulating Tumor Cells in Blood. *ACS Appl. Mater. Interfaces* **2017**, *9*, 5193–5203.
- (38) Zhang, Q.; Liu, W.; Sun, C.; Zhang, H.; Pang, W.; Zhang, D.; Duan, X. On-Chip Surface Modified Nanostructured ZnO as Functional pH Sensors. *Nanotechnology* **2015**, *26*, 355202.
- (39) Pachauri, V.; Vlandas, A.; Kern, K.; Balasubramanian, K. Site-Specific Self-Assembled Liquid-Gated ZnO Nanowire Transistors for Sensing Applications. *Small* **2010**, *6*, 589–594.

- (40) Park, J.; Lee, S.; Lee, J.; Yong, K. A Light Incident Angle Switchable ZnO Nanorod Memristor: Reversible Switching Behavior Between Two Non-Volatile Memory Devices. *Adv. Mater.* **2013**, *25*, 6423–6429.
- (41) Khaderbad, M. A.; Choi, Y.; Hiralal, P.; Aziz, A.; Wang, N.; Durkan, C.; Thiruvengatanathan, P.; Amaratunga, G. A. J.; Rao, V. R.; Seshia, A. A. Electrical Actuation and Readout in a Nanoelectromechanical Resonator Based on a Laterally Suspended Zinc Oxide Nanowire. *Nanotechnology* **2012**, *23*, 025501.
- (42) Wen, W.; Wu, J.-M.; Wang, Y.-D. Large-Size Porous ZnO Flakes with Superior Gas-Sensing Performance. *Appl. Phys. Lett.* **2012**, *100*, 262111.
- (43) Gao, P. X.; Ding, Y.; Wang, Z. L. Crystallographic Orientation-Aligned ZnO Nanorods Grown by a Tin Catalyst. *Nano Lett.* **2003**, *3*, 1315–1320.
- (44) Pan, Z. W.; Dai, Z. R.; Wang, Z. L.; Hughes, W. L.; Lao, C.; Wang, Z. L. Nanobelts of Semiconducting Oxides. *Science* **2001**, *291*, 1947–1949.
- (45) Hughes, W. L.; Wang, Z. L. Formation of Piezoelectric Single-Crystal Nanorings and Nanobows. *J. Am. Chem. Soc.* **2004**, *126*, 6703–6709.
- (46) Gao, P. X.; Ding, Y.; Mai, W.; Hughes, W. L.; Lao, C.; Wang, Z. L. Conversion of Zinc Oxide Nanobelts into Superlattice-Structured Nanohelices. *Science* **2005**, *309*, 1700–1704.
- (47) Chang, Y.-C.; Yang, W.-C.; Chang, C.-M.; Hsu, P.-C.; Chen, L.-J. Controlled Growth of ZnO Nanopagoda Arrays with Varied Lamination and Apex Angles. *Cryst. Growth Des.* **2009**, *9*, 3161–3167.
- (48) Cho, S.; Jung, S.-H.; Jang, J.-W.; Oh, E.; Lee, K.-H. Simultaneous Synthesis of Al-Doped ZnO Nanoneedles and Zinc Aluminum Hydroxides through Use of a Seed Layer. *Cryst. Growth Des.* **2008**, *8*, 4553–4558.
- (49) Kong, X. Y.; Wang, Z. L. Spontaneous Polarization-Induced Nanohelices, Nanosprings, and Nanorings of Piezoelectric Nanobelts. *Nano Lett.* **2003**, *3*, 1625–1631.
- (50) Mazeina, L.; Picard, Y. N.; Prokes, S. M. Controlled Growth of Parallel Oriented ZnO Nanostructural Arrays on Ga<sub>2</sub>O<sub>3</sub> Nanowires. *Cryst. Growth Des.* **2009**, *9*, 1164–1169.
- (51) Wei, A.; Sun, X. W.; Xu, C. X.; Dong, Z. L.; Yang, Y.; Tan, S. T.; Huang, W. Growth Mechanism of Tubular ZnO Formed in Aqueous Solution. *Nanotechnology* **2006**, *17*, 1740–1744.
- (52) Zhou, H. L.; Shao, P. G.; Chua, S. J.; van Kan, J. A.; Bettiol, A. A.; Osipowicz, T.; Ooi, K. F.; Goh, G. K. L.; Watt, F. Selective Growth of ZnO Nanorod Arrays on a GaN/Sapphire Substrate Using a Proton Beam Written Mask. *Cryst. Growth Des.* **2008**, *8*, 4445–4448.
- (53) Ng, A. M. C.; Chen, X. Y.; Djurisic, A. B. ZnO Nanostructures for Optoelectronics: Material Properties and Device Applications. *Prog. Quantum Electron.* **2010**, *34*, 191–259.
- (54) Avrutin, V.; Silversmith, D. J.; Morkoç, H. Doping Asymmetry Problem in ZnO: Current Status and Outlook. *Proc. IEEE* **2010**, *98*, 1269–1280.
- (55) Aydin, C.; Abd El-Sadek, M. S.; Zheng, K.; Yahia, I. S.; Yakuphanoglu, F. Synthesis, Diffused Reflectance and Electrical Properties of Nanocrystalline Fe-Doped ZnO via Sol-Gel Calcination Technique. *Opt. Laser Technol.* **2013**, *48*, 447–452.
- (56) George, S.; Pokhrel, S.; Xia, T.; Gilbert, B.; Ji, Z.; Schowalter, M.; Rosenauer, A.; Damoiseaux, R.; Bradley, K. A.; Mädler, L.; et al. Use of a Rapid Cytotoxicity Screening Approach To Engineer a Safer Zinc Oxide Nanoparticle through Iron Doping. *ACS Nano* **2010**, *4*, 15–29.
- (57) Wang, J. L.; Yang, P. Y.; Hsieh, T. Y.; Juan, P. C. Ionic pH and Glucose Sensors Fabricated Using Hydrothermal ZnO Nanostructures. *Jpn. J. Appl. Phys.* **2016**, *55*, 01AE16.
- (58) Wang, J.-L.; Yang, P.-Y.; Hsieh, T.-Y.; Hwang, C.-C.; Juang, M.-H. PH-Sensing Characteristics of Hydrothermal Al-Doped ZnO Nanostructures. *J. Nanomater.* **2013**, *2013*, 1–7.
- (59) Guinovart, T.; Valdés-Ramírez, G.; Windmiller, J. R.; Andrade, F. J.; Wang, J. Bandage-Based Wearable Potentiometric Sensor for Monitoring Wound pH. *Electroanalysis* **2014**, *26*, 1345–1353.
- (60) Yoon, J. H.; Hong, S. B.; Yun, S. O.; Lee, S. J.; Lee, T. J.; Lee, K. G.; Choi, B. G. High Performance Flexible pH Sensor Based on Polyaniline Nanopillar Array Electrode. *J. Colloid Interface Sci.* **2017**, *490*, 53–58.
- (61) Rojas, J. P.; Torres Sevilla, G. A.; Ghoneim, M. T.; Inayat, S. B.; Ahmed, S. M.; Hussain, A. M.; Hussain, M. M. Transformational Silicon Electronics. *ACS Nano* **2014**, *8*, 1468–1474.
- (62) Ghoneim, M. T.; Hussain, M. M. Study of Harsh Environment Operation of Flexible Ferroelectric Memory Integrated with PZT and Silicon Fabric. *Appl. Phys. Lett.* **2015**, *107*, 052904.
- (63) Ghoneim, M. T.; Rojas, J. P.; Young, C. D.; Bersuker, G.; Hussain, M. M. Electrical Analysis of High Dielectric Constant Insulator and Metal Gate Metal Oxide Semiconductor Capacitors on Flexible Bulk Mono-Crystalline Silicon. *IEEE Trans. Reliab.* **2015**, *64*, 579–585.
- (64) Ghoneim, M. T.; Kutbee, A.; Ghodsi Nasser, F.; Bersuker, G.; Hussain, M. M. Mechanical Anomaly Impact on Metal-Oxide-Semiconductor Capacitors on Flexible Silicon Fabric. *Appl. Phys. Lett.* **2014**, *104*, 234104.
- (65) Torres Sevilla, G. A.; Ghoneim, M. T.; Fahad, H.; Rojas, J. P.; Hussain, A. M.; Hussain, M. M. Flexible Nanoscale High-Performance FinFETs. *ACS Nano* **2014**, *8*, 9850–9856.
- (66) Ghoneim, M. T.; Zidan, M. A.; Salama, K. N.; Hussain, M. M. Towards Neuromorphic Electronics: Memristors on Foldable Silicon Fabric. *Microelectron. J.* **2014**, *45*, 1392–1395.
- (67) Ghoneim, M. T.; Rojas, J. P.; Hussain, A. M.; Hussain, M. M. Additive Advantage in Characteristics of MIMCAPs on Flexible Silicon (100) Fabric with Release-First Process. *Phys. Status Solidi RRL* **2014**, *8*, 163–166.
- (68) Nyein, H. Y. Y.; Gao, W.; Shahpar, Z.; Emaminejad, S.; Challa, S.; Chen, K.; Fahad, H. M.; Tai, L. C.; Ota, H.; Davis, R. W.; et al. A Wearable Electrochemical Platform for Noninvasive Simultaneous Monitoring of Ca<sup>2+</sup> and pH. *ACS Nano* **2016**, *10*, 7216–7224.
- (69) Humpolicek, P.; Kasparkova, V.; Saha, P.; Stejskal, J. Biocompatibility of Polyaniline. *Synth. Met.* **2012**, *162*, 722–727.
- (70) Sha, R.; Komori, K.; Badhulika, S. Amperometric pH Sensor Based on Graphene-Polyaniline Composite. *IEEE Sens. J.* **2017**, *17*, 5038–5043.
- (71) Ping, J.; Wang, Y.; Wu, J.; Ying, Y.; Ji, F. A Novel pH Sensing Membrane Based on an Ionic Liquid-Polymer Composite. *Microchim. Acta* **2012**, *176*, 229–234.
- (72) Maiolo, L.; Mirabella, S.; Maita, F.; Alberti, A.; Minotti, A.; Strano, V.; Pecora, A.; Shacham-Diamand, Y.; Fortunato, G. Flexible pH Sensors Based on Polysilicon Thin Film Transistors and ZnO Nanowalls. *Appl. Phys. Lett.* **2014**, *105*, 093501.
- (73) Shin, J.; Braun, P. V.; Lee, W. Fast Response Photonic Crystal pH Sensor Based on Templated Photo-Polymerized Hydrogel Inverse Opal. *Sens. Actuators, B* **2010**, *150*, 183–190.
- (74) Richter, A.; Paschew, G.; Klatt, S.; Lienig, J.; Arndt, K. F.; Adler, H. J. P. Review on Hydrogel-Based pH Sensors and Microsensors. *Sensors* **2008**, *8*, 561–581.
- (75) Richter, A.; Bund, A.; Keller, M.; Arndt, K. F. Characterization of a Microgravimetric Sensor Based on pH Sensitive Hydrogels. *Sens. Actuators, B* **2004**, *99*, 579–585.
- (76) Zong, S.; Wang, Z.; Yang, J.; Cui, Y. Intracellular pH Sensing Using P-Aminothiophenol Functionalized Gold Nanorods with Low Cytotoxicity. *Anal. Chem.* **2011**, *83*, 4178–4183.
- (77) Ma, D.; Zheng, J.; Tang, P.; Xu, W.; Qing, Z.; Yang, S.; Li, J.; Yang, R. Quantitative Monitoring of Hypoxia-Induced Intracellular Acidification in Lung Tumor Cells and Tissues Using Activatable Surface-Enhanced Raman Scattering Nanoprobes. *Anal. Chem.* **2016**, *88*, 11852–11859.
- (78) Qin, Y.; Kwon, H. J.; Subrahmanyam, A.; Howlader, M. M. R.; Selvaganapathy, P. R.; Adronov, A.; Deen, M. J. Inkjet-Printed Bifunctional Carbon Nanotubes for pH Sensing. *Mater. Lett.* **2016**, *176*, 68–70.
- (79) Ruan, C.; Zeng, K.; Grimes, C. A. A Mass-Sensitive pH Sensor Based on a Stimuli-Responsive Polymer. *Anal. Chim. Acta* **2003**, *497*, 123–131.
- (80) Lin, J. Recent Development and Applications of Optical and Fiber-Optic pH Sensors. *TrAC, Trends Anal. Chem.* **2000**, *19*, 541–552.

- (81) Li, L.-L.; Sun, H.; Fang, C.-J.; Xu, J.; Jin, J.-Y.; Yan, C.-H. Optical Sensors Based on Functionalized Mesoporous Silica SBA-15 for the Detection of Multianalytes ( $H^+$  and  $Cu^{2+}$ ) in Water. *J. Mater. Chem.* **2007**, *17*, 4492.
- (82) Islam, S.; Bakhtiar, H.; Bidin, N.; Riaz, S.; Naseem, S. Sol-gel Based Thermally Stable Mesoporous  $TiO_2$  Nanomatrix for Fiber Optic pH Sensing. *J. Sol-Gel Sci. Technol.* **2018**, *86*, 42–50.
- (83) Islam, S.; Bakhtiar, H.; Naseem, S.; Aziz, M. S. B. A.; Bidin, N.; Riaz, S.; Ali, J. Surface Functionality and Optical Properties Impact of Phenol Red Dye on Mesoporous Silica Matrix for Fiber Optic pH Sensing. *Sens. Actuators, A* **2018**, *276*, 267–277.
- (84) Tsou, C.-J.; Chu, C.; Hung, Y.; Mou, C.-Y. A Broad Range Fluorescent pH Sensor Based on Hollow Mesoporous Silica Nanoparticles, Utilising the Surface Curvature Effect. *J. Mater. Chem. B* **2013**, *1*, 5557–5563.
- (85) Peng, H.-S.; Chiu, D. T. Soft Fluorescent Nanomaterials for Biological and Biomedical Imaging. *Chem. Soc. Rev.* **2015**, *44*, 4699–4722.
- (86) Pospíšilová, M.; Kuncová, G.; Trögl, J. Fiber-Optic Chemical Sensors and Fiber-Optic Bio-Sensors. *Sensors* **2015**, *15*, 25208–25259.
- (87) Wolfbeis, O. S. Fiber-Optic Chemical Sensors and Biosensors. *Anal. Chem.* **2008**, *80*, 4269–4283.
- (88) Capel-Cuevas, S.; Cuéllar, M. P.; de Orbe-Payá, I.; Pegalajar, M. C.; Capitán-Vallvey, L. F. Full-Range Optical pH Sensor Based on Imaging Techniques. *Anal. Chim. Acta* **2010**, *681*, 71–81.
- (89) Fritzsche, M.; Barreiro, C. G.; Hitzmann, B.; Scheper, T. Optical pH Sensing Using Spectral Analysis. *Sens. Actuators, B* **2007**, *128*, 133–137.
- (90) Sheppard, N. F.; Lesho, M. J.; McNally, P.; Shaun Francomacaro, A. Microfabricated Conductometric pH Sensor. *Sens. Actuators, B* **1995**, *28*, 95–102.
- (91) Benson, K.; Ghimire, A.; Pattammattel, A.; Kumar, C. V. Protein Biophosphors: Biodegradable, Multifunctional, Protein-Based Hydrogel for White Emission, Sensing, and pH Detection. *Adv. Funct. Mater.* **2017**, *27*, 1702955.
- (92) Richter, A.; Howitz, S.; Kuckling, D.; Arndt, K. F. Influence of Volume Phase Transition Phenomena on the Behavior of Hydrogel-Based Valves. *Sens. Actuators, B* **2004**, *99*, 451–458.
- (93) Zhao, Y.; Lei, M.; Liu, S. X.; Zhao, Q. Smart Hydrogel-Based Optical Fiber SPR Sensor for pH Measurements. *Sens. Actuators, B* **2018**, *261*, 226–232.
- (94) You, Y. H.; Nagaraja, A. T.; Biswas, A.; Hwang, J. H.; Cote, G. L.; McShane, M. J. SERS-Active Smart Hydrogels with Modular Microdomains: From pH to Glucose Sensing. *IEEE Sens. J.* **2017**, *17*, 941–950.
- (95) Mishra, S. K.; Zou, B.; Chiang, K. S. Wide-Range pH Sensor Based on a Smart-Hydrogel-Coated Long-Period Fiber Grating. *IEEE J. Sel. Top. Quantum Electron.* **2017**, *23*, 284.
- (96) Shaibani, P. M.; Etayash, H.; Naicker, S.; Kaur, K.; Thundat, T. Metabolic Study of Cancer Cells Using a pH Sensitive Hydrogel Nanofiber Light Addressable Potentiometric Sensor. *ACS Sensors* **2017**, *2*, 151–156.
- (97) Ghoneim, M. T.; Smith, C. E.; Hussain, M. M. Simplistic Graphene Transfer Process and Its Impact on Contact Resistance. *Appl. Phys. Lett.* **2013**, *102*, 183115.
- (98) Chen, S. X.; Chang, S. P.; Chang, S. J. Investigation of InN Nanorod-Based EGFET pH Sensors Fabricated on Quartz Substrate. *Dig. J. Nanomater. Biostructures* **2014**, *9*, 1505–1511.
- (99) Lee, C. T.; Chiu, Y. S. Photoelectrochemical Passivated ZnO-Based Nanorod Structured Glucose Biosensors Using Gate-Recessed AlGaIn/GaN Ion-Sensitive Field-Effect Transistors. *Sens. Actuators, B* **2015**, *210*, 756–761.
- (100) Rout, C. S.; Kulkarni, G. U.; Rao, C. N. R. Electrical and Hydrogen-Sensing Characteristics of Field Effect Transistors Based on Nanorods of ZnO and WO<sub>2.27</sub>. *J. Nanosci. Nanotechnol.* **2009**, *9*, S652.
- (101) Al-Hilli, S. M.; Al-Mofarji, R. T.; Willander, M. Zinc Oxide Nanorod for Intracellular pH Sensing. *Appl. Phys. Lett.* **2006**, *89*, 173119.
- (102) Ahmad, Y.; Sharma, N. K.; Ahmad, M. F.; Sharma, M.; Garg, I.; Srivastava, M.; Bhargava, K. The Proteome of Hypobaric Induced Hypoxic Lung: Insights from Temporal Proteomic Profiling for Biomarker Discovery. *Sci. Rep.* **2015**, *5*, 1–20.
- (103) Tran, T.; Kwon, J.; Lee, K.; Lee, J.; Ju, B. pH Sensor Using Carbon Nanotubes as Sensing Material. In *IEEE ICCE'06. First International Conference on Communications and Electronics*; IEEE: Hanoi, Vietnam, 2007; pp 1–4.
- (104) Li, C. A.; Han, K. N.; Pham, X. H.; Seong, G. H. A Single-Walled Carbon Nanotube Thin Film-Based PH-Sensing Microfluidic Chip. *Analyst* **2014**, *139*, 2011–2015.
- (105) Gou, P.; Kraut, N. D.; Feigel, I. M.; Bai, H.; Morgan, G. J.; Chen, Y.; Tang, Y.; Bocan, K.; Stachel, J.; Berger, L.; et al. Carbon Nanotube Chemiresistor for Wireless pH Sensing. *Sci. Rep.* **2015**, *4*, 1–6.
- (106) Jung, D.; Han, M. E.; Lee, G. S. PH-Sensing Characteristics of Multi-Walled Carbon Nanotube Sheet. *Mater. Lett.* **2014**, *116*, 57–60.
- (107) Tsai, W.; Huang, B.; Wang, K.; Huang, Y.; Yang, P.; Cheng, H. Functionalized Carbon Nanotube Thin Films as the pH Sensing Membranes of Extended-Gate Field-Effect Transistors on the Flexible Substrates. *IEEE Trans. Nanotechnol.* **2014**, *13*, 760–766.
- (108) Jiao, L. H.; Barakat, N. Ion-Sensitive Field Effect Transistor as a pH Sensor Ion-Sensitive Field Effect Transistor as a pH Sensor. *J. Nanosci. Nanotechnol.* **2013**, *13*, 1194–1198.
- (109) Yuqing, M.; Jianguo, G.; Jianrong, C. Ion Sensitive Field Effect Transducer-Based Biosensors. *Biotechnol. Adv.* **2003**, *21*, 527–534.
- (110) van der Spiegel, J.; Lauks, I.; Chan, P.; Babic, D. The Extended Gate Chemically Sensitive Field Effect Transistor as Multi-Species Microprobe. *Sens. Actuators* **1983**, *4*, 291–298.
- (111) Chi, L. L.; Chou, J. C.; Chung, W. Y.; Sun, T. P.; Hsiung, S. K. Study on Extended Gate Field Effect Transistor with Tin Oxide Sensing Membrane. *Mater. Chem. Phys.* **2000**, *63*, 19–23.
- (112) Hussin, M. R. M.; Ismail, R.; Syono, I. Simulation and Fabrication of Extended Gate Ion Sensitive Field Effect Transistor for Biosensor Application. In *Computer Applications for Security, Control and System Engineering*; Springer: Heidelberg, 2012; pp 396–403.
- (113) Chiu, Y. S.; Tseng, C. Y.; Lee, C. T. Nanostructured EGFET pH Sensors with Surface-Passivated ZnO Thin-Film and Nanorod Array. *IEEE Sens. J.* **2012**, *12*, 930–934.
- (114) Batista, P. D.; Mulato, M. ZnO Extended-Gate Field-Effect Transistors as pH Sensors. *Appl. Phys. Lett.* **2005**, *87*, 143508.
- (115) Yang, P.-Y.; Wang, J.-L.; Chiu, P.-C.; Chou, J.-C.; Chen, C.-W.; Li, H.-H.; Cheng, H.-C. pH Sensing Characteristics of Extended-Gate Field-Effect Transistor Based on Al-Doped ZnO Nanostructures Hydrothermally Synthesized at Low Temperatures. *IEEE Electron Device Lett.* **2011**, *32*, 1603–1605.
- (116) Li, H. H.; Yang, C. E.; Kei, C. C.; Su, C. Y.; Dai, W. S.; Tseng, J. K.; Yang, P. Y.; Chou, J. C.; Cheng, H. C. Coaxial-Structured ZnO/Silicon Nanowires Extended-Gate Field-Effect Transistor as pH Sensor. *Thin Solid Films* **2013**, *529*, 173–176.
- (117) Manjakkal, L.; Sakthivel, B.; Gopalakrishnan, N.; Dahiya, R. Printed Flexible Electrochemical pH Sensors Based on CuO Nanorods. *Sens. Actuators, B* **2018**, *263*, 50–58.
- (118) Li, P.; Martin, C. M.; Yeung, K. K.; Xue, W. Dielectrophoresis Aligned Single-Walled Carbon Nanotubes as Ph Ensors. *Biosensors* **2011**, *1*, 23–35.
- (119) Yang, C. F.; Chen, C. L.; Busnaina, A.; Dokmeci, M. R. Single-Walled Carbon Nanotube Based pH Sensors on a Flexible Parylene-C Substrate. In *Proceedings of the 31st Annual International Conference of the IEEE Engineering in Medicine and Biology Society: Engineering the Future of Biomedicine, EMBC 2009*; IEEE: Minneapolis, MN, USA, 2009; pp 4102–4105.
- (120) Nordin, N.; Hashim, U.; Azizah, N. Interdigitated Electrode (IDE) Based on Titanium Dioxide ( $TiO_2$ ) Thin Films for Biosensor Application. In *AIP Conference Proceedings*; AIP Publishing: Selangor, Malaysia, 2016; Vol. 1733, p 020084.
- (121) Ali, G. M. Interdigitated Extended Gate Field Effect Transistor Without Reference Electrode. *J. Electron. Mater.* **2017**, *46*, 713–717.

- (122) Lakard, B.; Segut, O.; Lakard, S.; Herlem, G.; Gharbi, T. Potentiometric Miniaturized pH Sensors Based on Polypyrrole Films. *Sens. Actuators, B* **2007**, *122*, 101–108.
- (123) Mazlan, N. S.; Ramli, M. M.; Abdullah, M. M. A. B.; Halin, D. S. C.; Isa, S. S. M.; Talip, L. F. A.; Danial, N. S.; Murad, S. A. Z. Interdigitated Electrodes as Impedance and Capacitance Biosensors: A Review. In *AIP Conference Proceedings*; AIP Publishing: Krabi, Thailand, 2017; Vol. 1885, p 020276.
- (124) Tsouti, V.; Boutopoulos, C.; Zergioti, I.; Chatzandroulis, S. Capacitive Microsystems for Biological Sensing. *Biosens. Bioelectron.* **2011**, *27*, 1–11.
- (125) Farehanim, M. A.; Hashim, U.; Azizah, N.; Fatin, M. F.; Azman, A. H. Fabrication of Interdigitated Electrodes (IDEs) Using Basic Conventional Lithography for pH Measurement. In *AIP Conference Proceedings*; AIP Publishing: Penang, Malaysia, 2017; Vol. 1808.
- (126) Haarindraprasad, R.; Hashim, U.; Gopinath, S. C. B.; Kashif, M.; Veeradasan, P.; Balakrishnan, S. R.; Foo, K. L.; Poopalan, P. Low Temperature Annealed Zinc Oxide Nanostructured Thin Film-Based Transducers: Characterization for Sensing Applications. *PLoS One* **2015**, *10*, e0132755.
- (127) Chih, A.; Yang, F.; Chen, C. L.; Dokmeci, M. R. Single-Walled Carbon Nanotube Based pH Sensor. *Carbon N. Y.* **2009**, *124*, 12419.
- (128) Nguyen, H. D.; Nguyen, T. H.; Hoang, N. V.; Le, N. N.; Nguyen, T. N. N.; Doan, D. C. T.; Dang, M. C. pH Sensitivity of Emeraldine Salt Polyaniline and Poly(Vinyl Butyral) Blend. *Adv. Nat. Sci.: Nanosci. Nanotechnol.* **2014**, *5*, 045001.
- (129) Chinnathambi, S.; Euverink, G. J. W. Polyaniline Functionalized Electrochemically Reduced Graphene Oxide Chemiresistive Sensor to Monitor the pH in Real Time during Microbial Fermentations. *Sens. Actuators, B* **2018**, *264*, 38–44.
- (130) Zhang, Y.; Nayak, T. R.; Hong, H.; Cai, W. Biomedical Applications of Zinc Oxide Nanomaterials. *Curr. Mol. Med.* **2013**, *13*, 1633–1645.
- (131) Copa, V.; Tuico, A.; Mendoza, J.; Ferrolino, J.; Vergara, C.; Salvador, A.; Estacio, E.; Somintac, A. Development of Resistance-Based pH Sensor Using Zinc Oxide Nanorods. *J. Nanosci. Nanotechnol.* **2016**, *16*, 6102–6106.
- (132) Ghoneim, M. T.; Sadraei, A.; de Souza, P.; Moore, G. C.; Bazant, M. Z.; Dagdeviren, C. A Protocol to Characterize pH Sensing Materials and Systems. *Small Methods* **2019**, *3*, 1800265.
- (133) Kakooei, S.; Ismail, C.; Ari-Wahjoedi, B. An Overview of pH Sensors Based on Iridium Oxide: Fabrication and Application. *Int. J. Mater. Sci. Innov.* **2013**, *1*, 62–72.
- (134) Chen, P. Y.; Yin, L. T.; Cho, T. H. Optical and Impedance Characteristics of EGFET Based on SnO<sub>2</sub>/ITO Sensing Gate. *Life Sci.* **2014**, *11*, 871–875.
- (135) Oh, H.; Lee, K. J.; Baek, J.; Yang, S. S.; Lee, K. Development of a High Sensitive pH Sensor Based on Shear Horizontal Surface Acoustic Wave with ZnO Nanoparticles. *Microelectron. Eng.* **2013**, *111*, 154–159.
- (136) Huang, B.-R.; Lin, J.-C.; Yang, Y.-K. ZnO/Silicon Nanowire Hybrids Extended-Gate Field-Effect Transistors as pH Sensors. *J. Electrochem. Soc.* **2013**, *160*, B78–B82.
- (137) Chen, P.-Y.; Yin, L.-T.; Shi, M.-D.; Lee, Y.-C. Drift and Light Characteristics of EGFET Based on SnO<sub>2</sub>/ITO Sensing Gate. *Life Sci.* **2013**, *10*, 3132–3136.
- (138) Catts, J. G.; Langmuir, D. Adsorption of Cu, Pb and Zn by  $\Delta$ MnO<sub>2</sub>: Applicability of the Site Binding-Surface Complexation Model. *Appl. Geochem.* **1986**, *1*, 255–264.
- (139) Keysight Technology. Keysight Technologies, Digital Multimeters. *Datasheet* **2015**, 1–22.
- (140) Shee, D. B1500A Semiconductor Device Analyzer.
- (141) Keysight Technologies. Keysight B1500A Semiconductor Device Analyzer - Data Sheet, [www.keysight.com/find/b1500a](http://www.keysight.com/find/b1500a).
- (142) Mettler Toledo. *InLab Sensors*, 2017.
- (143) Lue, C. E.; Wang, I. S.; Huang, C. H.; Shiao, Y. T.; Wang, H. C.; Yang, C. M.; Hsu, S. H.; Chang, C. Y.; Wang, W.; Lai, C. S. pH Sensing Reliability of Flexible ITO/PET Electrodes on EGFETs Prepared by a Roll-to-Roll Process. *Microelectron. Reliab.* **2012**, *52*, 1651–1654.
- (144) Lin, J. L.; Chu, Y. M.; Hsaio, S. H.; Chin, Y. L.; Sun, T. P. Structures of Anodized Aluminum Oxide Extended-Gate Field-Effect Transistors on pH Sensors. *Japanese J. Appl. Physics, Part 1 Regul. Pap. Short Notes Rev. Pap.* **2006**, *45*, 7999–8004.
- (145) Queeney, K. M. Automated pH Cleaning and Calibration Systems - A Modular Approach. *Technical Papers of ISA* **2004**, 749–758.
- (146) Schöning, M. J.; Brinkmann, D.; Rolka, D.; Demuth, C.; Poghosian, A. CIP (Cleaning- in-Place) Suitable “Non-Glass” pH Sensor Based on a Ta<sub>2</sub>O<sub>5</sub>-Gate EIS Structure. *Sens. Actuators, B* **2005**, *111–112*, 423–429.
- (147) Wang, J. L.; Yang, P. Y.; Hsieh, T. Y.; Hwang, C. C.; Juang, M. H. PH-Sensing Characteristics of Hydrothermal Al-Doped ZnO Nanostructures. *J. Nanomater.* **2013**, *2013*, 1–7.
- (148) Nascimento, R. A. S.; Mulato, M. Mechanisms of Ion Detection for FET-Sensors Using FTO : Role of Cleaning Process, pH Sequence and Electrical Resistivity. *Mater. Res.* **2017**, *20*, 1369–1379.
- (149) Vasquez, R. P.; Lewis, B. F.; Grunthaler, F. J. X-Ray Photoelectron Spectroscopic Study of the Oxide Removal Mechanism of GaAs (100) Molecular Beam Epitaxial Substrates in in Situ Heating. *Appl. Phys. Lett.* **1983**, *42*, 293–295.
- (150) Ada, M. Y.; Ide, Y. Direct Observation of Species Liberated from GaAs Native Oxides during Atomic Hydrogen Cleaning. *Jpn. J. Appl. Phys.* **1994**, *33*, L683–L685.
- (151) Yamaguchi, K.; Qin, Z.; Nagano, H.; Kobayashi, M.; Yoshikawa, A.; Takahashi, K. Atomically Flat GaAs(001) Surfaces Obtained by High-Temperature Treatment with Atomic Hydrogen Irradiation. *Japanese J. Appl. Physics, Part 2 Lett.* **1997**, *36*, L1367.
- (152) King, S. W.; Barnak, J. P.; Bremser, M. D.; Tracy, K. M.; Ronning, C.; Davis, R. F.; Nemanich, R. J. Cleaning of AlN and GaN Surfaces. *J. Appl. Phys.* **1998**, *84*, S248–S260.
- (153) Hach Company; *pH Electrode Cleaning & Maintenance Guide*; 2014; Vol. 1.
- (154) Oh, J. Y.; Jang, H. J.; Cho, W. J.; Islam, M. S. Highly Sensitive Electrolyte-Insulator- Semiconductor pH Sensors Enabled by Silicon Nanowires with Al<sub>2</sub>O<sub>3</sub>/SiO<sub>2</sub> Sensing Membrane. *Sens. Actuators, B* **2012**, *171–172*, 238–243.
- (155) Rasheed, H. S.; Ahmed, N. M.; Matjafri, M. Z. Ag Metal Mid Layer Based on New Sensing Multilayers Structure Extended Gate Field Effect Transistor (EG-FET) for pH Sensor. *Mater. Sci. Semicond. Process.* **2018**, *74*, 51–56.
- (156) Ding, X.; Yang, S.; Miao, B.; Gu, L.; Gu, Z.; Zhang, J.; Wu, B.; Wang, H.; Wu, D.; Li, J. Molecular Gated-AlGaIn/GaN High Electron Mobility Transistor for pH Detection. *Analyst* **2018**, *143*, 2784–2789.
- (157) Coppa, B. J.; Fulton, C. C.; Kiesel, S. M.; Davis, R. F.; Pandarinath, C.; Burnette, J. E.; Nemanich, R. J.; Smith, D. J. Structural, Microstructural, and Electrical Properties of Gold Films and Schottky Contacts on Remote Plasma-Cleaned, n-Type ZnO{0001} Surfaces. *J. Appl. Phys.* **2005**, *97*, 103517.
- (158) Kumar, K.; Hughes, G.; Mcglynn, E.; Biswas, M. XPS Study of Cleaning Procedures of ZnO (0001), (000–1), (10–10) Surfaces. In *International Conference on Solid Films and Surfaces*; Dublin, Ireland, 2008; p 1.
- (159) Ali, G. M.; Ra'ad, H. D.; Abdullateef, A. A. pH Sensing Characteristics of EGFET Based on Pd-Doped ZnO Thin Films Synthesized by Sol-Gel Method In *Technological Advances in Electrical, Electronics and Computer Engineering (TAECE)*, 2015 Third International Conference on; IEEE: Beirut, Lebanon, 2015; pp 234–238.
- (160) Wang, L.; Bu, Y.; Ao, J. P. Effect of Oxygen Plasma Treatment on the Performance of AlGaIn/GaN Ion-Sensitive Field-Effect Transistors. *Diamond Relat. Mater.* **2017**, *73*, 1–6.
- (161) Coppa, B. J.; Fulton, C. C.; Hartlieb, P. J.; Davis, R. F.; Rodriguez, B. J.; Shields, B. J.; Nemanich, R. J. In Situ Cleaning and Characterization of Oxygen- and Zinc-Terminated, n-Type, ZnO{0001} Surfaces. *J. Appl. Phys.* **2004**, *95*, S856–S864.
- (162) Cao, H.; Landge, V.; Tata, U.; Seo, Y. S.; Rao, S.; Tang, S. J.; Tibbals, H. F.; Spechler, S.; Chiao, J. C. An Implantable, Batteryless, and Wireless Capsule with Integrated Impedance and pH Sensors for

Gastroesophageal Reflux Monitoring. *IEEE Trans. Biomed. Eng.* **2012**, *59*, 3131–3139.

(163) Linkohr, St.; Pletschen, W.; Schwarz, S. U.; Anzt, J.; Cimalla, V.; Ambacher, O. CIP (Cleaning-in-Place) Stability of AlGa<sub>N</sub>/Ga<sub>N</sub> pH Sensors. *J. Biotechnol.* **2013**, *163*, 354–361.

(164) Behnood, A.; Van Tittelboom, K.; De Belie, N. Methods for Measuring pH in Concrete: A Review. *Constr. Build. Mater.* **2016**, *105*, 176–188.

(165) Van Thanh, P.; Nhu, L. T. Q.; Mai, H. H.; Tuyen, N. V.; Doanh, S. C.; Viet, N. C.; Kien, D. T. Zinc Oxide Nanorods Grown on Printed Circuit Board for Extended-Gate Field-Effect Transistor pH Sensor. *J. Electron. Mater.* **2017**, *46*, 3732–3737.

(166) Rosli, A. B.; Abd Patah, N. D. H.; Rosdan, M. A.; Marbie, M. M.; Juhari, M. H.; Shariffudin, S. S.; Herman, S. H.; Rusop, M. Influence of Metal Catalyst for Zinc Oxide Nanostructures Grown by TCVD Method for Extended-Gate FET Sensor Application. In *Proceedings - RSM 2013:2013 IEEE Regional Symposium on Micro and Nano Electronics*; IEEE: Langkawi, Malaysia, 2013; pp 171–174.

(167) Fernandes, J. C.; Mulato, M. ZnO Thin Films Applied as pH Sensor in EGFET Devices. In *MRS Proceedings*; Cambridge University Press, 2015; Vol. 1805, pp mrs15–2136685.

(168) Li, Q.; Tang, W.; Su, Y.; Huang, Y.; Peng, S.; Zhuo, B.; Qiu, S.; Ding, L.; Li, Y.; Guo, X. Stable Thin-Film Reference Electrode on Plastic Substrate for All-Solid-State Ion-Sensitive Field-Effect Transistor Sensing System. *IEEE Electron Device Lett.* **2017**, *38*, 1469–1472.

(169) Chiu, Y. S.; Lee, C. T.; Lou, L. R.; Ho, S. C.; Chuang, C.-T. Wide Linear Sensing Sensors Using ZnO:Ta Extended-Gate Field-Effect-Transistors. *Sens. Actuators, B* **2013**, *188*, 944–948.

(170) Lin, J. C.; Huang, B. R.; Yang, Y. K. IGZO Nanoparticle-Modified Silicon Nanowires as Extended-Gate Field-Effect Transistor pH Sensors. *Sens. Actuators, B* **2013**, *184*, 27–32.

(171) Rasheed, H. S.; Ahmed, N. M.; Matjafri, M. Z.; Al-Hardan, N. H.; Almessiere, M. A.; Sabah, F. A.; Al-Hazeem, N. Z. Multilayer ZnO/Pd/ZnO Structure as Sensing Membrane for Extended-Gate Field-Effect Transistor (EGFET) with High pH Sensitivity. *J. Electron. Mater.* **2017**, *46*, 5901–5908.

(172) Lee, C. T.; Chiu, Y. S.; Ho, S. C.; Lee, Y. J. Investigation of a Photoelectrochemical Passivated ZnO-Based Glucose Biosensor. *Sensors* **2011**, *11*, 4648–4655.

(173) Chang, S.-P.; Li, C.-W.; Chen, K.-J.; Chang, S.-J.; Hsu, C.-L.; Hsueh, T.-J.; Hsueh, H.-T. ZnO-Nanowire-Based Extended-Gate Field-Effect-Transistor pH Sensors Prepared on Glass Substrate. *Sci. Adv. Mater.* **2012**, *4*, 1174–1178.

(174) Goldstein, S. R.; Peterson, J. I.; Fitzgerald, R. V. A Miniature Fiber Optic pH Sensor for Physiological Use. *J. Biomech. Eng.* **1980**, *102*, 141–146.

(175) Grant, S. A.; Bettencourt, K.; Krulevitch, P.; Hamilton, J.; Glass, R. In Vitro and in Vivo Measurements of Fiber Optic and Electrochemical Sensors to Monitor Brain Tissue pH. *Sens. Actuators, B* **2001**, *72*, 174–179.

(176) Chang, K. M.; Chang, C. T.; Chao, K. Y.; Lin, C. H. A Novel PH-Dependent Drift Improvement Method for Zirconium Dioxide Gated PH-Ion Sensitive Field Effect Transistors. *Sensors* **2010**, *10*, 4643–4654.

(177) Zhou, B.; Bian, C.; Tong, J.; Xia, S. Fabrication of a Miniature Multi-Parameter Sensor Chip for Water Quality Assessment. *Sensors (Switzerland)* **2017**, *17*, 1–14.

(178) Rigante, S.; Scarbolo, P.; Wipf, M.; Stoop, R. L.; Bedner, K.; Buitrago, E.; Bazigos, A.; Bouvet, D.; Calame, M.; Schönenberger, C.; et al. Sensing with Advanced Computing Technology: Fin Field-Effect Transistors with High-k Gate Stack on Bulk Silicon. *ACS Nano* **2015**, *9*, 4872–4881.

(179) Casey, J. R.; Grinstein, S.; Orłowski, J. Sensors and Regulators of Intracellular pH. *Nat. Rev. Mol. Cell Biol.* **2010**, *11*, 50–61.

(180) Shen, Y.; Liang, L.; Zhang, S.; Huang, D.; Zhang, J.; Xu, S.; Liang, C.; Xu, W. Organelle-Targeting Surface-Enhanced Raman Scattering (SERS) Nanosensors for Subcellular pH Sensing. *Nanoscale* **2018**, *10*, 1622–1630.

(181) Gerweck, L. E.; Seetharaman, K. Cellular pH Gradient in Tumor versus Normal Tissue: Potential Exploitation for the Treatment of Cancer. *Cancer Res.* **1996**, *56*, 1194–1198.

(182) Damaghi, M.; Wojtkowiak, J. W.; Gillies, R. J. pH Sensing and Regulation in Cancer. *Front. Physiol.* **2013**, *4*, 370.

(183) Susumu, K.; Field, L. D.; Oh, E.; Hunt, M.; Delehanty, J. B.; Palomo, V.; Dawson, P. E.; Huston, A. L.; Medintz, I. L. Purple-, Blue-, and Green-Emitting Multishell Alloyed Quantum Dots: Synthesis, Characterization, and Application for Ratiometric Extracellular pH Sensing. *Chem. Mater.* **2017**, *29*, 7330–7344.

(184) Chen, S.; Hong, Y.; Liu, Y.; Liu, J.; Leung, C. W. T.; Li, M.; Kwok, R. T. K.; Zhao, E.; Lam, J. W. Y.; Yu, Y.; et al. Full-Range Intracellular pH Sensing by an Aggregation-Induced Emission-Active Two-Channel Ratiometric Fluorogen. *J. Am. Chem. Soc.* **2013**, *135*, 4926–4929.

(185) Chandra, A.; Singh, N. Cell Microenvironment pH Sensing in 3D Microgels Using Fluorescent Carbon Dots. *ACS Biomater. Sci. Eng.* **2017**, *3*, 3620–3627.

(186) Düwel, S.; Hundshammer, C.; Gersch, M.; Feurecker, B.; Steiger, K.; Buck, A.; Walch, A.; Haase, A.; Glaser, S. J.; Schwaiger, A.; Schilling, F. Imaging of pH in Vivo Using Hyperpolarized <sup>13</sup>C-Labelled Zymonic Acid. *Nat. Commun.* **2017**, *8*, 15126.

(187) Koeppen, B. M. Renal Regulation of Acid-Base Balance. *Adv. Physiol. Educ.* **1998**, *20*, 275–S132.

(188) Cohen, R. S. Acidosis and Alkalosis. In *Fetal and Neonatal Brain Injury*, 4th ed.; 2009; Vol. 9780521888, pp 402–408.

(189) Mitchell, J. H.; Wildenthal, K.; Johnson, R. L. The Effects of Acid-Base Disturbances on Cardiovascular and Pulmonary Function. *Kidney Int.* **1972**, *1*, 375–389.

(190) Mark, P. R. G. *Renal Physiology*; Departments of Electrical Engineering, Mechanical Engineering, Massachusetts, and the Harvard-MIT Division of Health Sciences and Technology, 2004; pp 2–32.

(191) O'Donnell, M. E. Blood-Brain Barrier Na Transporters in Ischemic Stroke. *Adv. Pharmacol.* **2014**, *71*, 113–146.

(192) Hermansen, L.; Osnes, J. B. Blood and Muscle pH after Maximal Exercise in Man. *J. Appl. Physiol.* **1972**, *32*, 304–308.

(193) Osborn, J. J. Experimental Hypothermia: Respiratory and Blood pH Changes in Relation to Cardiac Function. *Am. J. Physiol.* **1953**, *175*, 389–398.

(194) Kuehnle, E.; Herms, S.; Kohls, F.; Kundu, S.; Hillemanns, P.; Staboulidou, I. Correlation of Fetal Scalp Blood Sampling pH with Neonatal Outcome Umbilical Artery pH Value. *Arch. Gynecol. Obstet.* **2016**, *294*, 763–770.

(195) Del Coso, J.; Hamouti, N.; Aguado-Jimenez, R.; Mora-Rodriguez, R. Respiratory Compensation and Blood pH Regulation during Variable Intensity Exercise in Trained versus Untrained Subjects. *Eur. J. Appl. Physiol.* **2009**, *107*, 83–93.

(196) Momiyama, Y.; Yamada, W.; Miyata, K.; Miura, K.; Fukuda, T.; Fuse, J.; Kikuno, T. Prognostic Values of Blood pH and Lactate Levels in Patients Resuscitated from Out-of-Hospital Cardiac Arrest. *Acute Med. Surg.* **2017**, *4*, 25–30.

(197) Kwong, T.; Robinson, C.; Spencer, D.; Wiseman, O. J.; Karet Frankl, F. E. Accuracy of Urine pH Testing in a Regional Metabolic Renal Clinic: Is the Dipstick Accurate Enough? *Urolithiasis* **2013**, *41*, 129–132.

(198) Cook, J. D.; Strauss, K. A.; Caplan, Y. H.; LoDico, C. P.; Bush, D. M. Urine pH: The Effects of Time and Temperature after Collection. *J. Anal. Toxicol.* **2007**, *31*, 486–496.

(199) Crouch, D. J. Oral Fluid Collection: The Neglected Variable in Oral Fluid Testing. *Forensic Sci. Int.* **2005**, *150*, 165–173.

(200) Kidwell, D. A.; Holland, J. C.; Athanaselis, S. Testing for Drugs of Abuse in Saliva and Sweat. *J. Chromatogr., Biomed. Appl.* **1998**, *713*, 111–135.

(201) Tabata, M.; Ratanaporncharoen, C.; Asano, A.; Kitasako, Y.; Ikeda, M.; Goda, T.; Matsumoto, A.; Tagami, J.; Miyahara, Y. Miniaturized Ir/IrO<sub>x</sub> pH Sensor for Quantitative Diagnosis of Dental Caries. *Procedia Eng.* **2016**, *168*, 598–601.

(202) Fujii, M.; Kitasako, Y.; Sadr, A.; Tagami, J. Roughness and pH Changes of Enamel Surface Induced by Soft Drinks in Vitro

Applications of Stylus Profilometry, Focus Variation 3D Scanning Microscopy and Micro pH Sensor. *Dent. Mater. J.* **2011**, *30*, 404–410.

(203) Murakami, K.; Kitasako, Y.; Burrow, M. F.; Tagami, J. In Vitro pH Analysis of Active and Arrested Dentinal Caries in Extracted Human Teeth Using a Micro pH Sensor. *Dent. Mater. J.* **2006**, *25*, 423–429.

(204) Ratanaporncharoen, C.; Tabata, M.; Kitasako, Y.; Ikeda, M.; Goda, T.; Matsumoto, A.; Tagami, J.; Miyahara, Y. pH Mapping on Tooth Surfaces for Quantitative Caries Diagnosis Using Micro Ir/IrOx pH Sensor. *Anal. Chem.* **2018**, *90*, 4925–4931.

(205) Chaisiwamongkhol, K.; Batchelor-Mcauley, C.; Compton, R. G. Amperometric Micro pH Measurements in Oxygenated Saliva. *Analyst* **2017**, *142*, 2828–2835.

(206) Baliga, S.; Muglikar, S.; Kale, R. Salivary PH: A Diagnostic Biomarker. *J. Indian Soc. Periodontol.* **2013**, *17*, 461.

(207) Seethalakshmi, C.; Jagat Reddy, R. C.; Asifa, N.; Prabhu, S. Correlation of Salivary PH, Incidence of Dental Caries and Periodontal Status in Diabetes Mellitus Patients: A Cross- Sectional Study. *J. Clin. Diagnostic Res.* **2016**, *10*, ZC12–ZC14.

(208) Rathnayake, N.; Åkerman, S.; Klinge, B.; Lundegren, N.; Jansson, H.; Tryselius, Y.; Sorsa, T.; Gustafsson, A. Salivary Biomarkers for Detection of Systemic Diseases. *PLoS One* **2013**, *8*, No. e61356.

(209) Yoshizawa, J. M.; Schafer, C. A.; Schafer, J. J.; Farrell, J. J.; Paster, B. J.; Wong, D. T. W. Salivary Biomarkers: Toward Future Clinical and Diagnostic Utilities. *Clin. Microbiol. Rev.* **2013**, *26*, 781–791.

(210) Jo, J.; Lee, C. H.; Kopelman, R.; Wang, X. In Vivo Quantitative Imaging of Tumor pH by Nanosonophore Assisted Multispectral Photoacoustic Imaging. *Nat. Commun.* **2017**, *8*, 471.

(211) Enriquez-Navas, P. M.; Gillies, R. J. Measuring PHi and PHe by MRS. *eMagRes.* **2015**, *4*, 643–650.

(212) Kaneniwa, N.; Otsuka, M. Evaluation of Acidogenicity of Commercial Isomaltooligosaccharides Mixture and Its Hydrogenated Derivative by Measurement of pH Response under Human Dental Plaque. *Chem. Pharm. Bull.* **1985**, *33*, 1660–1668.

(213) Parvinzadeh Gashti, M.; Asselin, J.; Barbeau, J.; Boudreau, D.; Greener, J. A Microfluidic Platform with pH Imaging for Chemical and Hydrodynamic Stimulation of Intact Oral Biofilms. *Lab Chip* **2016**, *16*, 1412–1419.

(214) Hashim, A. I.; Zhang, X.; Wojtkowiak, J. W.; Martinez, G. V.; Gillies, R. J. Imaging pH and Metastasis. *NMR Biomed.* **2011**, *24*, 582–591.

(215) Zhang, X.; Lin, Y.; Gillies, R. J. Tumor pH and Its Measurement. *J. Nucl. Med.* **2010**, *51*, 1167–1170.

(216) Gallagher, F. A.; Kettunen, M. I.; Day, S. E.; Hu, D.-E.; Ardenkjaer-Larsen, J. H.; Zandt, R.; Jensen, P. R.; Karlsson, M.; Golman, K.; Lerche, M. H.; Brindle, K. M. Magnetic Resonance Imaging of pH in Vivo Using Hyperpolarized <sup>13</sup>C-Labelled Bicarbonate. *Nature* **2008**, *453*, 940–943.

(217) Malhotra, D.; Casey, J. R. Intracellular pH Measurement. In *eLS*; 2015; pp 1–7.

(218) Lardner, A. The Effects of Extracellular pH on Immune Function. *J. Leukocyte Biol.* **2001**, *69*, 522–530.

(219) Paradise, R. K.; Lauffenburger, D. A.; van Vliet, K. J. Acidic Extracellular pH Promotes Activation of Integrin  $\alpha v\beta 3$ . *PLoS One* **2011**, *6*, No. e15746.

(220) Hayata, H.; Miyazaki, H.; Niisato, N.; Yokoyama, N.; Marunaka, Y. Lowered Extracellular pH Is Involved in the Pathogenesis of Skeletal Muscle Insulin Resistance. *Biochem. Biophys. Res. Commun.* **2014**, *445*, 170–174.

(221) Kenney, R. M.; Boyce, M. W.; Whitman, N. A.; Kromhout, B. P.; Lockett, M. R. A PH- Sensing Optode for Mapping Spatiotemporal Gradients in 3D Paper-Based Cell Cultures. *Anal. Chem.* **2018**, *90*, 2376–2383.

(222) Munteanu, R. E.; Stănică, L.; Gheorghiu, M.; Gáspár, S. Measurement of the Extracellular pH of Adherently Growing Mammalian Cells with High Spatial Resolution Using a Voltammetric pH Microsensor. *Anal. Chem.* **2018**, *90*, 6899–6905.

(223) Švastová, E.; Hulíková, A.; Rafajová, M.; Zat'ovičová, M.; Gibadulinová, A.; Casini, A.; Cecchi, A.; Scozzafava, A.; Supuran, C. T.; Pastorek, J.; et al. Hypoxia Activates the Capacity of Tumor-Associated Carbonic Anhydrase IX to Acidify Extracellular pH. *FEBS Lett.* **2004**, *577*, 439–445.

(224) Hu, J.; Stein, A.; Bühlmann, P. Rational Design of All-Solid-State Ion-Selective Electrodes and Reference Electrodes. *TrAC, Trends Anal. Chem.* **2016**, *76*, 102–114.

(225) Carneiro, a. a. O.; Vilela, G. R.; De Araujo, D. B.; Baffa, O. MRI Relaxometry: Methods and Applications. *Braz. J. Phys.* **2006**, *36*, 1–7.

(226) Marzouk, S. A. M.; Ufer, S.; Buck, R. P.; Johnson, T. A.; Dunlap, L. A.; Cascio, W. E. Electrodeposited Iridium Oxide pH Electrode for Measurement of Extracellular Myocardial Acidosis during Acute Ischemia. *Anal. Chem.* **1998**, *70*, 5054–5061.

(227) Das, A.; Ko, D. H.; Chen, C. H.; Chang, L. B.; Lai, C. S.; Chu, F. C.; Chow, L.; Lin, R. M. Highly Sensitive Palladium Oxide Thin Film Extended Gate FETs as pH Sensor. *Sens. Actuators, B* **2014**, *205*, 199–205.

(228) Lee, Y.; Howe, C.; Mishra, S.; Lee, D. S.; Mahmood, M.; Piper, M.; Kim, Y.; Tieu, K.; Byun, H.-S.; Coffey, J. P.; et al. Wireless, Intraoral Hybrid Electronics for Real-Time Quantification of Sodium Intake toward Hypertension Management. *Proc. Natl. Acad. Sci. U. S. A.* **2018**, *115*, 5377–5382.

(229) Wang, X.; Liu, Z.; Zhang, T. Flexible Sensing Electronics for Wearable/Attachable Health Monitoring. *Small* **2017**, *13*, 1–19.

(230) Hans, R.; Thomas, S.; Garla, B.; Dagli, R. J.; Hans, M. K. Effect of Various Sugary Beverages on Salivary PH, Flow Rate, and Oral Clearance Rate amongst Adults. *Scientifica* **2016**, *2016*, 3–8.

(231) Oncescu, V.; O'Dell, D.; Erickson, D. Smartphone Based Health Accessory for Colorimetric Detection of Biomarkers in Sweat and Saliva. *Lab Chip* **2013**, *13*, 3232–3238.

(232) Marzouk, S. A. M.; Buck, R. P.; Dunlap, L. A.; Johnson, T. A.; Cascio, W. E. Measurement of Extracellular PH, K<sup>+</sup>, and Lactate in Ischemic Heart. *Anal. Biochem.* **2002**, *308*, 52–60.

(233) Zhou, J.; Zhang, L.; Tian, Y. Micro Electrochemical pH Sensor Applicable for Real-Time Ratiometric Monitoring of pH Values in Rat Brains. *Anal. Chem.* **2016**, *88*, 2113–2118.

(234) Chung, H.-J.; Sulkin, M. S. Ultrathin, Stretchable, Multiplexing pH Sensor Arrays on Biomedical Devices With Demonstrations on Rabbit and Human Hearts Undergoing Ischemia. *Adv. Healthc. Mater.* **2015**, *3*, 59–68.

(235) Tait, G. A.; Young, R. B.; Wilson, G. J.; Steward, D. J.; MacGregor, D. C. Myocardial pH during Regional Ischemia: Evaluation of a Fiber-Optic Photometric Probe. *Am. J. Physiol.* **1982**, *243*, H1027–31.

(236) Watanabe, T.; Kobayashi, K.; Suzuki, T.; Oizumi, M.; Clark, G. T. A Preliminary Report on Continuous Recording of Salivary pH Using Telemetry in an Edentulous Patient. *Int. J. Prosthodont.* **1999**, *12*.

(237) Soller, B. R.; Stahl, R. F.; Knox, M. Microsensors for Monitoring Myocardial Ischemia: The Concept of pH Time Integral. In *Engineering in Medicine and Biology Society, 1993. Proceedings of the 15th Annual International Conference of the IEEE*; IEEE: San Diego, CA, USA, 1993; pp 1582–1583.

(238) Rai, P.; Jung, S.; Ji, T.; Varadan, V. K. Ion-Sensitive Field Effect Transistors for pH and Potassium Ion Concentration Sensing: Towards Detection of Myocardial Ischemia. In *Nanosensors and Microsensors for Bio-Systems 2008*; International Society for Optics and Photonics: San Diego, CA, USA, 2008; p 693101.

(239) Anastasova, S.; Kassanos, P.; Yang, G. Z. Multi-Parametric Rigid and Flexible, Low- Cost, Disposable Sensing Platforms for Biomedical Applications. *Biosens. Bioelectron.* **2018**, *102*, 668–675.

(240) Curto, V. F.; Coyle, S.; Byrne, R.; Angelov, N.; Diamond, D.; Benito-Lopez, F. Concept and Development of an Autonomous Wearable Micro-Fluidic Platform for Real Time pH Sweat Analysis. *Sens. Actuators, B* **2012**, *175*, 263–270.

(241) Callewaert, C.; Buysschaert, B.; Vossen, E.; Fievez, V.; Van de Wiele, T.; Boon, N. Artificial Sweat Composition to Grow and Sustain a Mixed Human Axillary Microbiome. *J. Microbiol. Methods* **2014**, *103*, 6–8.

- (242) Jadoon, S.; Karim, S.; Akram, M. R.; Kalsoom Khan, A.; Zia, M. A.; Siddiqi, A. R.; Murtaza, G. Recent Developments in Sweat Analysis and Its Applications. *Int. J. Anal. Chem.* **2015**, *2015*, 164974.
- (243) Caldara, M.; Colleoni, C.; Guido, E.; Re, V.; Rosace, G. Optical Monitoring of Sweat pH by a Textile Fabric Wearable Sensor Based on Covalently Bonded Litmus-3- Glycidoxypropyltrimethoxysilane Coating. *Sens. Actuators, B* **2016**, *222*, 213–220.
- (244) Levitt, D. G.; Schoemaker, R. C. Human Physiologically Based Pharmacokinetic Model for ACE Inhibitors: Ramipril and Ramiprilat. *BMC Clin. Pharmacol.* **2006**, *6*, 159–169.
- (245) Nikolajek, W. P.; Emrich, H. M. pH of Sweat of Patients with Cystic Fibrosis. *Klin. Wochenschr.* **1976**, *54*, 287–288.
- (246) Luckie, D. B.; Krouse, M. E. Cystic Fibrosis: Does CFTR Malfunction Alter pH Regulation? In *Genetic Disorders*; 2013; pp 319–344.
- (247) Dang, W.; Manjakkal, L.; Navaraj, W. T.; Lorenzelli, L.; Vinciguerra, V.; Dahiya, R. Stretchable Wireless System for Sweat pH Monitoring. *Biosens. Bioelectron.* **2018**, *107*, 192–202.
- (248) Caplan, Y. H.; Goldberger, B. A. Alternative Specimens for Workplace Drug Testing. *J. Anal. Toxicol.* **2001**, *25*, 396–399.
- (249) Curto, V. F.; Fay, C.; Coyle, S.; Byrne, R.; O'Toole, C.; Barry, C.; Hughes, S.; Moyna, N.; Diamond, D.; Benito-Lopez, F. Real-Time Sweat pH Monitoring Based on a Wearable Chemical Barcode Micro-Fluidic Platform Incorporating Ionic Liquids. *Sens. Actuators, B* **2012**, *171–172*, 1327–1334.
- (250) Bandodkar, A. J.; Wang, J. Non-Invasive Wearable Electrochemical Sensors: A Review. *Trends Biotechnol.* **2014**, *32*, 363–371.
- (251) Bandodkar, A. J.; Hung, V. W. S.; Jia, W.; Valdés-Ramírez, G.; Windmiller, J. R.; Martinez, A. G.; Ramírez, J.; Chan, G.; Kerman, K.; Wang, J. Tattoo-Based Potentiometric Ion-Selective Sensors for Epidermal pH Monitoring. *Analyst* **2013**, *138*, 123–128.
- (252) Guinovart, T.; Parrilla, M.; Crespo, G. A.; Rius, F. X.; Andrade, F. J. Potentiometric Sensors Using Cotton Yarns, Carbon Nanotubes and Polymeric Membranes. *Analyst* **2013**, *138*, 5208–5215.
- (253) Karyakin, A. A.; Vuki, M.; Lukachova, L. V.; Karyakina, E. E.; Orlov, A. V.; Karpachova, G. P.; Wang, J. Processible Polyaniline as an Advanced Potentiometric pH Transducer. Application to Biosensors. *Anal. Chem.* **1999**, *71*, 2534–2540.
- (254) Curto, V. F.; Coyle, S.; Byrne, R.; Angelov, N.; Diamond, D.; Benito-Lopez, F. Concept and Development of an Autonomous Wearable Micro-Fluidic Platform for Real Time pH Sweat Analysis. *Sens. Actuators, B* **2012**, *175*, 263–270.
- (255) Nakata, S.; Arie, T.; Akita, S.; Takei, K. Wearable, Flexible, and Multifunctional Healthcare Device with an ISFET Chemical Sensor for Simultaneous Sweat pH and Skin Temperature Monitoring. *ACS Sensors* **2017**, *2*, 443–448.
- (256) Lee, H.; Song, C.; Hong, Y. S.; Kim, M. S.; Cho, H. R.; Kang, T.; Shin, K.; Choi, S. H.; Hyeon, T.; Kim, D. Wearable/Disposable Sweat-Based Glucose Monitoring Device with Multistage Transdermal Drug Delivery Module. *Sci. Adv.* **2017**, *3*, e1601314.
- (257) Trovato, V.; Rosace, G.; Colleoni, C.; Plutino, M. R. Synthesis and Characterization of Halochromic Hybrid Sol-Gel for the Development of a pH Sensor Fabric. In *IOP Conference Series: Materials Science and Engineering*; IOP Publishing: Corfu, Greece, 2017; Vol. 254.
- (258) Caldara, M.; Colleoni, C.; Guido, E.; Re, V.; Rosace, G.; Vitali, A. Textile Based Colorimetric pH Sensing - A Platform for Future Wearable pH Monitoring. In *Proceedings - BSN 2012: 9th International Workshop on Wearable and Implantable Body Sensor Networks*; IEEE: London, UK, 2012; pp 11–16.
- (259) Tamayol, A.; Akbari, M.; Zilberman, Y.; Comotto, M.; Lesh, E.; Serex, L.; Bagherifard, S.; Chen, Y.; Fu, G.; Ameri, S. K.; et al. Flexible PH-Sensing Hydrogel Fibers for Epidermal Applications. *Adv. Healthcare Mater.* **2016**, *5*, 711–719.
- (260) Zhu, Z.; Liu, T.; Li, G.; Li, T.; Inoue, Y. Wearable Sensor Systems for Infants. *Sensors* **2015**, *15*, 3721–3749.
- (261) Sen, C. K.; Gordillo, G. M.; Roy, S.; Kirsner, R.; Lambert, L.; Hunt, T. K.; Gottrup, F.; Gurtner, G. C.; Longaker, M. T. Human Skin Wounds: A Major Snoballing Threat to Public Health and Economy. *Wound Repair Regen.* **2009**, *17*, 763–771.
- (262) Guinovart, T.; Valdés-Ramírez, G.; Windmiller, J. R.; Andrade, F. J.; Wang, J. Bandage- Based Wearable Potentiometric Sensor for Monitoring Wound pH. *Electroanalysis* **2014**, *26*, 1345–1353.
- (263) Roychoudhury, S.; Umasankar, Y.; Jaller, J.; Herskovitz, I.; Mervis, J.; Darwin, E.; Hirt, P. A.; Borda, L. J.; Lev-tov, H. A.; Kirsner, R.; Bhansali, S. Continuous Monitoring of Wound Healing Using a Wearable Enzymatic Uric Acid Biosensor. *J. Electrochem. Soc.* **2018**, *165*, B3168–B3175.
- (264) Mostafalu, P.; Tamayol, A.; Rahimi, R.; Ochoa, M.; Khalilpour, A.; Kiaee, G.; Yazdi, I. K.; Bagherifard, S.; Dokmeci, M. R.; Ziaie, B.; et al. Smart Bandage for Monitoring and Treatment of Chronic Wounds. *Small* **2018**, *14*, 1703509.
- (265) Stoppa, M.; Chiolerio, A. Wearable Electronics and Smart Textiles: A Critical Review. *Sensors* **2014**, *14*, 11957–11992.
- (266) Giachet, F. T.; Vineis, C.; Sanchez Ramirez, D. O.; Carletto, R. A.; Varesano, A.; Mazzuchetti, G. Reversible and Washing Resistant Textile-Based Optical pH Sensors by Dyeing Fabrics with Curcuma. *Fibers Polym.* **2017**, *18*, 720–730.
- (267) Rahimi, R.; Ochoa, M.; Tamayol, A.; Khalili, S.; Khademhosseini, A.; Ziaie, B. Highly Stretchable Potentiometric pH Sensor Fabricated via Laser Carbonization and Machining of Carbon-Polyaniline Composite. *ACS Appl. Mater. Interfaces* **2017**, *9*, 9015–9023.
- (268) Frost, M. C.; Meyerhoff, M. E. Implantable Chemical Sensors for Real-Time Clinical Monitoring: Progress and Challenges. *Curr. Opin. Chem. Biol.* **2002**, *6*, 633–641.
- (269) Hao, J.; Xiao, T.; Wu, F.; Yu, P.; Mao, L. High Antifouling Property of Ion-Selective Membrane: Toward in Vivo Monitoring of pH Change in Live Brain of Rats with Membrane-Coated Carbon Fiber Electrodes. *Anal. Chem.* **2016**, *88*, 11238–11243.
- (270) Wencel, D.; Kaworek, A.; Abel, T.; Efremov, V.; Bradford, A.; Carthy, D.; Coady, G.; McMorro, R. C. N.; McDonagh, C. Optical Sensor for Real-Time pH Monitoring in Human Tissue. *Small* **2018**, *14*, 1803627.
- (271) Wang, D.; Yang, C.; Xia, J.; Xue, Z.; Jiang, D.; Zhou, G.; Zheng, X.; Zheng, H.; Du, Y.; Li, Q. Improvement of the Ir/IrO<sub>2</sub> pH Electrode via Hydrothermal Treatment. *Ionics* **2017**, *23*, 2167–2174.
- (272) Wang, M.; Yao, S.; Madou, M. A Long-Term Stable Iridium Oxide pH Electrode. *Sens. Actuators, B* **2002**, *81*, 313–315.
- (273) Vanamo, U.; Bobacka, J. Instrument-Free Control of the Standard Potential of Potentiometric Solid-Contact Ion-Selective Electrodes by Short-Circuiting with a Conventional Reference Electrode. *Anal. Chem.* **2014**, *86*, 10540–10545.
- (274) Sabah, F. A.; Ahmed, N. M.; Hassan, Z.; Abdullah Almessiere, M. Influences of Substrate Type on the pH Sensitivity of CuS Thin Films EG-FET Prepared by Spray Pyrolysis Deposition. *Mater. Sci. Semicond. Process.* **2017**, *63*, 269–278.
- (275) Nguyen, C. M.; Huang, W.; Rao, S.; Cao, H.; Tata, U.; Chiao, M.; Chiao, J. Sol-Gel Iridium Oxide-Based pH Sensor Array on Flexible Polyimide Substrate. *IEEE Sens. J.* **2013**, *13*, 3857–3864.
- (276) Ghoneim, M. T.; Zidan, M. A.; Almassar, M. Y.; Hanna, A. N.; Kosel, J.; Salama, K. N.; Hussain, M. M. Thin PZT-Based Ferroelectric Capacitors on Flexible Silicon for Nonvolatile Memory Applications. *Adv. Electron. Mater.* **2015**, *1*, 1500045.
- (277) Ghoneim, M.; Hussain, M. Review on Physically Flexible Nonvolatile Memory for Internet of Everything Electronics. *Electronics* **2015**, *4*, 424–479.
- (278) Kutbee, A. T.; Bahabry, R. R.; Alamoudi, K. O.; Ghoneim, M. T.; Cordero, M. D.; Almuslem, A. S.; Gumus, A.; Diallo, E. M.; Nassar, J. M.; Hussain, A. M.; Khashab, N. M.; Hussain, M. M. Flexible and Biocompatible High-Performance Solid-State Micro-Battery for Implantable Orthodontic System. *npj Flex. Electron.* **2017**, *1*, 7.
- (279) Alfaraj, N.; Hussain, A. M.; Torres Sevilla, G. A.; Ghoneim, M. T.; Rojas, J. P.; Aljedaani, A. B.; Hussain, M. M. Functional Integrity of Flexible N-Channel Metal-oxide-semiconductor Field-Effect Transistors on a Reversibly Bistable Platform. *Appl. Phys. Lett.* **2015**, *107*, 174101.

- (280) Shaikh, S. F.; Ghoneim, M. T.; Bahabry, R. R.; Khan, S. M.; Hussain, M. M. Modular Lego-Electronics. *Adv. Mater. Technol.* **2018**, *3*, 1700147.
- (281) Ghoneim, M. T.; Alfaraaj, N.; Torres-Sevilla, G. A.; Fahad, H. M.; Hussain, M. M. Out-of-Plane Strain Effects on Physically Flexible FinFET CMOS. *IEEE Trans. Electron Devices* **2016**, *63*, 2657–2664.
- (282) Prats-Alfonso, E.; Abad, L.; Casañ-Pastor, N.; Gonzalo-Ruiz, J.; Baldrich, E. Iridium Oxide pH Sensor for Biomedical Applications. Case Urea-Urease in Real Urine Samples. *Biosens. Bioelectron.* **2013**, *39*, 163–169.
- (283) Huang, B. R.; Hsu, C. L.; Wang, Y. K.; Yang, W. L. Core-Shell P-N Junction Si Nanowires as Rapid Response and High-Sensitivity pH Sensor. *IEEE Sens. J.* **2017**, *17*, 3967–3974.
- (284) Wu, S.; Wu, Y.; Lin, C. High Performance EGFET-Based Ph Sensor Utilizing Low-Cost Industrial-Grade Touch Panel Film As the Gate Structure. *uTAS Proc.* **2014**, *15*, 2131–2133.
- (285) Salvo, P.; Calisi, N.; Melaj, B.; Dini, V.; Paoletti, C.; Lomonaco, T.; Pucci, A.; Di Francesco, F.; Piaggese, A.; Romanelli, M. Temperature- and PH-Sensitive Wearable Materials for Monitoring Foot Ulcers. *Int. J. Nanomed.* **2017**, *12*, 949–954.
- (286) Meruva, R. K.; Meyerhoff, M. E. Catheter-Type Sensor for Potentiometric Monitoring of Oxygen, pH and Carbon Dioxide. *Biosens. Bioelectron.* **1998**, *13*, 201–212.
- (287) Macdonald, D. D.; Liu, J.; Lee, D. Development of W/WO<sub>3</sub> Sensors for the Measurement of pH in an Emulsion Polymerization System. *J. Appl. Electrochem.* **2004**, *34*, 577–582.
- (288) Yang, J.; Kwak, T. J.; Zhang, X.; McClain, R.; Chang, W. J.; Gunasekaran, S. Digital pH Test Strips for In-Field pH Monitoring Using Iridium Oxide-Reduced Graphene Oxide Hybrid Thin Films. *ACS Sensors* **2016**, *1*, 1235–1243.
- (289) Lonsdale, W.; Wajrak, M.; Alameh, K. Effect of Conditioning Protocol, Redox Species and Material Thickness on the pH Sensitivity and Hysteresis of Sputtered RuO<sub>2</sub> Electrodes. *Sens. Actuators, B* **2017**, *252*, 251–256.
- (290) Voigt, H.; Schitthelm, F.; Lange, T.; Kullick, T.; Ferretti, R. Diamond-like Carbon-Gate PH-ISFET. *Sens. Actuators, B* **1997**, *44*, 441–445.
- (291) Bartic, C.; Palan, B.; Campitelli, A.; Borghs, G. Monitoring pH with Organic-Based Field-Effect Transistors. *Sens. Actuators, B* **2002**, *83*, 115–122.
- (292) Graham, D. J.; Jaselskis, B.; Moore, C. E. Development of the Glass Electrode and the pH Response. *J. Chem. Educ.* **2013**, *90*, 345–351.
- (293) Pantelis, D. M.; Experton, J.; Martin, C. R. Rearranging the Nernst Equation to Make a Dosage-Controllable Membrane Delivery System. *J. Electroanal. Chem.* **2018**, *819*, 73–77.
- (294) Scholz, F. Nikolsky's Ion Exchange Theory versus Baucke's Dissociation Mechanism of the Glass Electrode. *J. Solid State Electrochem.* **2011**, *15*, 67–68.
- (295) Durst, R. A. Mechanism of the Glass Electrode Response. *J. Chem. Educ.* **1967**, *44*, 175.
- (296) Baucke, F. G. K. The Modern Understanding of the Glass Electrode Response. *Fresenius' J. Anal. Chem.* **1994**, *349*, 582–596.
- (297) Cheng, K. L. A New Concept for PH-Potential Calculations. *J. Chem. Educ.* **1999**, *76*, 1029.
- (298) Mauro, A. Space Charge Regions in Fixed Charge Membranes and the Associated Property of Capacitance. *Biophys. J.* **1962**, *2*, 179–198.
- (299) Oldham, K. B. A Gouy-Chapman-Stern Model of the Double Layer at a (Metal)/(Ionic Liquid) Interface. *J. Electroanal. Chem.* **2008**, *613*, 131–138.
- (300) Al-Hilli, S.; Willander, M. The pH Response and Sensing Mechanism of N-Type ZnO/Electrolyte Interfaces. *Sensors* **2009**, *9*, 7445–7480.
- (301) Yates, D. E.; Levine, S.; Healy, T. W. Site-Binding Model of the Electrical Double Layer at the Oxide/Water Interface. *J. Chem. Soc., Faraday Trans. 1* **1974**, *70*, 1807–1818.
- (302) Parizi, K. B.; Xu, X.; Pal, A.; Hu, X.; Wong, H. S. P. ISFET pH Sensitivity: Counter-Ions Play a Key Role. *Sci. Rep.* **2017**, *7*, 1–10.
- (303) Huang, W. D.; Cao, H.; Deb, S.; Chiao, M.; Chiao, J. C. A Flexible pH Sensor Based on the Iridium Oxide Sensing Film. *Sens. Actuators, A* **2011**, *169*, 1–11.
- (304) Kofstad, P. Defects and Transport Properties of Metal Oxides. *Oxid. Met.* **1995**, *44*, 3–27.
- (305) Pilon, L.; Wang, H.; d'Entremont, A. Recent Advances in Continuum Modeling of Interfacial and Transport Phenomena in Electric Double Layer Capacitors. *J. Electrochem. Soc.* **2015**, *162*, A5158–A5178.
- (306) Batista, P. D.; Mulato, M. ZnO Extended-Gate Field-Effect Transistors as pH Sensors. *Appl. Phys. Lett.* **2005**, *87*, 143508.
- (307) Su, Y.; Dagdeviren, C.; Li, R. Measured Output Voltages of Piezoelectric Devices Depend on the Resistance of Voltmeter. *Adv. Funct. Mater.* **2015**, *25*, 5320–5325.
- (308) Su, Y.; Li, S.; Huan, Y.; Li, R.; Zhang, Z.; Joe, P.; Dagdeviren, C. The Universal and Easy-to-Use Standard of Voltage Measurement for Quantifying the Performance of Piezoelectric Devices. *Extrem. Mech. Lett.* **2017**, *15*, 10–16.